# ANDERSON-HOLSTEIN MODEL: SOME APPLICATIONS

**Ch. Narasimha Raju**

School of Physics
University of Hyderabad
Hyderabad, 500046
India

**Supervisor: Prof. Ashok Chatterjee**

April 2016

# DECLARATION

I hereby declare that the work reported in this thesis has been carried out by me independently in the school of physics, University of Hyderabad, under the supervision of Prof. Ashok Chatterjee, School of Physics, and University of Hyderabad. I also declare that this is my own work and effort, and it has not been submitted at any other University or Institution for any degree. Wherever contributions of others are involved, every effort is made to indicate that clearly with due reference to literature, and acknowledgement of collaborative research and discussions.

Place: Hyderabad

Date:

Ch. Narasimha Raju

# CERTIFICATE

This is to certify that the thesis work entitled "Anderson-Holstein model: Some Applications" being submitted to University of Hyderabad by **Narasimha Raju Chebrolu** with Reg.No. 09PHPH04, in partial fulfillment for the award of the degree of Doctor of Philosophy in physics, is a bona fide work carried out by him under my supervision.

Dean
School of Physics,

Prof. Ashok Chatterjee
Supervisor,

# ACKNOWLEDGEMENTS

I consider myself extremely fortunate to have had a chance to work with Prof. Ashok Chatterjee. He has always been encouraging, guiding, while at the same time he gave me enough freedom to pursue my research interests. He always help me financially, morally and mentally. Without his guidance, this thesis would not have been possible. I express my gratitude to Sri Ch. Sarat Babu, Smt. Naga Rajeswari, Sri C. Satyanarayana, Prof. Soma Mukhopadhyay, Prof. Uma maheswara Rao & family, Prof. Anantha Lakshmi for their support during my hard times. I would like to thank my doctoral review committee members, Dr. Srinath, and Dr. S. V. S. Nageshwara Rao for their valuable suggestions during doctoral review presentations. I am extremely grateful to the Dean, School of Physics and non-teaching staff for their help in administrative matters.

The financial assistance provided by University of Hyderabad and BSR fellowship of UGC is also greatly acknowledged.

I thank all my colleagues namely, I. V. Sankar, Aalu Boda, D. Sanjeev Kumar, P. J. Monisha, Uma Lavanya, Luhluh Jahan for their support and cooperation in throughout my work. I wish to thank I. V. Sankar and D. Sanjeev Kumar, who gave help in learning MATLAB programing.

Finally I would like to acknowledge my parents, sister, nieces Shara & Bhavana and all my friends for their unconditional love and support.

# PREFACE

The main objective of this thesis is to study the quantum impurity problem and quantum transport problem in three terminal devices. To study the above systems we consider the single level symmetric Anderson-Holstein model. Mainly we focus on the theoretical study of the effect of the local electron-phonon (*el-ph*) interaction on the properties of above systems. The major part of this thesis is dedicated to the study of the physics of a magnetic impurity atom in a non-magnetic host metal (dilute magnetic alloys). We also incorporate in the thesis our investigation on the problem of a magnetic impurity in a BCS superconductor (impure superconductors). Finally we take up and study the problem of quantum transport through an impurity quantum dot in a single molecular transistor.

In dilute magnetic alloys, the local electron-electron (*el-el*) as well as *el-ph* interaction present at the impurity site effects the properties of these systems substantially. We consider the single-impurity Anderson model together with an unperturbed phonon Hamiltonian relevant for the impurity atom and the Holstein *el-ph* interaction term to include the local *el-ph* interaction present at the impurity site. The resulting Hamiltonian is called the Anderson-Holstein Hamiltonian. We study the effect of *el-ph* interaction on the many-body bound state formed between the conduction and impurity electrons at the impurity. We furthermore investigate the effect of *el-ph* interaction on the local magnetic moment of the impurity, the polaron-bipolaron transition and also calculate the specific heat contribution from the impurity electron. We next consider the problem of the magnetic impurity in an impure superconducting host. Finally, we investigate the transport properties of a three-terminal device like single molecular transistor.

# LIST OF PUBLICATIONS BASED ON WHICH THE THESIS IS WRITTEN

[1] **Ch. Narasimha Raju**, **Ashok Chatterjee**,
*Binding energy between the magnetic impurity electron and the conduction electrons in the Anderson-Holstein model.*
Eur. Phys. J. B **86**, 493 (2013).

[2] **Ch. Narasimha Raju**, **Ashok Chatterjee**,
*Effect of external magnetic field on the bound state between the localized and conduction electrons in Anderson-Holstein model.*
Physica B **448**, 207 (2014).

[3] **Ch. Narasimha Raju**, **Ashok Chatterjee**,
*Effect of electron-phonon interaction and external magnetic field on the bound state between in the Anderson-Holstein model: An improved variational calculation.*
Eur. Phys. J. B **88**, 108 (2015).

[4] **Ch. Narasimha Raju**, **Ashok Chatterjee**,
*Ground state energy, binding energy and the impurity specific heat of Anderson-Holstein model.*
Can. J. Phys. **93**, 1024 (2015).

[5] **Ch. Narasimha Raju**, **Ashok Chatterjee**,
*Specific heat of a localized magnetic impurity in a non-magnetic host: A Spectral density method for the Anderson-Holstein model.*
Physica B **474**, 37 (2015).

[6] **Ch. Narasimha Raju**, **Ashok Chatterjee**,
*Properties of a localized magnetic impurity in a superconducting host: The Anderson-Holstein-BCS model.*
J. Magn. Magn. Mater. **396**, 71 (2015).

[7] **Ch. Narasimha Raju**, **Ashok Chatterjee**,
*Quantum dissipative effects on Non-equilibrium transport through a Single-molecular transistor.*
Scientific Reports **6**, 18511 (2016).

# PUBLICATIONS IN CONFERENCE PROCEEDINGS

[1] **Ch. Narasimha Raju**, **Ashok Chatterjee**,
*Spectral density method to Anderson-Holstein model*.
AIP Conference Proceedings **1512**, 1136 (2013).

# CONTENTS

Declaration form I

Certificate II

Acknowledgements III

Preface IV

List of publications V

Contents VII

**1. Introduction**

1.1 Importance of Anderson-Holstein model 1

1.2 Description of Anderson-Holstein Hamiltonian 3

1.3 Different extensions of Anderson-Holstein model 4

1.3.1 Anderson-Holstein-BCS model Hamiltonian 5

1.3.2 Anderson- Holstein-Caldeira Leggett model Hamiltonian 6

1.4 Organization of thesis 9

References 10

**2. Ground state energy of Anderson-Holstein model: The Equation of motion method**

2.1 Introduction 13

2.2 Effective Anderson-Holstein model 14

2.3 Equation of motion method 17

2.4 Specific heat contribution from the impurity 22

2.5 Results and Discussion 23

2.6 Summary 27

References 28

**3. Specific heat due to an impurity in a metal: The Spectral density approximation method**

3.1 Introduction 31
3.2 Spectral density approximation method 31
3.3 Results and Discussion 34
3.4 Summary 37
References 38

**4. Ground state energy of Anderson-Holstein model: The Cluster variation method**

4.1 Introduction 39
4.2 Cluster variation method 39
4.2.1 Ground state energy of Anderson-Holstein model 41
4.2.2 Binding energy 46
4.3 Results and Discussion
4.3.1 In the absence of magnetic field 48
4.3.2 In the presence of magnetic field 59
4.4 Summary 60
References 62

**5. Effect of external magnetic field on the bound state in Anderson-Holstein model: An improved variational treatment**

5.1 Introduction 63
5.2 Generalized Lang-Firsov transformation 64
5.3 Results and Discussion 65
5.4 Summary 75
References 76

**6. Magnetic impurity in a superconducting host: The Anderson-Holstein-BCS model**

6.1 Introduction 77
6.2 Effective Anderson-Holstein-BCS model 78
6.3 Cluster variation method 79
6.4 Results and Discussion 86
6.5 Summary 92
References 93

**7. Quantum dissipative effects on non-equilibrium transport through a single molecular transistor**

7.1 Introduction 95
7.2 Decoupling of oscillator-bath interaction 96
7.3 Effective Anderson-Holstein-Caldeira-Leggett model Hamiltonian 98
7.4 Tunneling current 99
7.5 Results and Discussion 104
7.6 Summary 109
References 109

**8. Conclusions** 111

# Chapter **1**

# Introduction

## 1.1 Importance of Anderson-Holstein model

In 1961, Anderson proposed his celebrated model called the Anderson model [1] to describe the physics of dilute magnetic alloys. Such alloys are produced by adding a few paramagnetic impurities in non-magnetic host metals. Two examples of such alloys are CuFe and LaCe [2-4]. At low temperatures (below a characteristic temperature called Kondo temperature $T_K$) these systems exhibit anomalous properties [5]. Basically the Anderson model describes the interaction between the conduction electrons and the strongly localized impurity level. The impurity is characterized by an onsite repulsive electron-electron (*el-el*) interaction and the interaction between the conduction band and impurity level is represented by a hybridization term. In the absence of hybridization interaction, the impurity will be in the magnetic doublet state. Below $T_k$ the impurity forms a many body-bound state with the continuum electrons due to hybridization interaction leading to the formation of a nonmagnetic singlet state [6-8].

Several researchers have used the Anderson model to study different condensed matter systems like heavy fermion systems [9, 10], mixed valence systems [11, 12], negative tunneling ($-U$) (bipolaron) centers in semiconductor glasses [13], superconductors [14-17] and so on. In many of these systems, the local charge on the impurity also couples with the displacement of the impurity (quanta of these oscillations are called phonons)

leading to the Holstein [18] type electron-phonon (*el-ph*) interaction. Thus the relevant physics for such systems can be unraveled by the well-known single-impurity Anderson-Holstein (AH) model [19-29]. In general, the *el-ph* interaction reduces the effective Coulomb repulsion between electrons at the impurity level and can even produce, under some suitable conditions, a net attractive *el-el* interaction. Since the AH model provides a suitable framework to deal with the interplay between the *el-el* and *el-ph* interactions, it can capture the interesting physics arising out of this interplay. The flexibility of the model also allows one to study transport through electronic devices like a single molecular transistor (SMT) [30-35]. In such devices a quantum dot or a molecule which may be envisaged as the Anderson impurity is placed between two metal leads and is known to play an active role in the electron transport. The AH model has been used by several groups to study the phenomenon of Coulomb blockade in quantum dots [36, 37], the Kondo effect [38-42] and the existence of the vibrational side bands [43, 44] in SMT. Because of general nature of the model and the variety of the phenomena it can describe both in bulk and nano-systems, the AH model has received considerable attention in recent years. Several analytical and numerical techniques like Green's function techniques [45], kinetic equation approach [46], numerical renormalization group (NRG) method [47], dynamical mean field theory DMFT [48] etc. have been employed to solve the AH model.

In the present thesis we study the AH model using various analytical methods like the equation of motion (EOM) method within the framework of Green's function technique, spectral density approximation (SDA) method, cluster variation (CV) approach and Keldysh non-equilibrium Green function technique.

## 1.2 Description of Anderson-Holstein model

The AH model Hamiltonian can be written as,

$$H = H_{band} + H_{imp} + H_{hyb} \tag{1.1}$$

where,

$$H_{band} = \sum\nolimits_{\boldsymbol{k},\sigma} \varepsilon_{\boldsymbol{k}\sigma} n_{\boldsymbol{k}\sigma} \ , \tag{1.2}$$

$$H_{imp} = \sum\nolimits_{\sigma} \varepsilon_d n_{d,\sigma} \ + U \, n_{d,\sigma} n_{d,-\sigma} + \hbar\omega_0 b^{\dagger} b + \lambda\hbar\omega_0 \sum\nolimits_{\sigma} n_{d,\sigma} \left(b^{\dagger} + b\right). \tag{1.3}$$

$$H_{hyb} = \sum\nolimits_{\boldsymbol{k},\sigma} \left(V_{\boldsymbol{k}} c^{\dagger}{}_{d\sigma} c_{\boldsymbol{k}\sigma} + h.c\right), \tag{1.4}$$

Here $H_{band}$ represents the Hamiltonian for the unperturbed conduction band electrons with $n_{\boldsymbol{k}\sigma} (= c^{\dagger}_{\boldsymbol{k}\sigma} c_{\boldsymbol{k}\sigma})$ as the number operator for the electrons with wave vector ***k,*** spin $\sigma$ and the single particle energy $\varepsilon_{\boldsymbol{k}\sigma}$, $c^{\dagger}_{\boldsymbol{k}\sigma}$ $(c_{\boldsymbol{k}\sigma})$ being the electron creation (annihilation) operator. We consider the continuum electrons to be non-interacting. $H_{imp}$ represents the impurity part of the Hamiltonian. The first term in $H_{imp}$ describes the unperturbed localized electron with the number operator $n_{d\sigma} (= c^{\dagger}_{d\sigma} c_{d\sigma})$ for the electron with energy $\varepsilon_d$ in the localized level $d$, $c^{\dagger}_{d\sigma} (c_{d\sigma})$ being the creation (annihilation) operator for the localized electron. The second term in $H_{imp}$ denotes the onsite repulsive Coulomb interaction between two localized electrons of opposite spins in the impurity energy level $\varepsilon_d$, the strength of the interaction being $U$. The third term in $H_{imp}$ refers to the local phonon Hamiltonian, $b^{\dagger}(b)$ being the creation (annihilation) operator for a local phonon of frequency $\omega_0$. The

last term in $H_{imp}$ describes the interaction between a localized electron and a local phonon, $\lambda$ being the *el-ph* coupling constant. The $H_{hyb}$ term represents the coupling between a localized electron and a conduction electron, $V_{\boldsymbol{k}}$ giving the amplitude of the probability of hopping of a conduction band electron from a state $\boldsymbol{k}$ on to the localized level $d$. Without the *el-el* interaction term, the AH Hamiltonian is referred as Fano-Anderson-Holstein model.

We consider, throughout this dissertation, a three-dimensional symmetric AH model i.e., $\varepsilon_d = -U/2$ and make a flat band approximation for the conduction electron density of states $g(0)$. It is a good enough approximation in many cases, as a small variation in the density of states does not significantly alter the physical properties. We choose $\hbar = \omega_0 = 1$ and measure all energies in units of $\hbar\omega_0$ from the chemical potential. We study the AH model in both adiabatic and anti-adiabatic regimes. In the adiabatic regime $(V > \omega_0)$, the time scale for the phonon dynamics is much slower than that of the electron motion so that the electrons can adjust their positions instantaneously to follow the ion dynamics. But in an anti-adiabatic case $(V < \omega_0)$, the impurity atom motion adjusts itself adiabatically to the electron motion.

## 1.3 Different extensions of the AH model

Recently the AH model has been used to understand the vibrational bound states in magnetic molecule with the Morse potential on superconducting surfaces [49]. Motivated by this work, we have considered an extension of the AH model namely the AH-BCS model to study the properties of a magnetic impurity in a BCS superconductor. We study this model in chapter 6. Another extension of the AH model we have studied is the AH-Caldeira-Leggett model [50]. We have considered this model to study the damping

effect in an SMT device in Chapter 7. We present the AH-BCS model and the AH-Caldeira-Leggett model explicitly in the following subsection.

### 1.3.1 AH-BCS model Hamiltonian

A magnetic impurity in a BCS superconducting bath can be described by the AH-BCS Hamiltonian as

$$H = \sum_{\boldsymbol{k},\sigma} \varepsilon_{\boldsymbol{k}\sigma} n_{\boldsymbol{k}\sigma} + \Delta \sum_{\boldsymbol{k},\sigma} \left( c^{\dagger}_{\boldsymbol{k},\sigma} c^{\dagger}_{-\boldsymbol{k},-\sigma} + h.c \right) + \sum_{\sigma} \varepsilon_d n_{d\sigma} + U n_{d\downarrow} n_{d\uparrow}$$

$$+ \sum_{\boldsymbol{k},\sigma} V_{\boldsymbol{k}} \left( c^{\dagger}_{\boldsymbol{k}\sigma} c_{d\sigma} + h.c \right) + \hbar\omega_0 \left( b^{\dagger} b \right) + \lambda \hbar\omega_0 \left( b + b^{\dagger} \right) \sum_{\sigma} n_{d\sigma} \,. \tag{1.5}$$

All the terms in the above equation except the second term have been introduced earlier. The second term is the BCS mean-field Hamiltonian with the superconducting gap parameter $\Delta$ defined as: $\Delta = |g| \sum_{\boldsymbol{k}} \langle c_{\boldsymbol{k}\downarrow} c_{-\boldsymbol{k}\uparrow} \rangle$, where $g$ is the coupling constant of the pairing interaction. Here we have neglected the superconductive contribution from the $d-$electrons. The effect of magnetic impurities on superconductivity is well known [51-53]. In this thesis we are interested to study the effect of superconductivity on the properties of a magnetic impurity embedded in a BCS superconductor. In this system the hybridization interaction between the conduction band and the impurity state tends to form a many-body bound state around the impurity (Kondo screening) at the expense of the breaking of the Cooper pairs. On the other hand, the superconductivity tends to keep the conduction electrons in singlet state (Cooper pair). The local *el-ph* interaction present on the impurity enhances the binding energy between the impurity and the conduction

electrons by reducing the local Coulomb correlation strength. The interplay of all these interactions leads to a quantum phase transition of the impurity system from the doublet to a singlet state.

### 1.3.2 Anderson-Holstein-Caldeira-Leggett model

Here we present another extension of the AH model called the AH-Caldeira-Leggett model which is useful to describe the quantum dissipative effects in an electronic device at the nanoscale called SMT. Fig 1 shows the schematic description of an SMT system. A typical SMT device consists of a single-level molecule or a QD coupled to two metal leads. The QD is assumed to have a single vibrational mode interacting with its charge by *el-ph* interaction. The entire structure is constructed on an insulating substrate (yellow colour part in Fig 1) that can be approximated as a bath of independent harmonic oscillators in the spirit of the Caldeira-Leggett model [54]. The substrate can cause a damping effect that can be described by a linear coupling term between the local phonon field of the QD and a set of independent harmonic oscillators of the substrate bath.

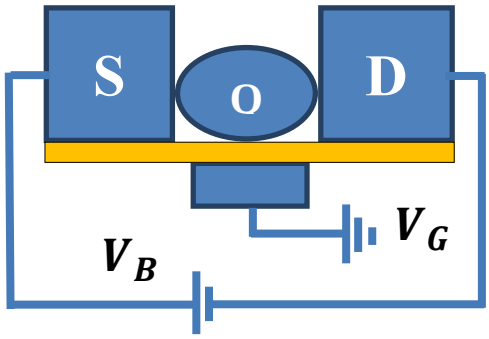


**Fig**.**1** Schematic diagram of the SMT device. In the above diagram **S**, **D** and **QD** refers source, drain and quantum dot respectively.

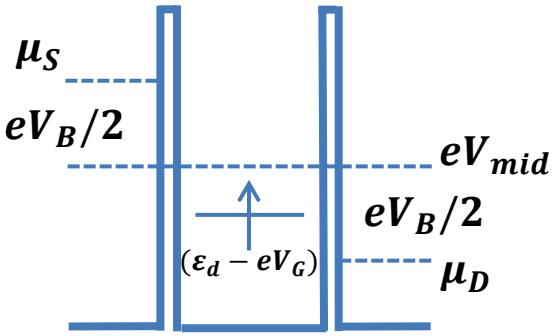


**Fig. 2** Schematic energy level diagram of the SMT device.

The AH-Caldeira-Leggett model Hamiltonian for the system is given by

$$H = H_l + H_m + H_t + H_B. \tag{1.6}$$

The first term $H_l$ in Eq. (1.6) describes the Hamiltonian for the source ($l = S$) and the drain ($l = D$) and is given by

$$H_l = \sum_{\boldsymbol{k},\sigma\in S,D} \varepsilon_{\boldsymbol{k}\sigma} n_{\boldsymbol{k}\sigma}\,, \tag{1.7}$$

where $n_{\boldsymbol{k}\sigma}$ is the number operator for conduction electrons in the continuum states of the source and drain with density of states $g_{S(D)}(\varepsilon)$. The second term $H_m$ describes the Hamiltonian of the molecule and is given by

$$H_m = H_{m0} + H_{vib} + H_{vib-e}, \tag{1.8}$$

where $H_{m0}$ is the Hamiltonian for the electronic part of the QD and reads as

$$H_{m0} = \sum_{\sigma} (\varepsilon_d - eV_G)\, n_{d\sigma} + U\, n_{d\uparrow} n_{d\downarrow}\,, \tag{1.9}$$

where $n_{d\sigma}$ is the number operator for the electrons on the QD with $\varepsilon_d$ as the onsite energy (that can be varied experimentally by tuning the gate voltage ($V_G$) and $U$ is the local Coulomb correlation strength on the QD. $H_{vib}$ describes the vibrational degree of freedom of the QD of mass $m_0$ and frequency $\omega_0$ and can be written as,

$$H_{vib} = \left(\frac{p_0^2}{2m_0} + \frac{1}{2}\, m_0 {\omega_0}^2 {x_0}^2\right), \tag{1.10}$$

and $H_{vib-e}$ represents the *el-ph* interaction on the QD and is given by

$$H_{vib-e} = \lambda x_0 \sum_{\sigma} n_{d\sigma}, \tag{1.11}$$

with $\lambda$ as the *el-ph* coupling constant. The leads-QD hybridization term with hybridization strength $V_{\boldsymbol{k}}$ is given by,

$$H_t = \sum_{\boldsymbol{k},\sigma\in S,D} \left(V_{\boldsymbol{k}} c_{d\sigma}^{\dagger} c_{\boldsymbol{k}\sigma} + h.c\right), \tag{1.12}$$

Finally, the damping effect is incorporated in the model by introducing the terms

$$H_B = H_{B0} + H_{vib-B}\,, \tag{1.13}$$

where $H_{B0}$ is the Hamiltonian of the bath oscillators and is given by

$$H_{B0} = \sum_{j=1}^{N} \left[\frac{p_j^2}{2m_j} + \frac{1}{2}\, m_j {\omega_j}^2 {x_j}^2\right], \tag{1.14}$$

where $\{x_j\}$ are the coordinates and $\{p_j\}$ the canonically conjugate momenta of the bath oscillators and $H_{vib-B}$ describes the interaction between the bath oscillators and the QD oscillator and is given by

$$H_{vib-B} = \sum_{j=1}^{N} \beta_j x_j x_0 \ , \tag{1.15}$$

where $\beta_j$ is the coupling strength between the QD oscillator and the $j^h$ bath oscillator.

## 1.4 Organization of thesis

In the chapter immediately following i. e., in Chapter **2**, we employ Green's function EOM method to AH model and use the mean-field approximation to calculate the ground state (GS) energy and the binding energy between the impurity electron and the conduction electrons. Using the Matsubara Green function technique we have also calculated the impurity specific heat. In Chapter **3**, we calculate the spectral function of the impurity using the SDA method and using the spectral function we again calculate the specific heat contribution from the impurity and analyze our results. In Chapter **4**, we calculate the GS energy and the bound state formation in the AH model by CV method in the strong coupling limit. In Chapter **5**, we employ an improved variational method to study more accurately the role of phonons on the bound state problem in the AH model by CV method in the presence of an external magnetic field over the entire range of *el-ph* interaction. In Chapter **6,** we consider a magnetic impurity in a BCS superconductor and study the effect of the superconducting background on the impurity using the AH model with the mean-field BCS term. Here we employ the CV method to calculate the GS energy and the binding energy and study the effect of *el-ph* interaction and the superconducting order-parameter on the GS energy and

the binding energy in the intermediate and strong coupling limits. In chapter **7,** we consider the AH-Caldeira-Leggett model to investigate the physics of an SMT device. Here we use the Keldysh non-equilibrium Green function technique to study the vibrational and damping effects on the tunneling current and the differential conductance of an SMT device. Finally in Chapter 8, we briefly summarize the findings and make some concluding remarks.

## References


[1] P. W. Anderson, Phys, Rev. **124**, 41 (1961).

[2] M. D. Daybell, in *Magnetism,* edited by H. Suhl (Academic Press, New York, 1973), Vol. **V**.

[3] A. M. Tsvelick & P. B. Wiegman, Adv. Phys. **32**, 453 (1983).

[4] C. Rizzuto, Rep. Prog. Phys. **37**, 147 (1974).

[5] J. Kondo, Prog. Theor. Phys. **32**, 37 (1964);
J. Kondo, *The Physics of Dilute Magnetic Alloys* (Cambridge University Press, 2012).

[6] Y. Nagaoka, Phys. Rev. **138**, A1112 (1965);
K. Yoshida, Phys. Rev. **147**, 223 (1966).

[7] A. J. Heeger & M. A. Jensen, Phys. Rev. Lett. **18**, 488 (1967).

[8] S. M. Bose & T. Tanaka, Phys. Rev. **176**, 600 (1968);
S. M. Bose & T. Tanaka, J. Phys. C: Solid State Phys. **3**, 958 (1970).

[9] P. Coleman, in *Theory of Heavy Fermions and Valence Fluctuations*, edited by T. Kasuya & T. Saso (Springer, New York, 1985).

[10] A. L. Kuzemsky, Phys. Part. Nucl. Lett. **3**, 13 (1993);
A. L. Kuzemsky, Int. J. Mod. Phys. B **10**, 1895 (1996);
A. L. Kuzemsky, arXiv: 150.00983 [cond-mat.str-el].

[11] C. M. Varma, Rev. Mod. Phys. **48**, 219 (1976).

[12] N. Grewe *et al*., Z. Physik. B **30**, 393 (1978).

[13] P. W. Anderson, Phys. Rev. Letters. **34**, 953 (1975).

[14] E. Simanek, Solid State Commun. **32**, 731 (1979).

[15] C. S. Ting *et al*., Phys. Rev. Lett. **45**, 1213 (1980).

[16] L. Zhang, Acta Physica Sinica. **32**, 1435 (1983).

[17] T. Hui & L. Zhang, Solid State Commun. **54**, 1 (1985).

[18] T. Holstein, Ann. Phys. **8**, 325 (1959).

[19] A. C. Hewson *et al*., J. Phys. C: Solid State Phys. **12**, 1665 (1979).

[20] H. Kaga *et al*., Prog. Theor. Phys. **64**, 1918 (1980).

[21] A. C. Hewson & D. M. Newns, J. Phys. C **13**, 4477 (1980).

[22] K. Schönhammer & O. Gunnarsson, Phys. Rev. B **30**, 3141(1984).

[23] H. B. Schüttler *et al*., Phys. Rev. Lett. **58**, 1147 (1987).

[24] H. B. Schüttler *et al*., J. Low Temp. Phys. **69**, 159 (1987).

[25] A. C. Hewson & D. Mayer, J. Phys.: Condens. Matter **14**, 427 (2002).

[26] D. Mayer & A. C. Hewson, Phys. Rev. Lett. **89**, 196401 (2002).

[27] H. C. Lee & H.-Y. Choi, Phys. Rev. B **69**, 075109 (2004).

[28] K. Mitsumoto & Y. Ōno, Physica B **378**, 265 (2006).

[29] M. Cheng & K. Ingersent, Phys. Rev. B **87**, 075145 (2013).

[30] D. M. T. Kuo & Y. C. Chang, Phys. Rev. B **66**, 085311 (2002).

[31] J. X. Zhu & A. V. Balatsky, Phys. Rev. B **67**, 165326 (2003).

[32] A. Mitra, I. Aleiner & A. J. Millis, Phys. Rev. B **69**, 245302 (2004).

[33] Z. Z. Chen *et al*., Phys. Rev. B **71**, 165324 (2005).

[34] M. Galperin *et al*., Phys. Rev. B **73**, 045314 (2006).

[35] P. S. Cornaglia *et al*., Phys. Rev. B **76**, 241403(R) (2007).

[36] H. Park *et al.*, Nature **407**, 57 (2000).

[37] M. Galperin *et al*., Phys. Rev. B **76**, 035301 (2007).

[38] P. S. Cornaglia *et al*., Phys. Rev. Lett. **93**, 147201 (2004).

[39] L. H. Yu *et al.*, Phys. Rev. Lett. **93**, 266802 (2004).

[40] J. Paaske & K. Flensberg, Phys. Rev. Lett. **94**, 176801 (2005).

[41] P. S. Cornaglia *et al*., Phys. Rev. B **71**, 075320 (2005).

[42] Z. Z. Chen *et al*., J. Phys.: Condens. Matter **18**, 5435 (2006).

[43] K. Flensberg, Phys. Rev. B **68**, 205323 (2003).

[44] M. C. Lüffe *et al*., Phys. Rev. B **77**, 125306 (2008).

[45] R. C. Monreal & A. Martin-Rodero, Phys. Rev. B **79**, 115140 (2009);
Z. Z. Chen *et al*., Phys. Rev B **71**, 165324 (2005).

[46] M. Leijnse & M. R. Wegewijs, Phys. Rev. B **78**, 235424 (2008).

[47] A. C. Hewson & D. Meyer, J. Phys.: Condens. Matter **14**, 427 (2002);
G. S. Jeon, T. H. Park & H. Y. Choi, Phys. Rev. B **68**, 045106 (2003);
A. C. Hewson *et al*., J. Phys.: Condens. Matter **22**, 114602 (2010);
H. J. Lee *et al*., Phys. Rev. B **82**, 054516 (2010).

[48] A. C. Hewson *et al*., J. Phys.: Condens. Matter **22**, 115602 (2010);
D. Meyer & A. C. Hewson, Phys. Rev. Lett. **89**, 196401 (2002).

[49] D. Golež *et al*., Phys. Rev. B **86**, 085142 (2012).

[50] S. Braig & K. Flensberg, Phys. Rev. B **68**, 205324 (2003).

[51] A. A. Abrikosov & L.P. Gorkov, Sov. Phys. JETP **12**, 1243 (1961).

[52] A. Sakurai, Prog. Theor. Phys. **44**, 1472 (1970).

[53] A. V. Balatsky *et al*., Rev. Mod. Phys. **78**, 373 (2006).

[54] A. O. Caldiera & A. J. Legget, Phys. Rev. Lett. **46**, 211 (1981);
A. O. Caldeira & A. J. Leggett, Ann. Phys. **149**, 374 (1983).

Chapter **2**

# Ground state energy of the Anderson-Holstein model: The Equation of motion method

## 2.1 Introduction

In this chapter we consider the system of a magnetic impurity atom in a non-magnetic host metal and study the ground state (GS) of this system using the single-level symmetric Anderson-Holstein (AH) model. One of the well-known examples of such a system is a gold sample containing a few atoms of gadolinium. Investigations [1-6] on such systems were inspired to a great extent by the discovery of the Kondo effect. Recently the AH model has also been used to study the electron-phonon (*el-ph*) interaction effects on the transport properties of a quantum dot coupled to two metallic leads and on the enhancement of Kondo temperature in molecular quantum dots [7-12]. A quantum dot (also referred to as an Anderson impurity) coupled to metallic leads resembles the $d$-level of a magnetic impurity in a non-magnetic metal.

In the present chapter, the AH Hamiltonian is solved by using the equation of motion (EOM) method within the framework of the Green function formalism in the strong *el-ph* coupling limit. It is well known that the GS of the single-impurity Anderson (SIAN) model is a many-body

singlet-like bound state formed between the impurity electron and the conduction electrons [13-28]. This happens because of quenching of the magnetic moment due to spin correlations through the s-d interaction. The s-d interaction between the localized and the conduction electrons tends to keep the impurity in singlet state. On the other hand, the onsite electron-electron (*el-el*) interaction tends to keep the impurity in the doublet state. The linear coupling between the impurity charge and the vibration of the impurity creates a local *el-ph* interaction which reduces the local *el-el* interaction and thus favours the formation of a singlet GS. Frankel et al. [29] have experimentally confirmed the singlet nature of the GS and have shown that the magnetic moment quenches because of spin correlations with conduction electrons [30]. In the presence of the local *el-ph* interaction, several aspects of the systems are however expected to change.

## 2.2 Effective Anderson-Holstein Hamiltonian

The AH model Hamiltonian reads as,

$$H = \sum_{k\sigma} \varepsilon_{\boldsymbol{k}} n_{\boldsymbol{k}\sigma} + \sum_{\sigma} \varepsilon_d n_{d,\sigma} + U n_{d,\sigma} n_{d,-\sigma} + \hbar\omega_0 b^{\dagger} b + \sum_{k,\sigma} \left( V_{\boldsymbol{k}} {c^{\dagger}}_{d\sigma} c_{\boldsymbol{k}\sigma} + h.c \right) + \lambda\, \hbar\omega_0 \sum_{\sigma} n_{d,\sigma} \left( b^{\dagger} + b \right), \qquad (2.1)$$

To solve the AH Hamiltonian, we first decouple the linear *el-ph* interaction term in the Hamiltonian. In order to accomplish this we employ the celebrated Lang-Firsov (LF) transformation (polaron transformation) [31-33] on $H$ to obtain the transformed Hamiltonian $\bar{H}$ which is written as

$$\bar{H} = e^{S}\, H\, e^{-S} \qquad (2.2)$$

where $S$ is an anti-Hermitian generator given by

$$S = \lambda\left(b^\dagger - b\right)\sum\nolimits_\sigma n_{d\sigma}. \tag{2.3}$$

To calculate the transformed Hamiltonian we use the Baker-Campbell-Hausdorff formula [34], which reads as

$$e^S a\, e^{-S} = \sum_{m=0}^{\infty} \frac{1}{m!}[S,a]_m = a + [S,a] + \frac{1}{2!}\big[S,[S,a]\big] + \cdots. \tag{2.4}$$

Using the above relation, we obtain the following results.

$$\bar{c}_{d\sigma} = e^S\, c_{d\sigma}\, e^{-S} = \sum_{m=0}^{\infty} \frac{(\lambda)^m\left(b^\dagger - b\right)^m}{m!}[n_{d\sigma}, c_{d\sigma}]_m = c_{d\sigma} e^{-\lambda\left(b^\dagger - b\right)}, \tag{2.5}$$

$$\bar{c}^\dagger_{d\sigma} = c^\dagger_{d\sigma} e^{\lambda\left(b^\dagger - b\right)}, \tag{2.6}$$

$$\bar{b}\ = e^S\, b\, e^{-S} = \sum_{m=0}^{\infty} \frac{(\lambda)^m {n_{d\sigma}}^m}{m!}\left[\left(b^\dagger - b\right), b\right]_m = (b - \lambda n_{d\sigma}), \tag{2.7}$$

$$\bar{b}^\dagger = \left(b^\dagger - \lambda n_{d\sigma}\right). \tag{2.8}$$

The transformed Hamiltonian thus reads as

$$\bar{H} = \sum\nolimits_{k,\sigma} \varepsilon_k n_{k\sigma} + \sum\nolimits_\sigma \tilde{\varepsilon}_d n_{d\sigma} + \tilde{U} n_{d,\sigma} n_{d,-\sigma} + \hbar\omega_0 b^\dagger b + \sum\nolimits_{k,\sigma} \left(\bar{V}_k c^\dagger_{k\sigma} c_{d\sigma} + \bar{V}^*_k c^\dagger_{d\sigma} c_{k\sigma}\right), \tag{2.9}$$

where,

$$\tilde{\varepsilon}_d = \varepsilon_d - \lambda^2 \hbar\omega_0, \tag{2.10}$$

$$\widetilde{U} = U - 2\lambda^2 \hbar\omega_0, \tag{2.11}$$

$$\bar{V}_k = V_k \, e^{\lambda(b-b^\dagger)}. \tag{2.12}$$

Thus we see that due to the *el-ph* interaction, the energy of the localized level $\varepsilon_d$ is renormalized to $\tilde{\varepsilon}_d$. The negative shift in the impurity energy level, $\varepsilon_p = -\lambda^2 \hbar\omega_0$ is the polaron self-energy or the polaron binding energy (BE). The *el-ph* interaction also reduces the *el-el* repulsive interaction at the localized level. This is also due to the polaronic effect. One can immediately see that the polaronic reductions in the localized electron energy and the onsite *el-el* correlation energy are of second order in the *el-ph* coupling. Since we are interested in the electron properties, we perform a zero-phonon averaging of Eq. (2.9) to obtain an effective AH Hamiltonian given by

$$H_{eff} = \sum\nolimits_{\boldsymbol{k},\sigma} \varepsilon_k n_{k\sigma} + \sum\nolimits_{\sigma} \tilde{\varepsilon}_d n_{d\sigma} + \widetilde{U}\, n_{d\sigma} n_{d,-\sigma} + \sum\nolimits_{\boldsymbol{k},\sigma} \tilde{V}_k \left( c_{k\sigma}^\dagger c_{d\sigma} + c_{d\sigma}^\dagger c_{k\sigma} \right), \tag{2.13}$$

where, $\tilde{V}_k = V_{\boldsymbol{k}} \, e^{-(\lambda^2/2)}$. Thus the hopping integrals $V_k$ and $V_k^*$ also get renormalized because of the *el-ph* interaction. The exponential reduction in the hopping integral is reminiscent of the Holstein reduction factor that occurs in the Holstein-Hubbard model. This suggests a mass renormalization leading to band narrowing for the continuous electron band. This also implies that the electron hopping is accompanied by a phonon cloud. Here we assume $V_{\boldsymbol{k}}$ to be independent of $\boldsymbol{k}$ for the sake of

mathematical simplicity and choose to write $V_{\boldsymbol{k}} = V$. This is a good enough approximation in the long-wavelength limit. In the following section we solve the effective Hamiltonian Eq. (2.13) using EOM method.

## 2.3 Equation of motion method

The EOM method is one of the simplest methods to calculate the Green function of strongly correlated systems. The basic idea of the EOM method is to generate a set of coupled differential equations of the Green functions (equations of motion of the Green functions) by differentiating the Green functions a number of times with respect to time. In this approach, the time derivative of a lower-order Green's function gets equated to a higher-order Green function. To proceed further one has to truncate the series of differential equations by decoupling some higher-order Green's function. This decoupling scheme can be implemented at different hierarchical levels. The higher the level at which the decoupling is done, the better is the approximation. Basically these decoupling schemes are nothing but neglecting higher-order correlations. To avoid these ambiguities one can choose the irreducible Green's function (IGF) method developed by Kuzemsky [35]. Now we define the single particle Green's functions as

$$G_{ij}^{>} = -i \langle 0 \left| c_{i\sigma}(t) c_{j\sigma}^{\dagger}(0) \right| 0 \rangle, \tag{2.14a}$$

$$G_{ij}^{<} = i \langle 0 \left| c_{i\sigma}^{\dagger}(0) c_{j\sigma}(t) \right| 0 \rangle, \tag{2.14b}$$

$$G_{ij}^{R} = -i\, \theta(t) \langle 0 \left| \{ c_{j\sigma}(t) c_{i\sigma}^{\dagger}(0) \} \right| 0 \rangle, \tag{2.14c}$$

where $i, j = k$ or $d$ and $|0\rangle$ represents the GS of the system. Where $G_{ij}^{>}(t)$, $G_{ij}^{<}(t)$ and $G_{ij}^{R}(t)$ are called the lesser, greater and the retarded Green's

functions respectively. In order to obtain the relationship between the GS energy and Green's functions, we consider the following commutation relations,

$$\left[c_{k\sigma}, H_{eff}\right] = \varepsilon_k c_{k\sigma} + \tilde{V}_k c_{d\sigma}, \tag{2.15}$$

$$\left[c_{d\sigma}, H_{eff}\right] = \tilde{\varepsilon}_d c_{d\sigma} + \tilde{U} c_{d\sigma} n_{d,-\sigma} + \sum\nolimits_k \tilde{V}_k c_{k\sigma}. \tag{2.16}$$

In terms of these commutators, $H_{eff}$ can be written as

$$H_{eff} = \sum\nolimits_{k\sigma} c_{k\sigma}^{\dagger}\left[c_{k\sigma}, H_{eff}\right] + \frac{1}{2}\sum\nolimits_{\sigma} c_{d\sigma}^{\dagger}\left[c_{d\sigma}, H_{eff}\right] + \frac{1}{2}\sum\nolimits_{\sigma} \tilde{\varepsilon}_d n_{d\sigma} + \frac{1}{2}\sum\nolimits_{k\sigma} \tilde{V}_k c_{d\sigma}^{\dagger} c_{k\sigma}. \tag{2.17}$$

Using the Heisenberg equation for $G_{kk}^{>}(t)_{t=0}$ and taking its Fourier transform over a contour $c$ consisting of the real axis and a semicircle at infinity in the upper half plane, we obtain

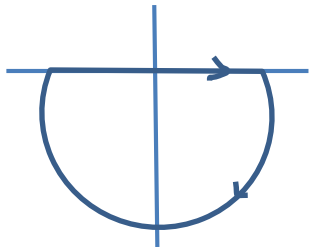

***Fig.1*** *The contour $C$ in Eqs. (2.18) to (2.20) consists of a real axis, and a semicircle at $\infty$ in the lower half plane.*

$$\left.\frac{dG_{kk}^{>}(t)}{dt}\right|_{t=0} = \frac{1}{2\pi i}\oint \varepsilon G_{kk}(\varepsilon) d\varepsilon = \left\langle 0\middle| c_{k\sigma}^{\dagger}\left[c_{k\sigma}, H_{eff}\right]\middle| 0\right\rangle. \tag{2.18}$$

In the same way we can obtain

$$\frac{1}{2\pi i}\oint \varepsilon G_{dd}(\varepsilon)d\varepsilon \;=\; \langle 0|c_{d\sigma}^{\dagger}[c_{d\sigma}\,,H_{eff}]|0\rangle\,, \tag{2.19}$$

$$\frac{1}{2\pi i}\oint G_{kd}^{<}(\varepsilon)d\varepsilon \;=\; \langle 0|c_{d\sigma}^{\dagger}c_{k\sigma}\,|0\rangle\,, \tag{2.20}$$

where Green's functions $G_{dd}$ and $G_{kd}$ are however coupled to each other. The equations of motion for the electron operators have the form

$$i\frac{dc_{k\sigma}}{dt} = \varepsilon_k c_{k\sigma} + \tilde{V}_k c_{d\sigma}, \tag{2.21}$$

and consequently the Green functions obey the following equations in the $\varepsilon$ - space:

$$\varepsilon\, G_{kd}(\varepsilon) = \varepsilon_k G_{kd}(\varepsilon) + \tilde{V}_k G_{dd}(\varepsilon)\,, \tag{2.22}$$

$$\varepsilon\, G_{kk'}(\varepsilon) = \delta_{kk'} + \varepsilon_k G_{kk'}(\varepsilon) + \tilde{V}_k G_{dk'}(\varepsilon), \tag{2.23}$$

which immediately yield

$$G_{kd}(\varepsilon) = \frac{\tilde{V}_k}{(\varepsilon-\varepsilon_k)}\, G_{dd}(\varepsilon)\,, \tag{2.24}$$

$$G_{kk}(\varepsilon) \;= \frac{\left[(\varepsilon-\varepsilon_k) + \left|\tilde{V}_k\right|^2 G_{dd}(\varepsilon)\right]}{(\varepsilon-\varepsilon_k)^2}. \tag{2.25}$$

It is useful to define the one-body self-energy $S(\varepsilon)$ as

$$S(\varepsilon) = \sum\nolimits_k \frac{\left|\tilde{V}_k\right|^2}{(\varepsilon-\varepsilon_k)}. \tag{2.26}$$

Following Anderson we ignore the real part of $S$, since it only shifts the impurity electron energy by a constant which can be incorporated by defining a renormalized energy $\tilde{\varepsilon}_d$. We also neglect the effect of spin in the self-energy. With the flat band approximation, Eq. (2.26) takes the form:

$$S(\varepsilon) = -\,i\,\tilde{\Gamma}\,sgn(\varepsilon), \tag{2.27}$$

where

$$\tilde{\Gamma} = \pi g(0)\left|\tilde{V}_k\right|^2 = \Gamma\, e^{-\lambda^2}, \tag{2.28}$$

Γ being the hybridization parameter. The Dyson equation for $G_{dd}(\varepsilon)$ can be written as

$$G_{dd}(\varepsilon) = G^0_{dd}(\varepsilon) \; + G^0_{dd}(\varepsilon)\,\Sigma^\sigma(\varepsilon)\,G_{dd}(\varepsilon), \tag{2.29}$$

where $G^0_{dd}(\varepsilon)$ is the Green function of the phonon-dressed localized electron without the *el-el* interaction and is given by

$$G^0{}_{dd}(\varepsilon) = \frac{1}{[\varepsilon - \tilde{\varepsilon}_d - S(\varepsilon)]}\,, \tag{2.30}$$

and $\Sigma^\sigma(\varepsilon)$ is the self-energy operator. Thus the GS energy can be written as

$$\begin{aligned} E_0 &= \langle 0|H_{eff}|0\rangle \\ &= \frac{1}{2\pi i}\sum\nolimits_\sigma \oint \left[\varepsilon - \tfrac{\Sigma^\sigma(\varepsilon)}{2}\right] G_{dd}(\varepsilon)\,d\varepsilon + \sum\nolimits_{k\le k_F} \varepsilon_k. \end{aligned} \tag{2.31}$$

Using the Hartree-Fock approximation we get

$$G_{dd}(\varepsilon) = \frac{1}{\left[\varepsilon - \tilde{\varepsilon}_d - \widetilde{U}\langle n_{d,-\sigma}\rangle + i\,\tilde{\Gamma}\,sgn(\varepsilon)\right]}, \tag{2.32}$$

$$\Sigma^{\sigma} = \widetilde{U}\,\langle n_{d,-\sigma}\rangle, \tag{2.33}$$

and the average occupation probability is given by

$$\langle n_{d,\sigma}\rangle = \frac{1}{2\pi i}\oint G_{dd}(\varepsilon)\,d\varepsilon = \frac{1}{\pi}cot^{-1}\left[\left(x + \langle n_{d,-\sigma}\rangle\right)y\right], \tag{2.34}$$

where $x = \tilde{\varepsilon}_d/\widetilde{U}$ and $y = \widetilde{U}/\tilde{\Gamma}$. The GS energy is now given by the expression

$$E_0 = \frac{1}{\pi}\sum_{\sigma}\int_{-\infty}^{0} d\varepsilon\;\varepsilon\;Im\;G_{dd}(\varepsilon) - \widetilde{U}\,\langle n_{d,+}\rangle\langle n_{d,-}\rangle + \sum_{k\le k_F}\varepsilon_k, \tag{2.35}$$

where $Im[G_{dd}(\varepsilon)] = -\pi A(\varepsilon)$, $A(\varepsilon)$ being the spectral function given by

$$A(\varepsilon) = 2\tilde{\Gamma}\left[\left(\varepsilon - \tilde{\varepsilon}_d - \widetilde{U}\langle n_{d,-\sigma}\rangle\right)^2 + \tilde{\Gamma}^2\right]^{-1}. \tag{2.36}$$

Using a suitable cut-off energy to make the integral in Eq. (2.35) convergent and neglecting the constant contribution, we obtain, for the GS energy [36], after simplifications

$$E_0 = xN\widetilde{U} - \frac{\widetilde{U}}{\pi y}\ln\left(\frac{cos(\pi m) - cos(\pi N)}{2}\right) + \frac{1}{4}(N^2 - m^2)\widetilde{U} + \sum_{k\le k_F}\varepsilon_k. \tag{2.37}$$

Here $m\ \left(=\langle n_{d,+}\rangle - \langle n_{d,-}\rangle\right)$ is the magnetic moment (in units of Bohr magneton) carried by the impurity electrons and $N\left(=\langle n_{d,+}\rangle + \langle n_{d,-}\rangle\right)$ is the total number of such electrons. The energy required to break the bound state on the impurity atom (the binding energy $W$) is given by

$$W = (1-N)\tilde{\varepsilon}_d + \left|\tilde{V}_k\right|^2 \ln\left[\cos\left(\frac{nm}{2}\right)\right] + \lambda^2\hbar\omega_0 - \frac{1}{4}(1-m^2)\tilde{U}\,. \qquad (2.38)$$

## 2.4 Specific heat contribution from the impurity

In this section we calculate the energy of the impurity electron at finite temperature. Using the Matsubara Green function technique, Eq. (2.31) can be written as

$$E(T) = K_B\,T\sum_{\sigma n}\left[i\varepsilon_n - \frac{\Sigma^\sigma(i\varepsilon_n)}{2}\right]G_{dd}(i\varepsilon_n)$$

$$= -\frac{1}{\pi}\sum_\sigma\int_{-\infty+i\delta}^{\infty+i\delta} f(\varepsilon)Im\left\{\left[\varepsilon - \frac{\Sigma^\sigma(\varepsilon)}{2}\right]G_{dd}(\varepsilon)\right\}d\varepsilon, \qquad (2.39)$$

where $f(\varepsilon) = 1/(e^{\beta\varepsilon}+1)$. Using the Hartree-Fock approximation and the Sommerfeld expansion we obtain

$$E(T) = \sum_\sigma\int_{-\infty}^{\mu(T)} A(\varepsilon)\left(\varepsilon - \frac{\tilde{U}}{2}\langle n_{d,-\sigma}\rangle\right)d\varepsilon$$

$$+\frac{1}{6}(\pi K_B T)^2\sum_\sigma\left[A(0) - \frac{\tilde{U}\langle n_{d,-\sigma}\rangle}{2}\left(\frac{\partial A}{\partial\varepsilon}\right)_{\varepsilon=0}\right], \qquad (2.40)$$

where $\mu(T)$ is the temperature dependent part of the chemical potential and terms up to quadratic in $K_B T$ have been retained. The contribution to the specific heat $C$ from the impurity electron is obtained after some manipulations as

$$C = \frac{1}{3}(\pi K_B)^2 T \sum_\sigma A(0)$$

$$= \frac{2}{3}(\pi K_B)^2 T \sum_\sigma \frac{\tilde{\Gamma}}{\left[\left(\tilde{\varepsilon}_d + \tilde{U}\langle n_{d,-\sigma}\rangle\right)^2 + \tilde{\Gamma}^2\right]} \tag{2.41}$$

## 2.5 Results and discussion

It may be noted that Eq. (2.34) is symmetric under $\sigma \longrightarrow -\sigma$. Therefore, a nonmagnetic solution always exists. However for definite values of $x$ and $y$, there also exists a magnetic solution i.e., a solution corresponding to: $\langle n_{d,\sigma}\rangle \neq \langle n_{d,-\sigma}\rangle$. The expression for the impurity magnetic moment [37] is given by

$$m \cong \langle n_{d\sigma}\rangle - \langle n_{d,-\sigma}\rangle = 1 - [\pi x y(1-x) - 1]^{-1}, \tag{2.42}$$

which shows the possibility of existence of a magnetic moment in the GS. It is however well known that the GS of the single impurity Anderson model is a Kondo singlet with $m = 0$. The existence of a finite magnetic moment in the present work is thus an artifact of the approximation used in the calculation. However, we find that even if our approximation gives rise to a magnetic moment, it would be killed if the *el-ph* interaction is strong enough. Therefore, in what follows, we shall assume $m = 0$. In Fig. 1, we plot the GS energy $E_0$ as a function of the onsite Coulomb correlation

strength $U$ for two values of the *el-ph* coupling constant in an anti-adiabatic regime. $E_0$ increases almost in a linear way with $U$.

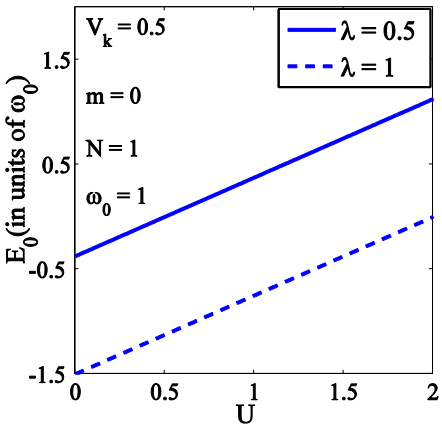


***Fig. 1*** *GS energy as a function of* $U$.

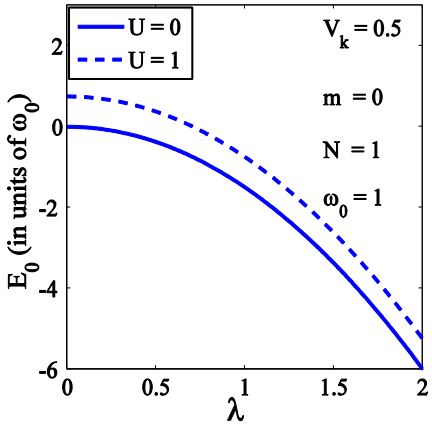


***Fig.2*** *GS energy as a function of* $\lambda$.

This is of course an expected behavior. The figure also shows that $\lambda = 1$ corresponds to a lower GS than $\lambda = 0.5$. In Fig. 2, we show the explicit behavior of $E_0$ as a function of $\lambda$ for $U = 0$ and $U = 1$ for an anti-adiabatic case. It is evident that $E_0$ decreases with increasing $\lambda$ in a nonlinear way. This is the polaronic effect which reduces the electron's energy by a term that is quadratic in $\lambda$ for small $\lambda$. In Fig. 3, we have plotted the BE ($W$) as a function of $U$ for a couple of $\lambda$ values, in the anti-adiabatic regime. It is clearly evident that as $U$ increases, binding decreases. This behaviour can be understood in the following way. Since there is only one electron on the impurity site, one may not expect the $U$-term to play an important role. But the s-d interaction causes hybridization between the wave functions of the localized and the conduction electrons and because of this there exists a possibility of double occupancy on the impurity site which will of course be inhibited by the onsite correlation term leading to a decrease in $W$. It is also clear that $W$ increases with $\lambda$. This can be explained as follows. The *el-ph*

interaction provides a phonon-mediated attractive *el-el* interaction in the second order which reduces the effect of the usual Coulomb repulsion and therefore has an opposite effect on $W$ i.e., it increases the binding. This is explicitly shown in Fig. 4 where we have plotted $W$ as a function of $\lambda$ for a couple of $U$ values for an anti-adiabatic case.

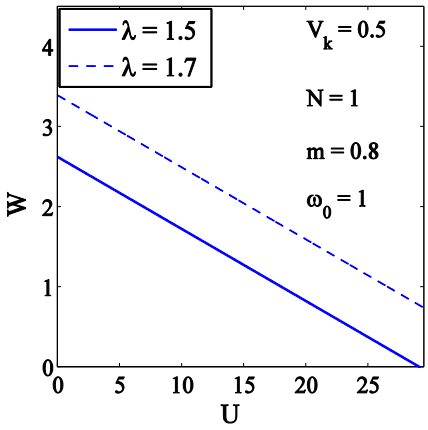


***Fig. 3*** *$W$ as a function of $U$.*

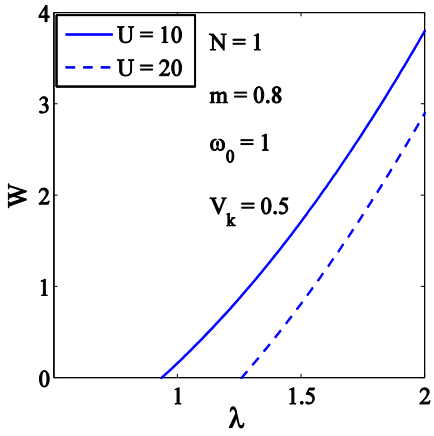


***Fig. 4*** *$W$ as a function of $\lambda$.*

$W$ is shown to increase with $\lambda$. The behavior is a little convex from below. Next we plot the spectral density $A(\varepsilon)$ as a function of the energy $\varepsilon$ for $\lambda = 0.5$ in Fig. 5. To assess the effect of the *el-ph* interaction, we plot in Fig. 6 $A(\varepsilon)$ for $\lambda = 0$. Several observarions are in order. First of all, we find that the peak in $A(\varepsilon)$ shifts towards the left when the *el-ph* interaction is switched on. This is the polaronic effect which reduces the electron energy by an amount that is quadratic in $\lambda$. This also leads to an asymmetry in the spectral density. Another notable observation is that the height and width of the peak also become greater due to the *el-ph* interaction. However, one shortcoming of this investigation is the absence of the side-peaks in the spectral densiy. This could be because of the use of the mean-field approximation or the zero-phonon averaging.

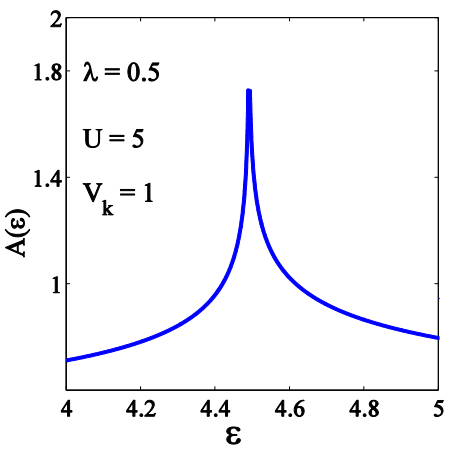


***Fig. 5*** *$A(\varepsilon)$ as a function of $\varepsilon$ for $\lambda = 0.5$.*

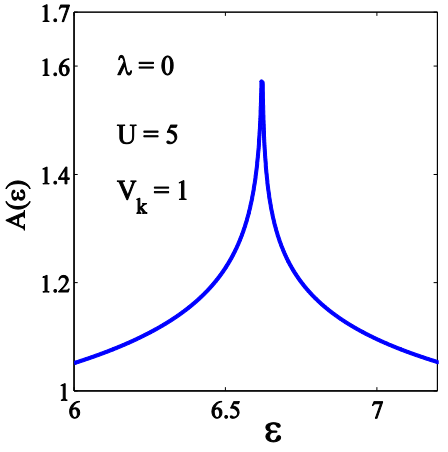


***Fig. 6*** *$A(\varepsilon)$ as a function of $\varepsilon$ for $\lambda = 0$.*

In Fig. 7 we plot $C$ as a function of temperature for three values of $\lambda$. As predicted by Eq. (2.41), the specific heat of the impurity electron is linear in $T$. Of course this is valid only at low temperature where the Sommerfeld expansion would be acceptable.

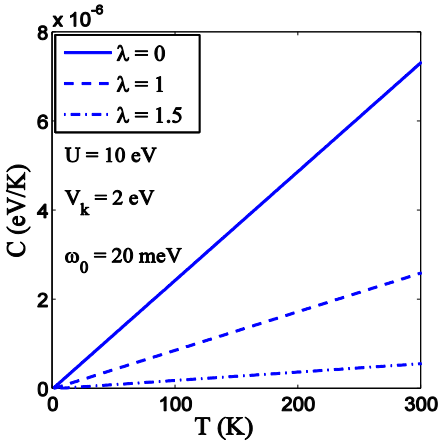


***Fig. 7*** *$C$ vs $T$ for different values of $\lambda$.*

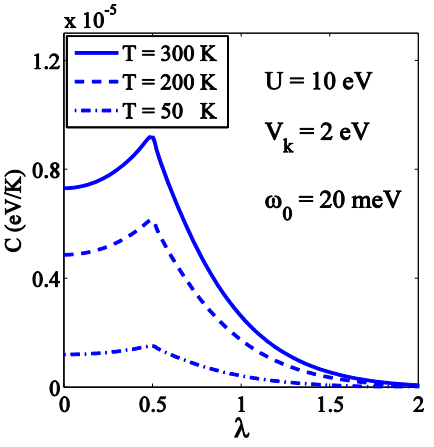


***Fig. 8*** *$C$ vs $\lambda$ for different values of $T$.*

The Fig. 7 shows that the behaviour of the specific heat with respect to $\lambda$ would be interesting. Therefore, in Fig. 8 we plot $C$ as a function of $\lambda$. Initially $C$ increases with $\lambda$, attains a peak value and then decreases with further increase in $\lambda$. Finally at some critical value of $\lambda$, $C$ becomes zero. It is indeed a rather curious behaviour and eludes an explanation at the moment.

## 2.6 Summary

In this chapter, we have studied the three dimensional AH model using the LF transformation followed by a zero-phonon averaging. The resulting effective AH Hamiltonian has been solved by using the EOM Green function technique within the framework of a mean-filed approximation to obtain the GS energy of the system. Our method does yield a magnetic solution which, we believe, is an artifact of the mean-field approximation. However we find that the magnetic moment, even if present, is reduced by the *el-ph* interaction. We have shown that there exists a bound state between the impurity electron and the conduction electrons. It is a many-body bound state and is of singlet type. The corresponding BE decreases with increasing $U$ and increases with increasing $\lambda$. We have also obtained the spectral function for the impurity electron. The asymmetry in the spectral function in the presence of *el-ph* interaction is pretty clear and is consistent with the more sophisticated calculations.

## References

[1] G. Gruner & A. Zawadowski, Rep. Prog. Phys. **37**, 1497 (1974).

[2] Y. Nagaoka, Phys. Rev. **138**, A1112 (1967).

[3] K. Yosida, Phys. Rev. **147**, 223 (1966);
K. Yosida, Progr. Theoret. Phys. (Kyoto) **36**, 875 (1966).
[4] A. Okiji, Progr. Theoret. Phys. (Kyoto) **36**, 875 (1966).
[5] A. J. Heeger & M. A. Jensen, Phys. Rev. Lett. **18**, 485 (1967).
[6] J. Kondo, Progr. Theoret. Phys. (Kyoto) **36**, 429 (1966)**.**
[7] Z. Z. Chen *et al*., Phys. Rev. B **71**, 165324 (2005).
[8] T. Koch *et al*., J. Phys.: Conf. Ser. **220**, 012014 (2010).
[9] J. Loos *et al*., J. Phys.: Condens. Matter **21**, 395601 (2009).
[10] J. X. Zhu & A. V. Balatsky, Phys. Rev. B **67**, 165326 (2003).
[11] R. Świrkowicz *et al*., Phys. Rev. B **68**, 195318 (2003).
[12] D. M. T. Kuo & Y. C. Chang, Phys. Rev. B **66**, 085311 (2002).
[13] S. Nakajima, Prog. Theor. Phys. **39**, 1402 (1968).
[14] J. Solyom, Phys. Lett. **23**, 305 (1966).
[15] M. D. Daybell & W. A. Steyert, Phys. Rev. Lett. **18**, 574 (1967).
[16] J. S. Lim & M. S. Choi, J. Phys.: Condens. Matter **20**, 415225 (2008).
[17] M. D. Daybell & W. A. Steyert, Rev. Mod. Phys. **40**, 354 (1968).
[18] K. Yosida, Phys. Rev. **147**, 223 (1966).
[19] J. R. Schrieffer, J. Appl. Phys. **38**, 1143 (1967).
[20] G. Kemeny, Phys. Rev. **156**, 740 (1967).
[21] H. Suhl & D. Wong, Physics **3**, 17 (1967).
[22] H. Suhl, Phys. Rev. Lett. **17**, 1140 (1966).
[23] A. A. Abrikosov, Physics **2**, 5 (1965).
[24] D. R. Hamann, Phys. Rev. **158**, 570 (1967).
[25] P. E. Bloomfield & D. R. Hamann, Phys. Rev. **164**, 856 (1967).
[26] R. B. Frankel *et al*., Phys. Rev. Lett. **18**, 1051 (1967).
[27] M. A. Jenseen *et al*., Phys. Rev. Lett. **18**, 997 (1967).
[28] K. Kume, J. Phys. Soc. Japan **22**, 1116 (1967).
[29] R. B. Frankel *et al*., Phys. Rev. Lett., **18**, 1051(1967).
[30] M. D. Daybell & W. A. Steyert, Phys. Rev. Lett., **18**, 398 (1967).
[31] I. G. Lang & Y. A. Firsov, Zh. Eksp. Teor. Fiz.**43**, 1843 (1962);

[Sov. Phys. JETP.**16**, 1301 (1963)].

[32] A. N. Das & S. Sil, J. Phys.: Condens. Matter **5**, 8265 (1993).

[33] Y. Takada & A. Chatterjee, Phys. Rev. B **67**, 081102 (R) (2003).

[34] J. Campbell, Proc. London Math. Soc. **28**, 381 (1897).

[35] A.L. Kuzemsky, Rivista Nuovo Cimento **25**, 1 (2002).

[36] B. KjÖllerstrÖm *et al*., Phys. Rev. **148**, 665 (1966).

[37] P.W. Anderson. Phys. Rev. **124**, 41 (1961).

Chapter **3**

# Specific heat due to an impurity in a metal: Spectral density approximation method

## 3.1 Introduction

In the previous chapter, we have calculated the impurity-level occupation and the specific heat of a magnetic impurity in a non-magnetic metal using the Matsubara Green function technique within the framework of the Hartree-Fock (HF) approximation, which however overestimates the effects of electron-electron (*el-el*) interaction. In the present chapter we make an attempt to improve those results by employing the spectral density approximation (SDA) method, which treats the *el-el* interaction beyond the HF approximation.

## 3.2 Spectral density approximation method

The spectral density (SD) function gives the same information of the system as does the Green function. The SD function can be obtained from the double-time-temperature Green functions using the equation of motion method. However, in this method, one has to use some decoupling approximation for the higher-order Green functions, which restricts the

validity of the method. The SDA method, proposed by Kalashnikov and Fradkin [1] and later used by others [2-8] avoids this problem. In this method, instead of the Green functions one considers the corresponding spectral densities and writes closed equations between them to calculate the SD function. Once the SD function is calculated, it becomes straight-forward to calculate the Green function and dynamical correlation functions of the impurity electrons. This method is based on the choice of a physically motivated single-particle SD function with some free parameters. In this work we use a modified Gaussian ansatz for SD function to consider the damping effect of quasi-particles on the impurity.

$$\Lambda_{d\sigma}(\omega) = \frac{f(\omega)}{M_{d\sigma}^{(0)}(\omega)}\, e^{-\left[\frac{(\omega-\alpha)}{\Gamma}\right]^2} \tag{3.1}$$

where $M_{d\sigma}^{(0)}(\omega)$ is the normalization constant, $f(\omega)$ is the Fermi distribution function and $\alpha$ and $\Gamma$ are the free parameters which denote the position and width of the peak of SD function respectively and are calculated self-consistently by using the spectral moment relation given by

$$M_{d\sigma}^{(m)}(\omega) = \frac{1}{\hbar}\int \omega^m \Lambda_{d\sigma}(\omega)\, d\omega = \langle\left\{\left[c_{d\sigma}, H_{eff}\right]_m, c_{d\sigma}^{\dagger}\right\}\rangle\,, \tag{3.2}$$

where $M_{d\sigma}^{(m)}(\omega)$ is the $m$-th moment of the SD function $\Lambda_{d\sigma}(\omega)$. Let us calculate the first three moments of the SD function using the above relation with the effective AH Hamiltonian given in the previous chapter [Eq. 2.6].

$$M_{d\sigma}^{(0)}(\omega) = \left[c_{d\sigma}, H_{eff}\right]_0 = c_{d\sigma},$$

$$M_{d\sigma}^{(1)}(\omega) = \left[c_{d\sigma}, H_{eff}\right]_1 = \left[c_{d\sigma}, H_{eff}\right],$$

$$M_{d\sigma}^{(2)}(\omega) = \left[c_{d\sigma}, H_{eff}\right]_2 = \left[\left[c_{d\sigma}, H_{eff}\right], H_{eff}\right], \tag{3.3}$$

and so on. After solving the spectral moment relation in Eq. (3.2) for $m = 0, 1, 2$, we obtain

$$M_{d\sigma}^{(0)}(\omega) = \Gamma\sqrt{\pi}, \tag{3.4}$$

$$M_{d\sigma}^{(1)}(\omega) = \alpha = \tilde{\varepsilon}_d + \tilde{U}\langle n_{d,-\sigma}\rangle, \tag{3.5}$$

$$M_{d\sigma}^{(2)}(\omega) = \alpha^2 + \frac{\Gamma^2}{2} = 2\tilde{\varepsilon}_d\tilde{U}\langle n_{d,-\sigma}\rangle + \tilde{\varepsilon}_d^2 + \tilde{U}^2\langle n_{d,-\sigma}\rangle + \sum\nolimits_k \tilde{V}^2. \tag{3.6}$$

Eqs. (3.5) and (3.6) yield

$$\Gamma = \sqrt{2}\left[\tilde{U}^2\left(\langle n_{d,-\sigma}\rangle - \langle n_{d,-\sigma}\rangle^2\right) + \sum\nolimits_k \tilde{V}^2\right]^{1/2}. \tag{3.7}$$

Once the SD function is obtained, the average occupancy of the impurity electron can be determined in a self-consistent way at finite temperature.

$$n_{d\sigma} = \int_{-\infty}^{\infty} \Lambda_{d\sigma}(\omega)\, d\omega = \frac{1}{2} erfc\left(\frac{\alpha - \mu}{\Gamma}\right) + \frac{(\pi K_B T)^2 \alpha}{3\sqrt{\pi}\Gamma^3} e^{-(\alpha/\Gamma)^2}. \tag{3.8}$$

To solve the above integral we use the Sommerfeld expansion and retain terms up to quadratic in $K_B T$. The contribution to the specific heat $C$ from the impurity electron [9] can be obtained using the expression as

$$C = \tfrac{1}{3}(\pi K_B)^2\, T \sum\nolimits_\sigma \Lambda_{d\sigma}(0)\ . \tag{3.9}$$

## 3.3 Results and Discussion

In Figs. 1(a) and 1(b), we study the SD function as a function of $\omega$ for different values of the *el-ph* interaction strength $\lambda$ for $U = 2$ and $U = 5$ respectively. Comparison of Figs. 1(a) and 1(b) shows that as the *el-el* interaction strength increases, the height of the peak of the SD function also increases. The effect of the *el-ph* interaction on the SD function is also clearly visible from both the figures. In the absence of the *el-ph* interaction i.e., for $\lambda = 0$, the SD function has a peak at $\omega = 0$. As the *el-ph* interaction increases, the peak position of the SD function shifts towards the left. It indicates the formation of polaron at the impurity. The amount of shift in the peak gives the polaron binding energy (BE). Interestingly, with increasing *el-ph* interaction, the width of the SD function decreases, while with increasing *el-el* interaction, the width of the SD function increases. From the Heisenberg uncertainty principal, the width of the SD function is inversely proportional to the life time of an excitation on the impurity. So the figures tell us that with increasing $\lambda$,

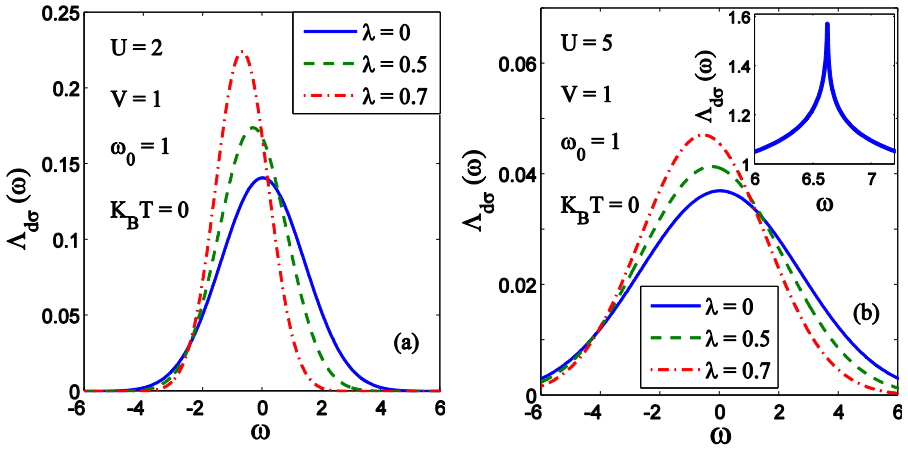


***Fig.1*** *SP function $\Lambda_{d\sigma}(\omega)$ as a function of energy for three values of $\lambda$. (a) $\Lambda_{d\sigma}(\omega)$ vs $\omega$ for $U = 2$. (b) $\Lambda_{d\sigma}(\omega)$ vs $\omega$ for $U = 5$. (**Inset:** Our previous chapter result using EOM method.*

the impurity electron becomes more localized and as a result the conductivity contribution from impurity should decrease. On the other hand, the effect of $U$ should be just opposite. The inset in Fig. 1(b) shows the behavior of the spectral function obtained using the Green function method with the mean-field approximation. In view of the accuracy of the present method, we believe that the results of the present method are more trustworthy. To further confirm the phenomenon of electron localization at the impurity, we plot in Figs. 2(a) and 2(b) the impurity specific heat $C$ as a function of $\lambda$ at different temperature $(T)$ for $U = 2$ and $U = 4$ respectively.

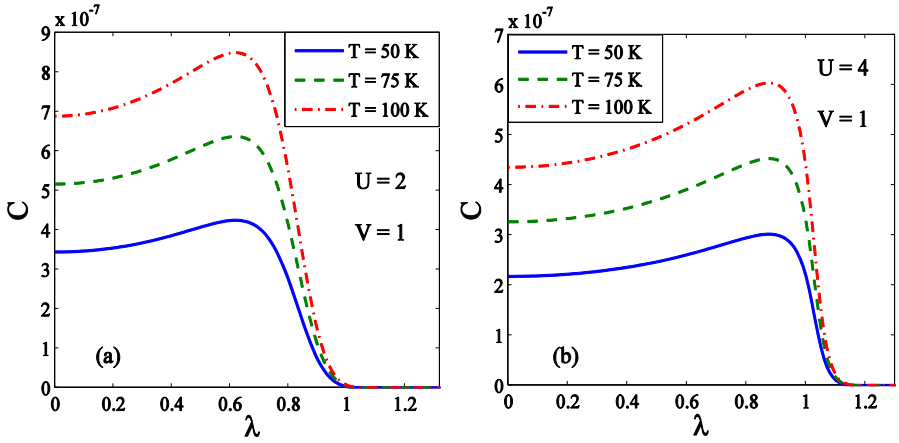


***Fig. 2*** *Specific heat $(C)$ as a function of el-ph interaction strength $\lambda$ for difereent values of temperature.* ***(a)*** *$C$ vs $\lambda$ for $U = 2$.* ***(b)*** *$C$ vs $\lambda$ for $U = 4$.*

At small $\lambda$, $C$ increases with $\lambda$, attains a maximum value at some critical value of $\lambda$ $(\lambda_c)$ and then falls continuously to zero and the value of $\lambda_c$ is almost independent of $T$. However we also observe from Figs. 2(a) and 2(b) that as $U$ increases, the value of $\lambda_c$ increses. This can be explained in a simple-minded way as follows. The *el-ph* interaction induces an attractive *el-el* interaction in the second order and as a result the effective onsite

Coulomb repulsion decreases with increasing $\lambda$. This effectively favours the hopping process and increases the specific heat. Mathematically speaking, in the weak-coupling limit, the polaron energy is linear in the coupling constant, while in the strong-coupling limit it is quadratic. Qualitatively, then, one would expect a similar behaviour in the specific heat as a function of $\lambda$. This is however true only in the single-particle polaron picture. In the many-body system, correlation plays an important role and therefore the specific heat behaves in a little more complicated way. In the strong-coupling limit, the situation becomes entirely different because the polaron goes into a completely localized or the self-trapped state. In this limit the electron at the impurity site does not respond to the environment and the specific heat falls off to zero. Eq. (3.9) shows that the the specific heat $C$ is linear in temperature $T$.

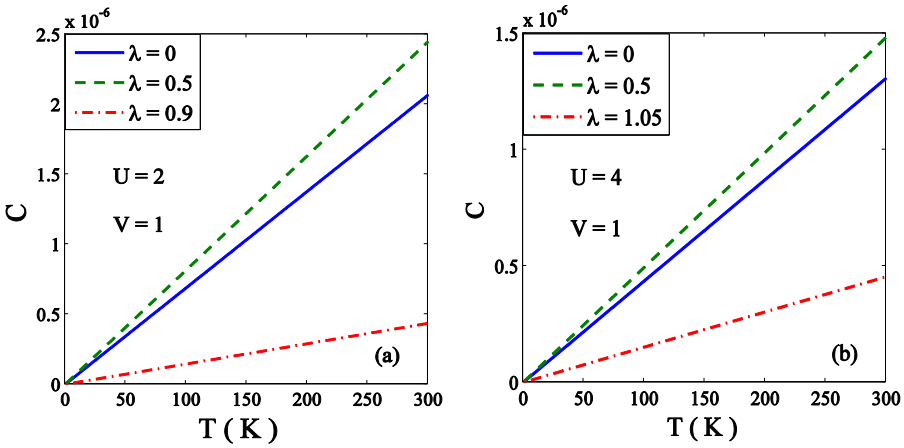


***Fig. 3*** *Specific heat ($C$) as a function of temperature for different values of el-ph interaction strength.* ***(a)*** *$C$ vs $T$ for $U = 2$.* ***(b)*** *$C$ vs $T$ for $U = 4$.*

But we would still like to plot $C - T$ curves to show how they change their gradient with $\lambda$ and $U$. Figs. 3(a) and 3(b) show the behaviour of $C$ as a function of $T$ for different values of $\lambda$ and for $U = 2$ and $U = 4$

respectively. The figures clearly confirm that beyond a certain value of $\lambda$ , specific heat would go to zero. Finally, we make a three-dimensional plot in Fig. 4 to show the dependence of $C$ on both $\lambda$ and $U$ together at $T = 100\,K$.

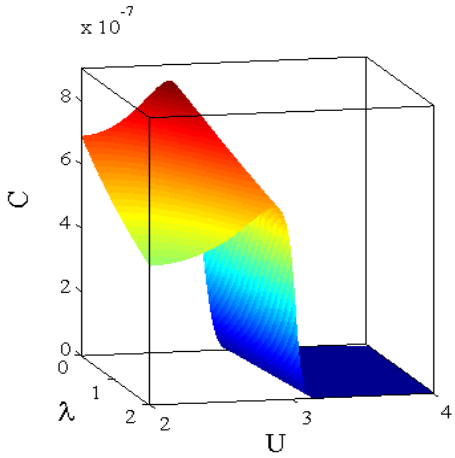


***Fig. 4*** *$C$ as a function of $\lambda$ and $U$ fot $T = 100\,K$.*

## 3.4 Summary

In this chapter we have studied the effect of *el-ph* interaction on the specific heat of a magnetic impurity atom in a non-magnetic host metal using the AH model in the strong *el-ph* coupling limit. The model Hamiltonian is studied by using the SDA method with a modified Gaussian ansatz for the SD function of the impurity atom. We have shown that as $\lambda$ increases, the width of the of SD function decreases as a result of which the life time of an electron on the impurity increases leading to the electron localization on the impurity. To confirm the electron localization we have calculated the specific heat contribution from the impurity electron and shown that the specific heat increases in the weak *el-ph* interaction regime and falls sharply to zero at a critical *el-ph* coupling constant which is independent of temperature.

# References

[1] O. K. Kalashnikov & E. S. Fradkin: Sov. Phys. JEPT **28**, 317 (1969).

[2] A. Cavallo *et al*., Eur. Phys. J. B **50**, 73 (2006).

[3] T. Herrmann & W. Nolting, J. Magn. Magn. Mater, **170**, 253 (1997).

[4] M. Maska, Phys. Rev. B **48**, 1160 (1993).

[5] M. Potthoff & W. Nolting, Phys. Rev. B **55**, 2741(1997).

[6] M. Potthoff & W. Nolting, Surf. Sci. **377**, 457(1997).

[7] B. Mehlig *et al*., Phys. Rev. B **52**, 2463 (1995).

[8] J. Beenen & D. M. Edwards, Phys. Rev. B **52**, 13636 (1995).

[9] B. KjÖllerstrÖm *et al*., Phys. Rev. **148**, 665 (1966).

Chapter **4**

# Ground state energy of the Anderson-Holstein model: The Cluster variation method

## 4.1 Introduction

In Chapter 2, we have studied problem of a magnetic impurity atom in a non-magnetic metal using the single-level symmetric Anderson-Holstein (AH) model and calculated the ground state (GS) energy and the binding energy (BE) between the impurity and conduction electrons using the Equation of motion approach of the Green function technique within the Hartree-Fock (HF) approximation scheme. As we have already mentioned, the HF approximation neglects the charge and spin fluctuations. So to improve the results of Chapter 2, we employ in this chapter a variational method known as the Cluster variation (CV) method (which is based on the variational principal of equilibrium statistical mechanics) to solve the AH Hamiltonian both in the presence and absence of an external magnetic field.

## 4.2 Cluster variation method

The CV method was first introduced by Kikuchi in 1951 [1], and later generalized by Morita in 1957 [2]. The free energy of a system is defined according to statistical mechanics as

$$F = tr[\rho_t(H + K_B T\, ln\rho_t)], \tag{4.1}$$

where $Tr$ is the trace operation, $K_B$ is the Boltzmann constant, $T$ is the absolute temperature, $H$ is the Hamiltonian of the system and $\rho_t$ is the normalized trial density matrix given by

$$\rho_t = \frac{e^{-\beta H}}{tr\,[e^{-\beta H}]}, \tag{4.2}$$

with $\beta = 1/K_B T$. According to the Gibbs variational principle the free energy of a system of $N$ particles in thermal equilibrium can be calculated by minimizing the expression for $F$ with $\rho_t$. The expectation value of any operator can be calculated as

$$\langle a \rangle = \frac{tr\left[a\, e^{-\beta H}\right]}{tr[\, e^{-\beta H}]}. \tag{4.3}$$

The free energy of the system, $F$ can be written as [3, 4]

$$F = \sum_j tr_j h^{(1)}(j)\rho_t^{(1)}(j) + \sum_{j>\boldsymbol{k}} tr_{j,k} h^{(2)}(j,\boldsymbol{k})\, \rho_t^{(2)}(j,\boldsymbol{k})$$

$$+K_B T \sum_j \gamma^{(1)}(j) + K_B T \sum_{j>\boldsymbol{k}} \gamma^{(2)}(j,\boldsymbol{k}) + \cdots \quad , \tag{4.4}$$

where $h^{(1)}(j)$ is the part of the Hamiltonian that involves single particle operators acting on particles in state $j$, $h^{(2)}(j,\boldsymbol{k})$ is the one involving two-particle operators acting on particles in states $i$ and $j$, $\rho_t^{(1)}(j)$ and $\rho_t^{(2)}(j,\boldsymbol{k})$ are one- and two-particle reduced density matrices,

$$tr_j h^{(1)}(j)\rho_t^{(1)}(j) = \langle j|h^{(1)}(j)\rho_t^{(1)}(j)|j\rangle,$$

$$tr_{j,\boldsymbol{k}} h^{(2)}(j,\boldsymbol{k})\rho_t^{(2)}(j,\boldsymbol{k}) = \langle j,\boldsymbol{k}|h^{(2)}(j,\boldsymbol{k})\rho_t^{(2)}(j,\boldsymbol{k})|j,\boldsymbol{k}\rangle, \tag{4.5}$$

and $\gamma^{(1)}(j)$, $\gamma^{(2)}(j,\boldsymbol{k})$ etc. are cumulants given by

$$\gamma^{(1)}(j) = tr_j \rho_t^{(1)}(j)\, ln\rho_t^{(1)}(j),$$

$$\gamma^{(2)}(j,\boldsymbol{k}) = tr_j \rho_t^{(2)}(j,\boldsymbol{k})\, ln\rho_t^{(2)}(j,\boldsymbol{k}) - tr_j \rho_t^{(1)}(j)\, ln\rho_t^{(1)}(j)$$

$$- tr_{\boldsymbol{k}} \rho_t^{(1)}(\boldsymbol{k})\, ln\rho_t^{(1)}(\boldsymbol{k}). \tag{4.6}$$

### 4.2.1 Ground state energy of Anderson-Holstein model

After decoupling the *el-ph* interaction using the Lang-Firsov (LF) transformation followed by the zero phonon average, the effective AH Hamiltonian in the presence of an external magnetic field ($\boldsymbol{B}$) reads as

$$H_{eff} = \sum\nolimits_{\boldsymbol{k},\sigma} \varepsilon_{\boldsymbol{k}} n_{\boldsymbol{k}\sigma} + \sum\nolimits_{\sigma} \tilde{\varepsilon}_{d\sigma} n_{d\sigma} + \widetilde{U}\, n_{d\sigma} n_{d,-\sigma}$$

$$+ \sum\nolimits_{\boldsymbol{k},\sigma} \tilde{V}_{\boldsymbol{k}} \left(c_{\boldsymbol{k}\sigma}^{\dagger} c_{d\sigma} + c_{d\sigma}^{\dagger} c_{\boldsymbol{k}\sigma}\right), \tag{4.7}$$

where,

$$\tilde{\varepsilon}_{d\sigma} = (\tilde{\varepsilon}_d - \mu_B\, \boldsymbol{B}.\boldsymbol{\sigma}). \tag{4.8}$$

Since the effective AH Hamiltonian $H_{eff}$ has up to two particle interaction terms, it is reasonable to retain terms up to $\gamma^{(2)}(j,\boldsymbol{k})$ in the free energy expression (4.6). Thus we have

$$F = \sum_{\boldsymbol{k},\sigma} \varepsilon_{\boldsymbol{k}} tr_{\boldsymbol{k}\sigma} \rho_t^{(1)}(\boldsymbol{k}\sigma) n_{\boldsymbol{k}\sigma} + \sum_{\sigma} \tilde{\varepsilon}_{d\sigma}\, tr_{d\sigma} \rho_t^{(1)}(d\sigma) n_{\boldsymbol{d}\sigma}$$

$$+ \tilde{U} \left( tr_{d\sigma} \rho_t^{(1)}(d\sigma) n_{\boldsymbol{d}\sigma} \right) \left( tr_{d,-\sigma} \rho_t^{(1)}(d,-\sigma) n_{\boldsymbol{d},-\sigma} \right)$$

$$+ \tilde{V} \sum_{\boldsymbol{k},\sigma} tr_{\boldsymbol{k}\sigma,d\sigma}\, \rho_t^{(2)}(\boldsymbol{k}\sigma, d\sigma) \left( c_{d\sigma}^{\dagger} c_{\boldsymbol{k}\sigma} + h.c \right)$$

$$+ K_B T \sum_{\boldsymbol{k},\sigma} tr_{k\sigma} \rho_t^{(1)}(\boldsymbol{k}\sigma)\, ln \rho_t^{(1)}(\boldsymbol{k}\sigma)$$

$$+ K_B T \sum_{\sigma} tr_{\sigma} \rho_t^{(1)}(d\sigma)\, ln \rho_t^{(1)}(d\sigma)$$

$$+ K_B T \sum_{\boldsymbol{k}\sigma} \Big[ tr_{\boldsymbol{k}\sigma,d\sigma} \rho_t^{(2)}(\boldsymbol{k}\sigma, d\sigma)\, ln \rho_t^{(2)}(\boldsymbol{k}\sigma, d\sigma)$$

$$- tr_{\boldsymbol{k}\sigma} \rho_t^{(1)}(\boldsymbol{k}\sigma)\, ln \rho_t^{(1)}(\boldsymbol{k}\sigma) - tr_{\sigma} \rho_t^{(1)}(d\sigma)\, ln \rho_t^{(1)}(d\sigma) \Big]. \quad (4.9)$$

Now we write the reduced trial density matrices in terms of the unknown expectation values $\langle n_{\boldsymbol{k}\sigma} \rangle$, $\langle n_{d\sigma} \rangle$ and $\langle c_{d\sigma}^{\dagger}\, c_{\boldsymbol{k}\sigma} \rangle$ which can be determined by minimizing the free energy with respect to them. The one-particle and two-particle density matrices are written as [5]

$$\rho_t^{(1)}(\boldsymbol{k}\sigma) = \begin{bmatrix} \langle n_{\boldsymbol{k}\sigma} \rangle & 0 \\ 0 & 1 - \langle n_{\boldsymbol{k}\sigma} \rangle \end{bmatrix}, \quad (4.10)$$

$$\rho_t^{(1)}(d\sigma) = \begin{bmatrix} \langle n_{d\sigma} \rangle & 0 \\ 0 & 1 - \langle n_{d\sigma} \rangle \end{bmatrix}, \quad (4.11)$$

$$\rho_t^{(2)}(\boldsymbol{k}\sigma, d\sigma)$$

$$= \begin{bmatrix} \langle n_{\boldsymbol{k}\sigma} n_{d\sigma}\rangle & 0 & 0 & 0 \\ 0 & \langle n_{\boldsymbol{k}\sigma}\rangle - \langle n_{\boldsymbol{k}\sigma} n_{d\sigma}\rangle & \langle c_{\boldsymbol{k}\sigma}^{\dagger} c_{d\sigma}\rangle & 0 \\ 0 & \langle c_{d\sigma}^{\dagger} c_{\boldsymbol{k}\sigma}\rangle & \langle n_{d\sigma}\rangle - \langle n_{\boldsymbol{k}\sigma} n_{d\sigma}\rangle & 0 \\ 0 & 0 & 0 & 1 - \langle n_{\boldsymbol{k}\sigma}\rangle - \langle n_{d\sigma}\rangle + \langle n_{\boldsymbol{k}\sigma} n_{d\sigma}\rangle \end{bmatrix}$$

(4.12)

After diagonalization of $\rho_t^{(2)}(\boldsymbol{k}\sigma, d\sigma)$, the free energy reads

$$F = U^{(1)} + U^{(2)} - T\,S^{(1)} - T\,S^{(2)}, \tag{4.13}$$

with

$$U^{(1)} = \sum_{\boldsymbol{k},\sigma} \varepsilon_{\boldsymbol{k}} \langle n_{\boldsymbol{k}\sigma}\rangle + \sum_{\sigma} \tilde{\varepsilon}_{d\sigma}\, \langle n_{d\sigma}\rangle, \tag{4.14}$$

$$U^{(2)} = \widetilde{U}\langle d_{d\sigma}\rangle\langle n_{d-\sigma}\rangle + \tilde{V} \sum_{\boldsymbol{k},\sigma} \left(\xi_{\boldsymbol{k}d\sigma} + \xi_{\boldsymbol{k}d\sigma}^{\dagger}\right), \quad \xi_{\boldsymbol{k}d\sigma} = \langle c_{\boldsymbol{k}\sigma}^{\dagger} c_{d\sigma}\rangle, \tag{4.15}$$

$$S^{(1)} = -K_B \sum_{\boldsymbol{k},\sigma} [\langle n_{\boldsymbol{k}\sigma}\rangle\, ln\langle n_{\boldsymbol{k}\sigma}\rangle + (1 - \langle n_{\boldsymbol{k}\sigma}\rangle)\, ln(1 - \langle n_{\boldsymbol{k}\sigma}\rangle)]$$

$$-K_B \sum_{\sigma} [\langle n_{\boldsymbol{d}\sigma}\rangle\, ln\langle n_{\boldsymbol{d}\sigma}\rangle + (1 - \langle n_{\boldsymbol{d}\sigma}\rangle)\, ln(1 - \langle n_{\boldsymbol{d}\sigma}\rangle)], \tag{4.16}$$

$$S^{(2)} = -\,K_B \sum_{\boldsymbol{k},\sigma} \{\, A\, ln(A) + B\, ln(B) + C\, ln(C)\}$$

$$+\, D\, ln(D) - \langle n_{\boldsymbol{k}\sigma}\rangle\, ln\langle n_{k\sigma}\rangle - (1 - \langle n_{\boldsymbol{k}\sigma}\rangle)\, ln[1 - \langle n_{\boldsymbol{k}\sigma}\rangle]$$

$$-\langle n_{d\sigma}\rangle\, ln\langle n_{d\sigma}\rangle - (1 - \langle n_{d\sigma}\rangle)\, ln[1 - \langle n_{d\sigma}\rangle], \tag{4.17}$$

where,

$$A = \langle n_{\boldsymbol{k}\sigma}\rangle\langle n_{\boldsymbol{d}\sigma}\rangle\,,$$

$$B = \left[\langle n_{\boldsymbol{k}\sigma}\rangle + \langle n_{\boldsymbol{d}\sigma}\rangle - 2\langle n_{\boldsymbol{k}\sigma}\rangle\langle n_{\boldsymbol{d}\sigma}\rangle + \sqrt{a}\,\right]/2\,,$$

$$C = \left[\langle n_{\boldsymbol{k}\sigma}\rangle + \langle n_{d\sigma}\rangle - 2\langle n_{\boldsymbol{k}\sigma}\rangle\langle n_{d\sigma}\rangle + \sqrt{a}\,\right]/2\,,$$

$$a = ((\langle n_{\boldsymbol{k}\sigma}\rangle - \langle n_{d\sigma}\rangle)^2 + 4|\xi_{\boldsymbol{k}d\sigma}|^2),$$

$$D = [1 - \langle n_{\boldsymbol{k}\sigma}\rangle - \langle n_{\boldsymbol{d}\sigma}\rangle + \langle n_{\boldsymbol{k}\sigma}\rangle\langle n_{\boldsymbol{d}\sigma}\rangle]\,,$$

where we have used: $\langle n_{d\uparrow}n_{d\downarrow}\rangle = \langle n_{d\uparrow}\rangle\,\langle n_{d\downarrow}\rangle$ and $\langle n_{\boldsymbol{k}\sigma}n_{d\sigma}\rangle = \langle n_{\boldsymbol{k}\sigma}\rangle\,\langle n_{d\sigma}\rangle$, $\langle n_{a\sigma}\rangle$ representing the distribution function of the electron of spin $\sigma$ in state $a$ in the presence of all the interactions. This is equivalent to neglecting the correlation between the $d$ electrons of opposite spins and also that between the conduction and $d$ electrons. As explained in [3], this should not be confused with the Hartree-Fock approximation. Now $F$ has to be minimized with respect to $\xi_{\boldsymbol{k}d\sigma}$, $\langle n_{\boldsymbol{k}\sigma}\rangle$, and $\langle n_{d\sigma}\rangle$ to obtain the equilibrium state. Minimization of $F$ with respect to $\xi_{\boldsymbol{k}d\sigma}$ in the limit $T = 0$ yields

$$\xi_{\boldsymbol{k}d\sigma} = -[\langle n_{\boldsymbol{k}\sigma}\rangle\langle n_{d\sigma}\rangle(1 - \langle n_{\boldsymbol{k}\sigma}\rangle)(1 - \langle n_{d\sigma}\rangle)]^{1/2}. \tag{4.18}$$

The free energy at $T = 0$, which is the GS energy, then becomes

$$F_{T=0} = E_0 = \sum_{\boldsymbol{k},\sigma} \varepsilon_{\boldsymbol{k}}\langle n_{\boldsymbol{k}\sigma}\rangle + \sum_{\sigma} \tilde{\varepsilon}_{d\sigma}\,\langle n_{d\sigma}\rangle + \tilde{U}\,\langle n_{d\sigma}\rangle\langle n_{d,-\sigma}\rangle$$

$$-2\left|\tilde{V}\right|\sum_{\boldsymbol{k},\sigma}[\langle n_{\boldsymbol{k}\sigma}\rangle\langle n_{d\sigma}\rangle(1 - \langle n_{\boldsymbol{k}\sigma}\rangle)(1 - \langle n_{d\sigma}\rangle)]^{1/2}. \tag{4.19}$$

Minimization of $E_0$ with respect to $\langle n_{\boldsymbol{k}\sigma}\rangle$ and $\langle n_{\boldsymbol{d}\sigma}\rangle$ gives

$$\varepsilon_{\boldsymbol{k}} - \left|\tilde{V}\right|\sqrt{\eta_{d\sigma}/\eta_{k\sigma}}\ (1 - 2\langle n_{k\sigma}\rangle) = 0, \tag{4.20}$$

$$\tilde{\varepsilon}_{d\sigma} - \left(\varepsilon_{0\sigma}/2\sqrt{\eta_{d\sigma}}\right)(1 - 2\langle n_{d\sigma}\rangle) = 0, \tag{4.21}$$

where,

$$\eta_{d\sigma} = \langle n_{d\sigma}\rangle(1 - \langle n_{d\sigma}\rangle),$$

$$\eta_{\boldsymbol{k}\sigma} = \langle n_{\boldsymbol{k}\sigma}\rangle(1 - \langle n_{\boldsymbol{k}\sigma}\rangle),$$

$$\varepsilon_{0\sigma}\ = 2\left|\tilde{V}\right|\sum\nolimits_{\boldsymbol{k}}[\langle n_{\boldsymbol{k}\sigma}\rangle(1 - \langle n_{\boldsymbol{k}\sigma}\rangle)]^{1/2}. \tag{4.22}$$

After some algebraic manipulation we obtain

$$\langle n_{\boldsymbol{k}\sigma}\rangle = \frac{1}{2}\left[1 - \frac{\varepsilon_{\boldsymbol{k}}}{\left(\varepsilon_{\boldsymbol{k}}^2 + 4\eta_{d\sigma}\left|\tilde{V}\right|^2\right)^2}\right], \tag{4.23}$$

$$\varepsilon_{0\sigma} = \ 4g(0)\left|\tilde{V}\right|^2\eta_{d\sigma}^{1/2}\left[\tilde{\varepsilon}_{d\sigma}/2g(0)\left|\tilde{V}\right|^2(1 - 2\langle n_{d\sigma}\rangle)\right]. \tag{4.24}$$

$$E_0 = \sum_{\boldsymbol{k}>\boldsymbol{k}_F,\sigma}\varepsilon_{\boldsymbol{k}}\langle n_{k\sigma}\rangle\ + \sum_{\boldsymbol{k}<\boldsymbol{k}_F,\sigma}|\varepsilon_{\boldsymbol{k}}|(1 - \langle n_{k\sigma}\rangle) + \sum_{\sigma}\tilde{\varepsilon}_{d\sigma}\ \langle n_{d\sigma}\rangle$$

$$+\ \tilde{U}\ (N^2 - m^2)/4 - \sum_{\sigma}\varepsilon_{0\sigma}\,\eta_{d\sigma}^{1/2}, \tag{4.25}$$

$$\sinh^{-1}\left[\frac{Z}{2[\langle n_{d\downarrow}\rangle(1 - \langle n_{d\downarrow}\rangle)]^{1/2}}\right] = \frac{(\tilde{\varepsilon}_d - \mu_B B + \langle n_{d\uparrow}\rangle)y}{(1 - 2\langle n_{d\downarrow}\rangle)},$$

$$\sinh^{-1}\left[\frac{Z}{2[\langle n_{d\uparrow}\rangle(1 - \langle n_{d\uparrow}\rangle)]^{1/2}}\right] = \frac{(\tilde{\varepsilon}_d + \mu_B B + \langle n_{d\downarrow}\rangle)y}{(1 - 2\langle n_{d\uparrow}\rangle)}, \tag{4.26}$$

$$Z = \frac{D}{|\tilde{V}|} \quad , \qquad y = \frac{\tilde{U}}{2g(0)|\tilde{V}|^2} \, . \tag{4.27}$$

where $\langle n_{k\sigma} \rangle$ in Eq. (4.23) gives the electron distribution for $\boldsymbol{k} > \boldsymbol{k}_F$ and hole distribution for $\boldsymbol{k} < \boldsymbol{k}_F$. The value of $\varepsilon_{0\sigma}$ has been obtained by replacing the summation over $\boldsymbol{k}$ by an integral over $\varepsilon_{\boldsymbol{k}}$ using the constant density of states $g(0)$ at the Fermi level, $D$ being the half band-width of the conduction band. Eq. (4.25) gives the total ground state energy of the interacting system.

## 4.2.2 Binding Energy

The binding energy (BE) between the localized and the conduction electrons is defined as:

$$W = \varepsilon_{d\sigma} - E_0 = (\varepsilon_{d\sigma} - \lambda^2 \hbar\omega_0) - (E_0 - \lambda^2 \hbar\omega_0)$$

$$= \tilde{\varepsilon}_{d\sigma} - E_0 + \lambda^2 \hbar\omega_0 \, , \tag{4.28}$$

which yields on substituting for $E_0$,

$$W = g(0)|\tilde{V}|^2 \sum\nolimits_{\sigma} \left\{ \eta_{d\sigma} \left[ 1 + 2 \sinh^{-1} \left( Z/2\eta_{d\sigma}^{1/2} \right) \right] \right\} - \tilde{\varepsilon}_d (N-1)$$

$$+ (m-1)\mu_B B - \tilde{U}\,(N^2 - m^2)/4 + \lambda^2 \hbar\omega_0 . \tag{4.29}$$

Here $m$ is the magnetic moment (in units of Bohr magneton) carried by the impurity electrons and is given by: $m = [\langle n_{d,\uparrow} \rangle - \langle n_{d,\downarrow} \rangle]$. The condition $\langle n_{d\uparrow} \rangle + \langle n_{d\downarrow} \rangle = N = 1$ is always satisfied irrespective of the value of *el-ph* coupling constant. This gives: $\eta_{d\uparrow} = \eta_{d\downarrow} = \eta_d$. Using Appelbaum approximation $\left( \tilde{U}/g(0)|\tilde{V}|^2 \right) \to \infty$, in Eq. (4.25) we write

$$\widetilde{U} = 4g(0)\left|\tilde{V}\right|^2 \sinh^{-1}\left(\frac{D}{2\eta_{d\sigma}^{1/2}\left|\tilde{V}\right|}\right) + \frac{2\mu_B B}{\langle n_{d\uparrow}\rangle - \langle n_{d\downarrow}\rangle}\,. \tag{4.30}$$

Then BE becomes

$$W = 2g(0)\left|\tilde{V}\right|^2 \eta_d + \frac{2\mu_B B\,\langle n_{d\downarrow}\rangle^2}{\langle n_{d\uparrow}\rangle - \langle n_{d\downarrow}\rangle} + \lambda^2\hbar\omega_0, \tag{4.31}$$

The second term in the Eq. (4.31) is much smaller than the other terms and so we can neglect it. Thus Eq. (4.31) reduces to

$$W \cong 2g(0)\left|\tilde{V}\right|^2 \eta_d + \lambda^2\hbar\omega_0\,. \tag{4.32}$$

In the weak-coupling limit ( $|\tilde{\varepsilon}_d| \gg g(0)|\widetilde{V}|^2$ ), Eq. (4.26) and Eq. (4.30) lead to the following equations

$$\tilde{\varepsilon}_{d\sigma} + 2g(0)\left|\tilde{V}\right|^2 \sinh^{-1}\left(\frac{D}{2\eta_{d\sigma}^{1/2}\left|\tilde{V}\right|}\right) = 0, \tag{4.33}$$

$$\left|\tilde{V}\right|^2 \eta_d = D^2 \exp\left[-\frac{(\tilde{\varepsilon}_d + \mu_B B)}{g(0)|\tilde{V}|^2}\right], \tag{4.34}$$

$$W = 2g(0)D^2\, exp\left[-\frac{(\tilde{\varepsilon}_d+\mu_B B)}{g(0)|\tilde{V}|^2}\right] + \lambda^2\hbar\omega_0, \tag{4.35}$$

which show that the GS energy of the fully interacting system is lower than the GS energy of the unperturbed electrons.

## 4.3 Results and Discussion

### 4.3.1 Results in the absence of magnetic field

We take $m = 0$. In Fig. 1, we plot $\langle n_{d\sigma} \rangle$ vs $\langle n_{d-\sigma} \rangle$ for different values of the *el-ph* coupling constant $\lambda$. Fig. 1(a) shows results in an adiabatic regime ( $V = 2 > \hbar\omega_0$ ). In the adiabatic region considered, there are three pairs of solutions for three values of $\lambda$. The first one is at $\langle n_{d\uparrow} \rangle = n_1$ and $\langle n_{d\downarrow} \rangle = n_2$, where $n_1 \neq n_2$ , the second one is at $\langle n_{d\uparrow} \rangle = \langle n_{d\downarrow} \rangle$ and the third one is at $\langle n_{d\downarrow} \rangle = n_1$ and $\langle n_{d\uparrow} \rangle = n_2$. The solutions $n_1 \neq n_2$ correspond to a magnetic solution. As $\lambda$ increases, the magnetic solutions disappear. This is understandable because the *el-ph* interaction provides a phonon-mediated attractive *el-el* interaction in the second order which reduces the effect of the usual Coulomb repulsion. In Fig. 1(b), we plot

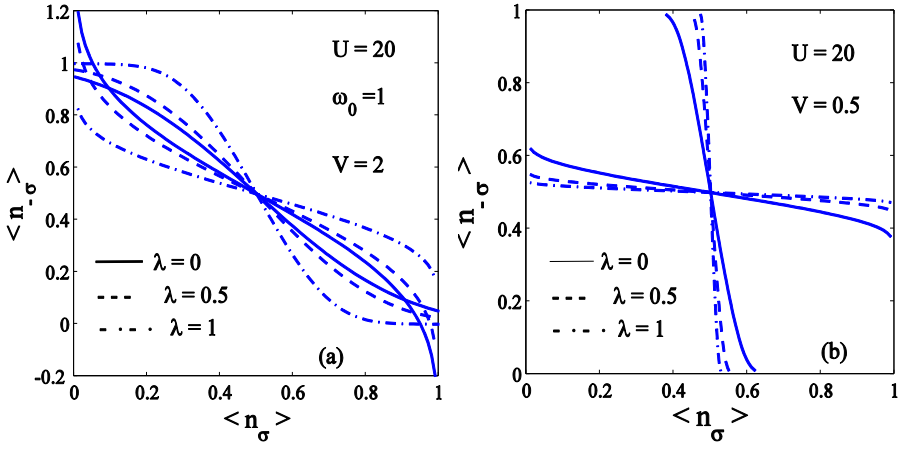


***Fig. 1*** *Self-consistent plot of* $\langle n_\sigma \rangle$ *vs* $\langle n_{-\sigma} \rangle$ *for* $\omega_0 = 1$ , $g(0) = \frac{1}{2}$, $D = 5$. *(a) shows an adiabatic case with* $V = 2$ *and (b) an anti-adiabatic case with* $V = 0.5$.

the opposite regime, i.e., the anti-adiabatic case ($V = 0.5 < \hbar\omega_0$). We have shown results for $\lambda = 0,\ 0.5$ and 1.0 for which magnetic solutions exist. Our

study shows that for $\lambda = 1.9$ onwards, magnetic solutions do not exist. At this point it is important to emphasize that the magnetic solution obtained in the adiabatic regime in the present calculation is probably an artifact of the approximation used. Since it is well known that the GS of the single-impurity Anderson model is the Kondo singlet, and since the *el-ph* interaction suppresses the local moment, one does not expect the existence of magnetic moment in the GS of the AH model. One of the main aims of this work is to study the effect of *el-ph* interaction on the GS energy of the system. In Fig. 2 we have studied the GS energy as a function of the onsite Coulomb correlation strength, $U$ for a couple of $\lambda$ values in an adiabatic and an anti-adiabatic case. Fig. 2(a) shows the results for an anti-adiabatic case ( $V = 0.5$ ), and Fig. 2(b) shows the results for an adiabatic case ( $V = 2$ ). We find that, as expected, the GS energy in general increases with increasing $U$. This is understandable because $U$ increases the onsite repulsive energy and consequently the total GS energy increases.

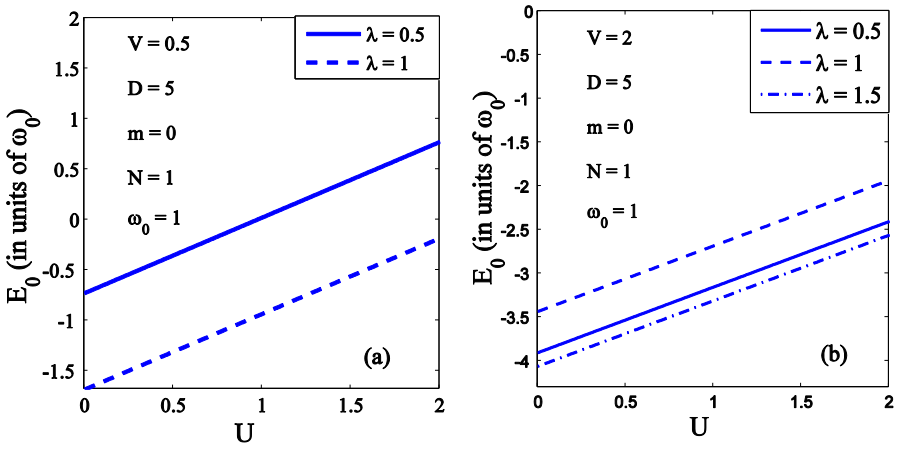


***Fig. 2*** *$E_0$ vs. U for different values of $\lambda$ with $(a)\ V = 0.5,\ (b)\ V = 2$.*

The GS energy is found to be lower in the adiabatic case than in the anti-adiabatic case, other parameters remaining the same. This can be explained

in the following way. The adiabaticity parameter, $V$ is larger than 1 (in our units) in the adiabatic case while it is smaller than 1 in an anti-adiabatic case. With increasing $V$, the $s-d$ interaction favours hybridization between the localized and the conduction electrons. In that case, the hopping of electrons from the localized to delocalized states and vice versa becomes stronger and in the process the system can adjust itself to a configuration of lower energy. Thus an increase in $V$ will reduce the GS energy. In Fig.3 we have studied the GS energy as a function of the onsite *el-ph* interaction strength for a couple of values of $U$. Fig. 3(a) shows the results for an anti-adiabatic case ( $V = 0.5$ ), while the results for an adiabatic case ( $V = 2$ ) are plotted in Fig. 3(b).

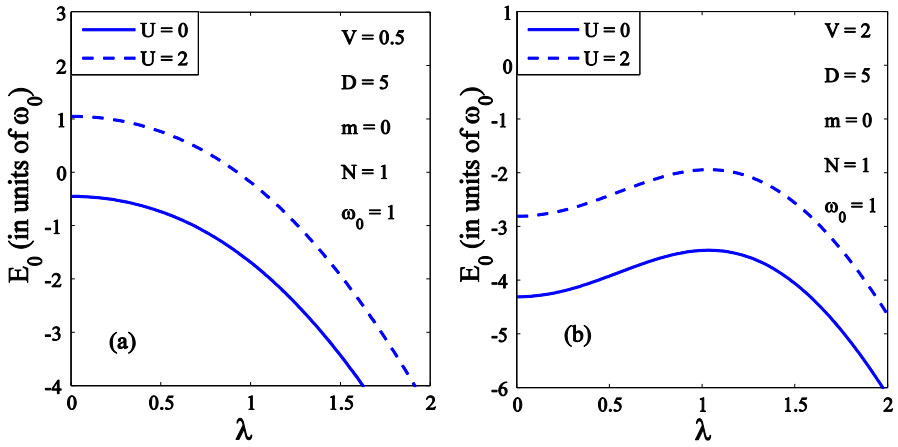


***Fig. 3*** $E_0$ *vs.* $\lambda$ *for different values of* $U$ *with* $(a)\ V = 0.5,\ (b)\ V = 2.$

In the anti-adiabatic case, we find that the energy decreases with increasing *el-ph* interaction. This can be explained physically by the simple polaronic effect in which the *el-ph* interaction provides an effective *el-el* attractive interaction which is of second-order in the *el-ph* coupling constant. So essentially it reduces the effect of the repulsive onsite Coulomb interaction and therefore the GS energy decreases with increasing $\lambda$. It seems that in an

adiabatic case, the GS energy first increases with increasing $\lambda$, attains a maximum and then decreases with further increase in $\lambda$. This is a very interesting behaviour and may be explained in the following way. The *el-ph* interaction has several effects. One of the effects which are relevant for the present discussion is the reduction in the onsite Coulomb repulsion $U$ and the other is the reduction in the $s-d$ overlap strength $V$. Reduction in $U$ suppresses the GS energy, while that in $V$ enhances it. There are a few other energies such as the impurity electron energy etc. which are reduced with increasing *el-ph* interaction strength $\lambda$. It seems that at low values of $\lambda$, the enhancement in energy due to reduction in $V$ dominates over all other effects and as a result the energy increases as $\lambda$ increases. However, beyond a critical value of $\lambda$, the decrease in the energy due to the reduction in $U$ and other energies wins over the increase in the energy due to the reduction in $V$ and as a result, the energy starts decreasing and continues to decrease monotonically thereafter. The main objective of this work is to examine the effect of *el-ph* interaction on the BE $W$ between the localized and the conduction electrons. In Fig. 4, we plot the BE $W$ as a function of $\lambda$ for several values of $U$ in the ant-adiabatic case. In particular, we show the results for $V = 0.5$. Fig. 4(a) shows the BE results for $U = 0.5, 1$ and $2$. It is evident that, in general, $W$ increases with increasing $\lambda$. However at small $\lambda$, the increase is slow and becomes rapid above a certain value of $\lambda$. In fact, with increasing $U$ the increase in $W$ with $\lambda$ at small $\lambda$ becomes even slower. For example, for $U = 2$, the increase in $W$ with $\lambda$ is almost zero up to about $\lambda = 0.8$ beyond which, of course, $W$ increases with $\lambda$ very rapidly. Furthermore, for a given value of $\lambda$, $W$ decreases as $U$ increases. Figs. 4(b) and 4(c) show the behavior for $U = 3$ and 3.5 respectively. Here one can see that as $\lambda$ increases, $W$ increases monotonically with $\lambda$ and also the results in Fig. 4(b) and Fig. 4(c) are almost same and independent of $U$. This can be understood from the expression of $W$. In the anti-adiabatic region, since $V$ is small, for large $U$, the quantity, $exp[-|\tilde{\varepsilon}_d|/g(0)|\tilde{V}|^2]$

becomes negligibly small as compared to $\lambda^2$ and consequently $W$ becomes essentially independent of $U$ and varies with $\lambda$ as $\lambda^2$.

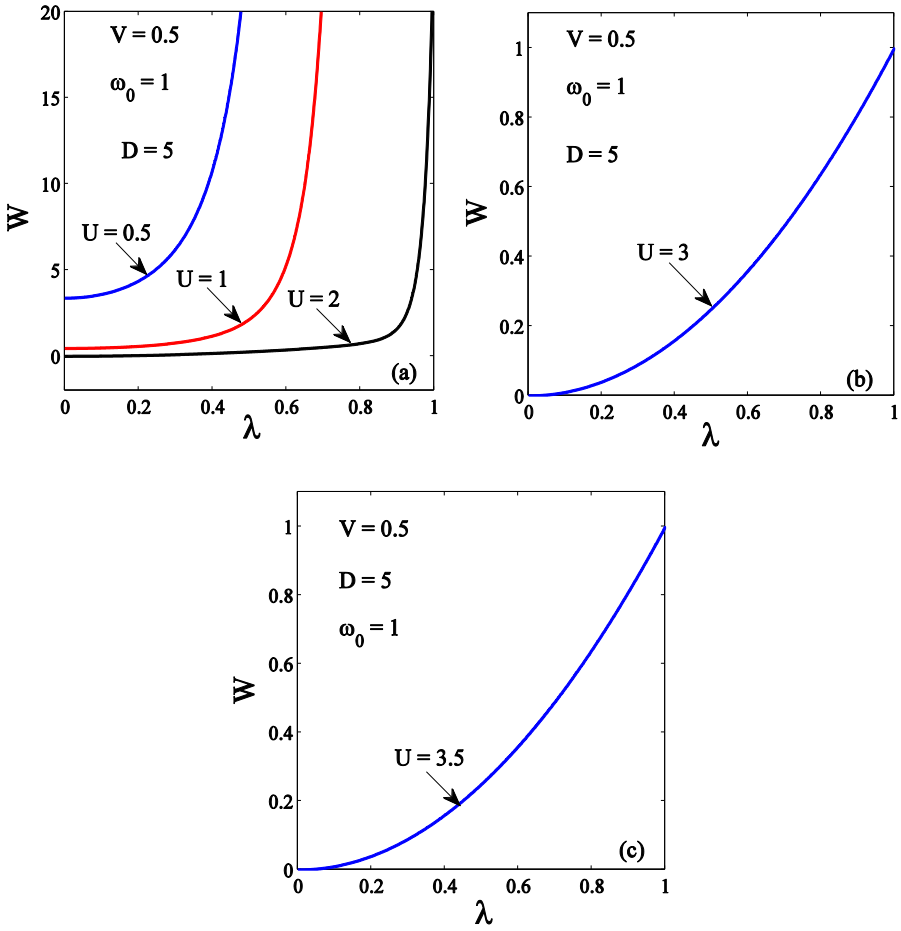


***Fig. 4*** *$W$ as a function of $\lambda$ with $D = 5$, $g(0) = 0.5$, $\omega_0 = 1$, $V = 0.5$ and different values of $U$.*

In Figs. 5, we plot the variation of the BE $W$ as a function of $\lambda$ for $V = 3$ for different values of $U$. One can immediately observe from Fig. 5(a) that the qualitative behavior of the BE $W$ as a function of $\lambda$ in an adiabatic region for small values of $U$ is more or less the same as in an anti-adiabatic

case. Quantitatively, however, the binding is much stronger in the adiabatic case. The reason is of course clear. We have already mentioned above that the $s-d$ interaction favours hybridization and reduces the GS energy and hence the energy of the bound state of the impurity electron and the itinerant electrons becomes lower and therefore it requires more energy to break the bound state. Therefore an increase in $V$ will favour binding. Figs. 5(b), 5(c) and 5(d) show the behavior for $U = 3,\ 3.5$ and 4. Now the results look more interesting. In fact, the results are qualitatively different from the

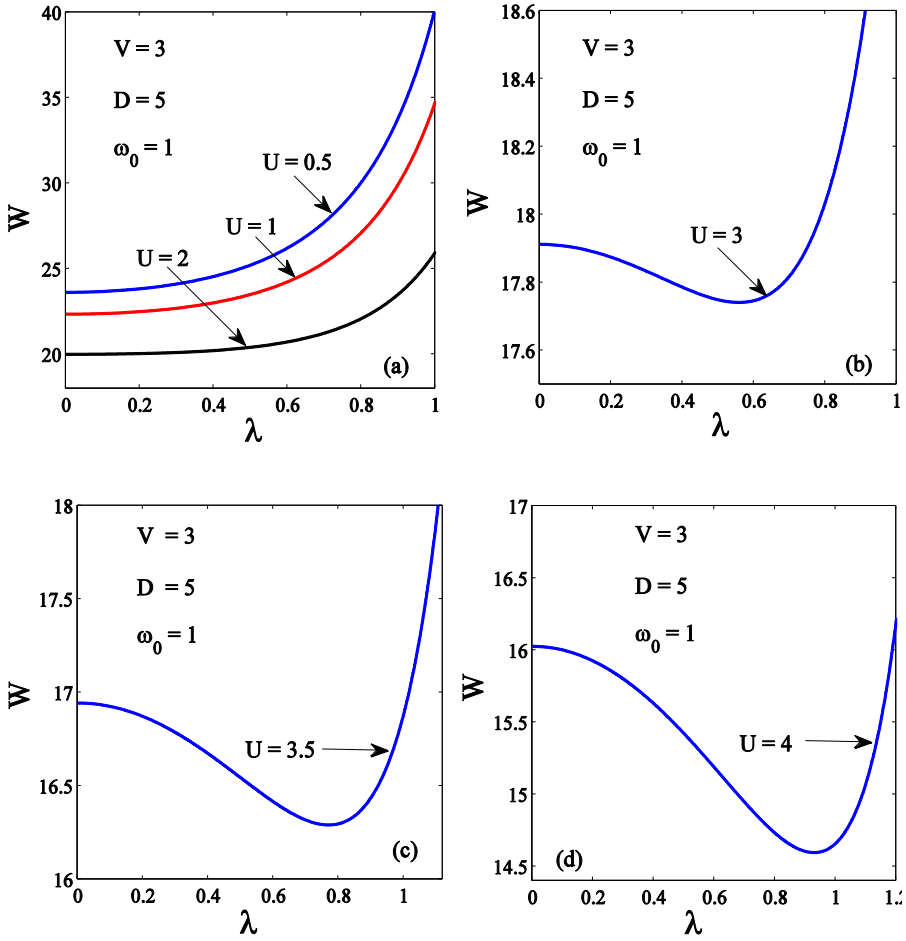


***Fig. 5*** *W vs λ with* $D = 5,\ g(0) = 0.5, \omega_0 = 1, V = 3.0$ *and different values of* $U$.

corresponding antiadiatic cases. The reason is the following. For large $U$, the quantity, $exp[-|\tilde{\varepsilon}_d|/g(0)|\tilde{V}|^2]$ is no more ignorable and therefore unlike in the anti-adiabatic cases, now $W$ depends both on $U$ and $\lambda$. One can see that as $\lambda$ increases, $W$ decreases, reaches a minimum at some value of $\lambda$ (depending on the value of $U$) and then increases monotonically with $\lambda$. All these behaviour can be understood in view of the fact that an increase in $\lambda$ reduces both $U$ and $V$ because of polaronic effect leading to an effective $U$ and an effective $V$. For small $U$, the decrease in $U$ plays a more important role than the decrease in $V$ and as a result $W$ increases with $\lambda$. However for large $U$, at small $\lambda$, the decrease in $U$ is not so significant as compared to $V$ and therefore the decrease in $V$ dominates and as a result $W$ decreases. As $\lambda$ increases substantially, effective $V$ becomes very small because of the exponential polaronic reduction and then the decrease in the effective $U$ becomes more important and consequently $W$ increases. Thus BE goes through a minimum at a certain value of $\lambda$. For $U > 2$, the value of $\lambda$ at which $W$ shows a minimum increases with $U$. It seems that $U = 2$ is some kind of an intermediate case for which the effects of the changes in $U$ and $V$ cancel each other up to a certain value of $\lambda$ beyond which of course effective $U$ dominates and $W$ increases with $\lambda$ thereafter. The decrease in $W$ with increasing $U$ at small $\lambda$ in Fig. 5(a) is again because of the dominating effect of effective $U$ over $V$ at small $\lambda$. The effect reverses when $U$ becomes larger than 2. The exact determination of the value of $\lambda$ where the minimum in $W$ should occur and the understanding of the special role of the case $U = 2$, require a simple mathematical analysis which involves minimizing $W$ with respect to $\lambda$. This in general gives two equations out of which only one gives self-consistent results for the minimum value of $\lambda$. The relevant equation reads

$$exp\left[-\left(\frac{\left(2\lambda_{min}^2-U\right)\ e^{\lambda_{min}^2}}{V^2}+\lambda_{min}^2\right)\right]=\left(\frac{D}{V}\right)^2\left[U-\left(2+2\lambda_{min}^2\right)\right], \tag{4.23}$$

which immediately suggests that $\lambda_{min}$ has to be smaller than $\left(\frac{U}{2}-1\right)^{1/2}$ and also tells us that the minimum in $W$ as a function of $\lambda$ cannot occur below $U=2$. This is precisely what we observe in Figs. 5(b) and 5(d). The actual value of $\lambda_{min}$ of course depends on both $U$ and $V$. It is important to realize that the minimum structure in BE occurs only when both $U$ and $V$ are above certain values. We show in Fig. 6 the curve in the $U-V$ plane above which the minimum structure would occur in the $W-\lambda$ plot. The figure clearly shows that $W$ as a function of $\lambda$ exhibits a minimum structure only in the adiabatic region and that too above $U=2$.

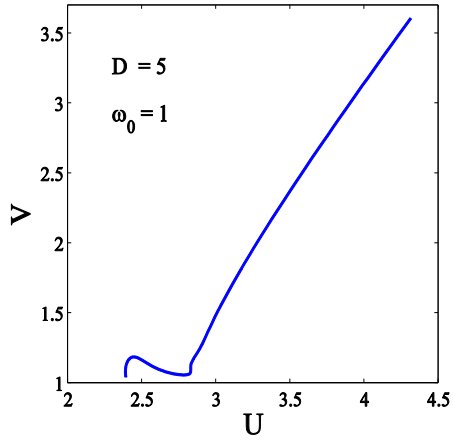


***Fig. 6*** *Curve in the $U-V$ plane above which minimum occurs in the $W-\lambda$ graph.*

It would be interesting to study the variation of $W$ with respect to $U$ explicitly. We show this variation in Fig. 7. Fig. 7(a) shows the results for an anti-adiabatic case ($V=0.5$), while the results for an adiabatic case ($V=3$) are plotted in Fig. 7(b). As is understandable, for $\lambda=0$, $W$

decreases with increasing $U$ for both the adiabatic and the anti-adiabatic cases and becomes zero eventually because the on-site repulsive interaction would not allow any itinerant electron to occupy the impurity site for a large value of $U$. For $V = 0.5$, as the *el-ph* interaction is switched on, the effective on-site correlation effect is reduced which leads to a larger BE. Thus the binding energy increases with $\lambda$ for a given $U$ as shown in Fig. 7(a). In this case the decrease in $U$ with increasing $\lambda$ has a more dominant effect than that in $V$. In Fig. 7(b) we see that the increase in $W$ with $\lambda$ takes place only up to a certain value of $U$. The reason is again simple. As $\lambda$ increases, the decrease in effective $U$ becomes more dominating than that in effective $V$ at small $U$. As a result of this, the over-all GS energy decreases with increase in $\lambda$ and consequently BE increases with $\lambda$ at small $U$. At large $U$, as the *el-ph* interaction increases, the change in $U$ does not matter much, while the reduction in $V$ dominates and consequently the GS energy increases and $W$ decreases with increase in $\lambda$. Thus one expects that beyond a certain value of $U$, BE will have a sharper fall for higher values of $\lambda$ leading to a crossing behaviour. This is what is exactly observed in Fig. 7(b). We would like to study the effect of the adiabaticity parameter $V$ on the $\lambda$-dependence of the $W$.

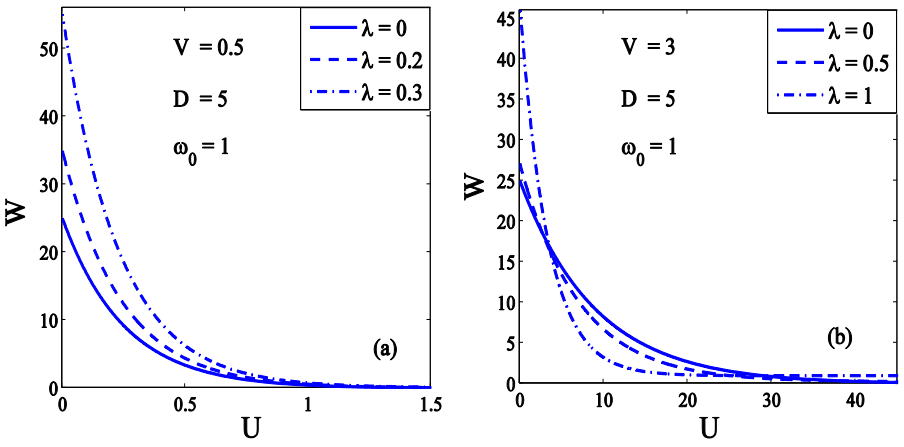


***Fig. 7*** *W vs. U for different values of* $\lambda$ *with* $(a)\ V = 0.5,\ (b)\ V = 3.$

To study this effect we plot in Fig. 8, $W$ vs $\lambda$ for three values of $V$. We show two cases, one for $U = 2$ (Fig. 8(a)) and another for $U = 2.5$ (Fig. 8(b)). The qualitative behavior is same for $U = 2$ and $U = 2.5$. First of all we note that below a certain value of $\lambda$, $W$ is larger for larger $V$. This is an expected behavior because as $V$ increases for a given $\lambda$ (below a certain $\lambda$), the GS energy decreases and therefore BE increases.

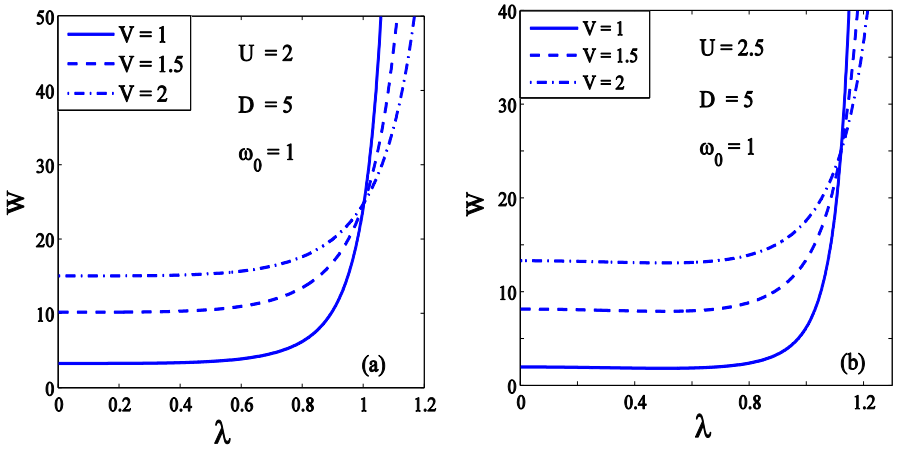


***Fig. 8*** *$W$ vs $\lambda$ with $D = 5$, $g(0) = 0.5$ and $\omega_0 = 1$ with (a) $U = 2$ ,(b) $U = 2.5$.*

We also observe that in general, $W$ increases with increasing $\lambda$. This is an expected behavior because in the present case, essentially the effective $U$ has a more dominant role than the effective $V$ as $\lambda$ increases. Strictly speaking, for an initial range of $\lambda$, BE does not change much with $\lambda$. Such a scenario has already been discussed in Fig. 4(a). With the increase in $\lambda$, the decrease in $V$ will tend to reduce BE and that in $U$ will enhance it. We have already seen before that for $U$ close to 2, these two effects essentially cancel each other making $W$ almost independent of $\lambda$ up to a certain value of $\lambda$. However as we have discussed earlier, at large $\lambda$, $V$ decreases substantially due to exponential reduction and consequently the behavior is

then determined essentially by effective $U$. It is understandable that the value of $\lambda$ above which the effective $U$ will take over depends on $V$. Obviously, this value of $\lambda$ will be larger if $V$ is larger. This explains the crossing behavior observed in Fig. 8. To show the dependence of BE on both the *el-el* interaction and the *el-ph* interaction together, we present three-dimensional plots for $W$ as a function of both $U$ and $\lambda$ in Figs. 9 and 10. One can see from Fig. 9 that in the adiabatic case, for a given value of $\lambda$, $W$ decreases with increasing $U$ and for a given value $U$, $W$ increases with increasing $\lambda$ below a critical $U$ above which $W$ decreases with increasing $\lambda$.

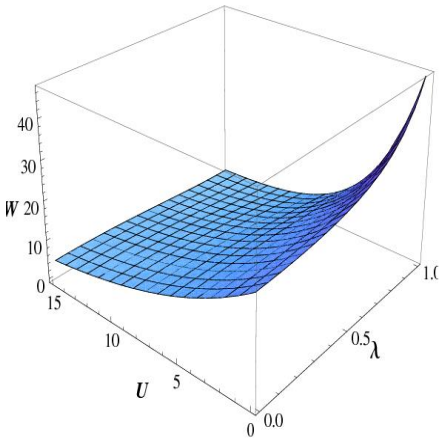


***Fig. 9*** *$W$ as a function of $U$ and $\lambda$ for $V = 3$.*

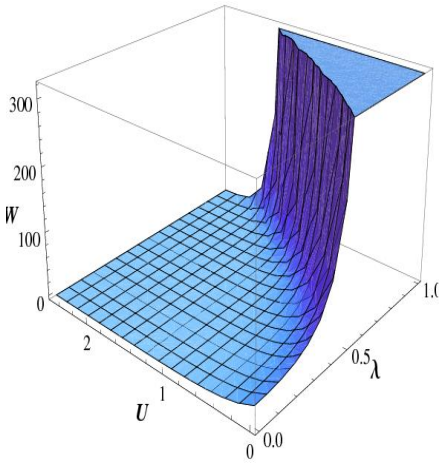


***Fig. 10*** *$W$ as a function of $U$ and $\lambda$ for $V = 0.5$.*

In the anti-adiabatic case (Fig. 10), it is clear that for a given value of $\lambda$, $W$ decreases with increasing $U$ and for a given value of $U$, it increases with increasing $\lambda$. It is also evident that the increase in $W$ with $\lambda$ is much more rapid at smaller values of $U$. At large values of $U$, $W$ becomes zero for all $\lambda$. All these observations are consistent with the arguments we presented earlier.

### 4.3.2 Results in the presence of magnetic field

In this section we analyze the results in the presence of an external magnetic field. Here $E_0$ is minimized with respect to $m$ to obtain the GS energy. In Figs. 11 and 12 we plot the GS energy as a function of $U$ and $\lambda$ respectively for different values of $B$ in an anti-adiabatic case $(V < \omega_0)$.

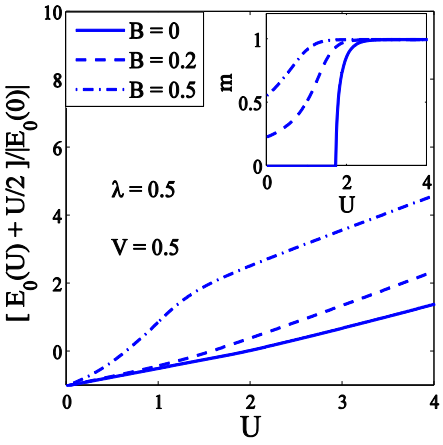


***Fig. 11*** *GS energy as a function of $U$. (**Inset:** $m$ as a function of $U$.)*

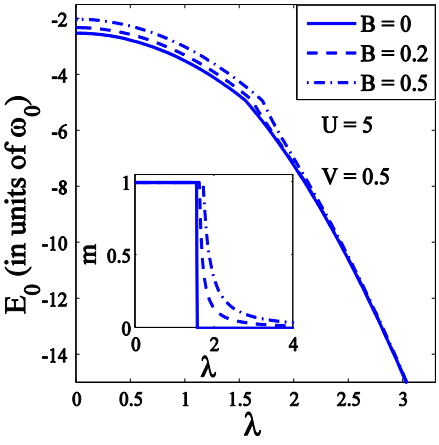


***Fig. 12*** *GS energy as a function of $\lambda$. (**Inset:** $m$ as a function of $\lambda$.)*

As expected, the GS energy increases with increasing $U$ and decreases as $\lambda$ increases. The reason for the increase in $E_0$ with $U$ is obvious. The decrease in $E_0$ with increasing $\lambda$ is due to the polaronic effect. One can observe from the insets that $m$ increases with increasing $U$ and $B$, but decreases as $\lambda$ increases. The onsite correlation opposes two electrons occupying the same impurity site and thus enhances $m$, while the magnetic field tries to align spins in its own direction leading to an increase in $m$. The *el-ph* interaction induces an attractive *el-el* interaction leading to an over-all reduction in the effective $U$ as a result of which $m$ decreases with increasing $\lambda$. Another

important observation one can make from the figures is that the reduction in $m$ with increasing $\lambda$ becomes slower as $B$ increases.

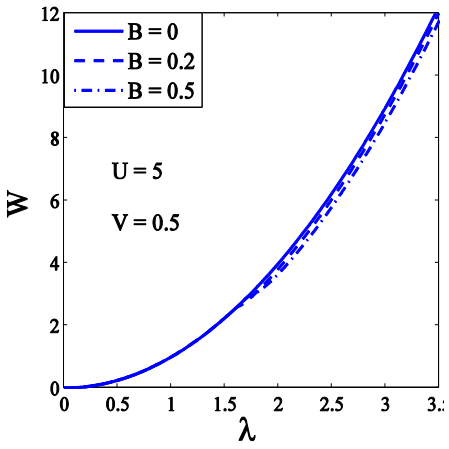


***Fig. 13*** *W energy as a function of* $\lambda$.

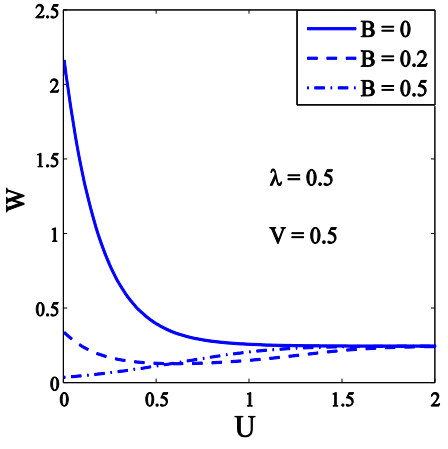


***Fig. 14*** *W energy as a function of* $U$.

Finally we examine the effect of *el-ph* and *el-el* interactions on the BE $W$ in the presence of an external magnetic field. In Figs. 13 and 14 we plot $W$ as a function of $\lambda$ and $U$ respectively for several values of $B$. As expected the *el-el* interaction and the magnetic field reduce $W$, while the *el-ph* interaction enhances it.

## 4.4 Summary

In this chapter, we have investigated the effect of Holstein's *el-ph* interaction on the total GS energy of the single-impurity AH system, local magnetic moment and BE between the impurity electron and the conduction electrons using the CV method. We have presented the results both in the presence and absence of a magnetic field. We have obtained the equations to determine the number of $d$ electrons of a given spin. Though we have

obtained magnetic solutions, the existence of these solutions is probably an artifact of the approximation used in the present calculation. We find that the GS energy in general increases with increasing $U$ which is of course an expected behavior. Furthermore, the GS energy is found to be lower in the adiabatic case than in the anti-adiabatic case, other parameters remaining same. We have shown that in the anti-adiabatic case, $W$ increases with increasing $\lambda$. Even for an adiabatic case, $W$ increases with increasing $\lambda$ for small values of $U$. However, for large $U$, we have shown that as $\lambda$ increases, BE initially decreases, reaches a minimum at some value of $\lambda$ $(\lambda_{min})$, which depends on the value of $U$, and then increases monotonically with $\lambda$. As a function of $U$, $W$ decreases with increasing $U$ for $\lambda = 0$ in both the adiabatic and the anti-adiabatic cases and becomes zero eventually. For $\lambda \neq 0$, the reduction in the effective on-site correlation has a more dominating effect than the decrease in the effective hopping parameter in the anti-adiabatic case $(V = 0.5)$ and consequently BE increases with $\lambda$ for a given $U$. For $V = 3$, i.e., in an adiabatic case, we have found that the increase in $W$ with $\lambda$ takes place only up to a certain value of $U$. This implies that as $\lambda$ increases, the effect of the decrease in effective $U$ continues to have a more dominating effect than the decrease in effective $V$ does at small $U$. At large $U$, as the *el-ph* interaction increases, the change in $U$ does not seem to have much effect as compared to the reduction in $V$ has and $W$ decreases with increase in $\lambda$. Thus above a certain value of $U$, $W$ undergoes a sharper fall for higher values of $\lambda$ leading to a crossing behaviour. We have also shown that $W$ increases with increasing $V$ below a certain value of $\lambda$ above which however, $W$ decreases with increasing $V$ again giving rise to a crossing behavior. Finally we have presented the three-dimensional phase diagrams for BE as a function of $\lambda$ and $U$ for both the adiabatic and anti-adiabatic cases.

In the presence of a magnetic field, the GS energy is found to increase with increasing onsite correlation $U$ and the magnetic field $B$, but it is found to decrease with the *el-ph* interaction strength $\lambda$. We have next shown that, in general, both the onsite Coulomb interaction $U$ and the external magnetic field $B$ suppress the binding between the local and the conduction electrons, while a large *el-ph* interaction enhances it. We have finally shown that the local magnetic moment $m$ increases with increasing $U$, and $B$, while it decreases as $\lambda$ increases.

## References

[1] R. Kikuchi, Phys. Rev. **81**, 988 (1951).

[2] T. Morita, J. Phys. Soc. Japan **12**, 1060 (1957).

[3] S. M. Bose & T. Tanaka, Phys. Rev. **176**, 600 (1968);
S. M. Bose & T. Tanaka, J. Phys. C: Solid State Phys. **3**, 958 (1970).

[4] T. Morita & T. Tanaka, Phys. Rev. **145**, 288 (1966).

[5] J. Halow, T. Tanaka & T. Morita, Phys. Rev. **175**, 680 (1968).
T. Tanaka, *Methods of statistical physics* (Cambridge University Press, 2002).

# Chapter **5**

# Effect of external magnetic field on the bound state in Anderson-Holstein model: An improved variational treatment

## 5.1 Introduction

In the preceding chapters we have employed conventional Lang-Firsov (LF) transformation to decouple the electron-phonon (*el-ph*) interaction in the Anderson-Holstein (AH) model, which is a good treatment in the strong-coupling limit. To improve the earlier results, in this chapter we employ the generalized (variational) LF transformation to treat the *el-ph* interaction for the entire range of the *el-ph* coupling strength. The aim of this chapter is to study the effects of the *el-ph* interaction and the magnetic field on the ground state (GS) energy, local magnetic moment and the binding energy (BE) between the magnetic impurity and the conduction electrons using the variational LF transformation and the CV method. We also study the phase diagram for the polaron-bipolaron transition.

## 5.2 Generalized Lang-Firsov transformation

The AH Hamiltonian in the presence of a magnetic field ($\boldsymbol{B}$) reads as

$$H = \sum_{\boldsymbol{k},\sigma} \varepsilon_{\boldsymbol{k}} n_{\boldsymbol{k}\sigma} + \sum_{\sigma} (\varepsilon_d - \mu_B \, \boldsymbol{B}.\boldsymbol{\sigma}) n_{d\sigma} + U n_{d\sigma} n_{d,-\sigma} + \hbar\omega_0 b^\dagger b + \sum_{\boldsymbol{k},\sigma} \left( V_{\boldsymbol{k}} {c^\dagger}_{d\sigma} c_{\boldsymbol{k}\sigma} + h.c \right) + \lambda \, \hbar\omega_0 \left( b^\dagger + b \right) \sum_{\sigma} n_{d\sigma}, \qquad (5.1)$$

As promised in the introduction we now employ a generalized or the variational LF transformation [1] with a generator: $S = \lambda \, \eta \left( b^\dagger - b \right) \sum_\sigma n_{d\sigma}$ to eliminate the *el-ph* interaction from the problem. In the conventional LF transformation, $\eta = 1$ which is a good prescription in the strong-coupling limit. Here we consider $\eta$ as a variational parameter to minimize the GS energy. Physically $\eta$ gives a measure of the polarization potential created by the *el-ph* interaction. The transformed Hamiltonian reads

$$\bar{H} = \sum_{\boldsymbol{k},\sigma} \varepsilon_{\boldsymbol{k}} \, n_{\boldsymbol{k}\sigma} + \sum_{\sigma} \tilde{\varepsilon}_{d\sigma} \, n_{d\sigma} + \tilde{U} n_{d\sigma} n_{d,-\sigma} + \hbar\omega_0 b^\dagger b + \sum_{\boldsymbol{k},\sigma} \left( V'_{\boldsymbol{k}} c^\dagger_{\boldsymbol{k}\sigma} c_{d\sigma} + h.c \right), \qquad (5.2)$$

where

$$\tilde{\varepsilon}_{d\sigma} = \varepsilon_d - \mu_B B\sigma - \hbar\omega_0 \lambda^2 \eta (2 - \eta), \qquad (5.3)$$

$$\tilde{U} = U - 2\lambda^2 \eta \hbar\omega_0 (2 - \eta), \qquad (5.4)$$

$$V'_{\boldsymbol{k}} = V_{\boldsymbol{k}} e^{\lambda\eta(b - b^\dagger)}. \qquad (5.5)$$

Since we are interested in the electron properties in this work, we perform a zero-phonon averaging of Eq. (5.2) to obtain an effective AH Hamiltonian given by

$$H_{eff} = \sum_{\boldsymbol{k},\sigma} \varepsilon_{\boldsymbol{k}} n_{\boldsymbol{k}\sigma} + \sum_{\sigma} \tilde{\varepsilon}_{d\sigma}\, n_{d\sigma} + \tilde{U}\, n_{d\sigma} n_{d,-\sigma} + \sum_{\boldsymbol{k},\sigma} \tilde{V}\left(c^{\dagger}_{\boldsymbol{k}\sigma} c_{d\sigma} + c^{\dagger}_{d\sigma} c_{\boldsymbol{k}\sigma}\right), \tag{5.6}$$

where,

$$\tilde{V} = V\, e^{-(\lambda^2\eta^2/2)}. \tag{5.7}$$

## 5.3 Results and discussion

We now proceed to calculate the GS energy $E_0$ and the binding energy $W$ between the impurity and the conduction electrons using the CV method as explained in the previous chapter. $E_0$ and $W$ are finally given by

$$E_0 = \sum_{\boldsymbol{k}>\boldsymbol{k}_F,\sigma} \varepsilon_{\boldsymbol{k}} \langle n_{\boldsymbol{k}\sigma}\rangle + \sum_{\boldsymbol{k}<\boldsymbol{k}_F,\sigma} |\varepsilon_{\boldsymbol{k}}|(1 - \langle n_{\boldsymbol{k}\sigma}\rangle) + \sum_{\sigma} \tilde{\varepsilon}_{d\sigma}\langle n_{d\sigma}\rangle + \frac{1}{4}\tilde{U}(N^2 - m^2) - \sum_{\sigma} \varepsilon_{0\sigma}\, \eta_{d\sigma}^{1/2}, \tag{5.8}$$

$$W = 2D^2 g(0) \exp\left[-\frac{|\tilde{\varepsilon}_d| + \mu_B B}{g(0)\left|\tilde{V}\right|^2}\right] - (N-1)\tilde{\varepsilon}_d + \lambda^2\eta(2-\eta)\hbar\omega_0 + (m-1)\mu_B B. \tag{5.9}$$

We minimize $E_0$ with respect to $\eta$ and $m$ numerically. We find that $E_0$ in general increases with increasing $U$ in both adiabatic and anti-adiabatic cases. In Figs. 1 and 2 we show the explicit variation of $E_0$ as a function of

$\lambda$ for a couple of values of $B$. Fig. 1 shows the behavior for an anti-adiabatic case while Fig. 2 represents an adiabatic case. It is evident that $E_0$ decreases with increasing $\lambda$ in both cases. Furthermore, the figures show that the decrease is nonlinear which is understandable because the *el-ph* interaction contributes to the energy in the second order. This is the so-called polaronic effect which reduces the energy by a factor that is quadratic in $\lambda$ in the weak *el-ph* coupling regime. As $\lambda$ increases, the polaronic correction gets significant contributions from higher powers of $\lambda$ as well, justifying the sharper fall in the GS energy at large values of $\lambda$. It seems from Fig. 1 that in the presence of the magnetic field, as $\lambda$ increases, at some critical value of $\lambda$, $E_0$ changes its gradient discontinuously. As $B$ increases, the discontinuity in $dE_0/d\lambda$ occurs at a larger value of $\lambda$. This discontinuity at some critical value of $\lambda$ is symptomatic of a transition in the polaron system. However the details of the transition are not clear from this figure. Some changes also take place in the adiabatic case as a function of $\lambda$, but the effect looks less severe as can be seen from Fig. 2.

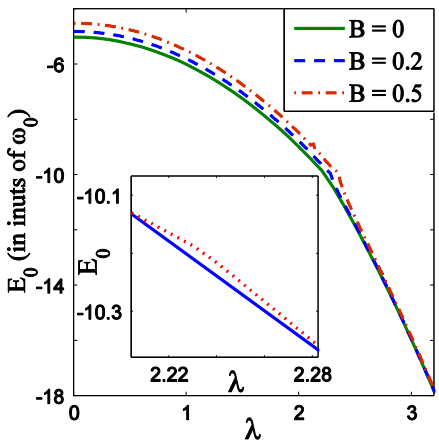


***Fig. 1*** *$E_0$ vs $\lambda$ for $B$= 0, 0.2, 0.5 and $V = 0.5$. (**Inset**: Present results (solid line) vis-à-vis those with $\eta = 1$ (dotted line) for $B = 0$.)*

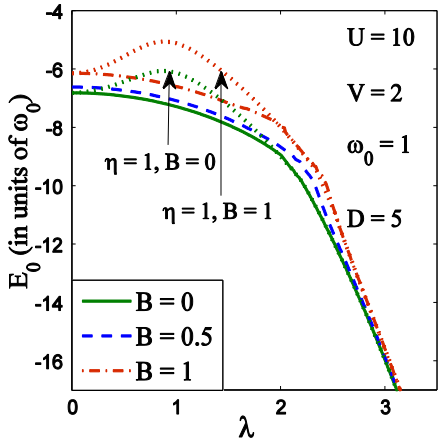


***Fig. 2*** *$E_0$ vs $\lambda$ for $B$ = 0, 0.5, 1 and $V = 2$.*

In Fig. 1, the inset compares the $B = 0$ results of the variational LF transformation with those with LF transformation ($\eta = 1$). The improvement is however only marginal. In Fig. 2 also, we plot the results for $\eta = 1$ in the absence of the magnetic field. It is clearly evident that the introduction of $\eta$ lowers the GS energy $E_0$ substantially in the adiabatic case. Thus the variational LF transformation provides more accurate results particularly in the adiabatic regime. In Fig. 3, we show the variation of $m$ as a function of *el-ph* interaction strength $\lambda$ for different values of $B$. Fig. 3(a) shows that the magnetic field has no effect on the $\lambda$ dependence of $m$ up to a certain value of $\lambda$. This is because $m$ is influenced by both the magnetic field and the *el-ph* interaction. As $\lambda$ increases, the effective onsite Coulomb correlation decreases leading to a reduction in the value of $m$.

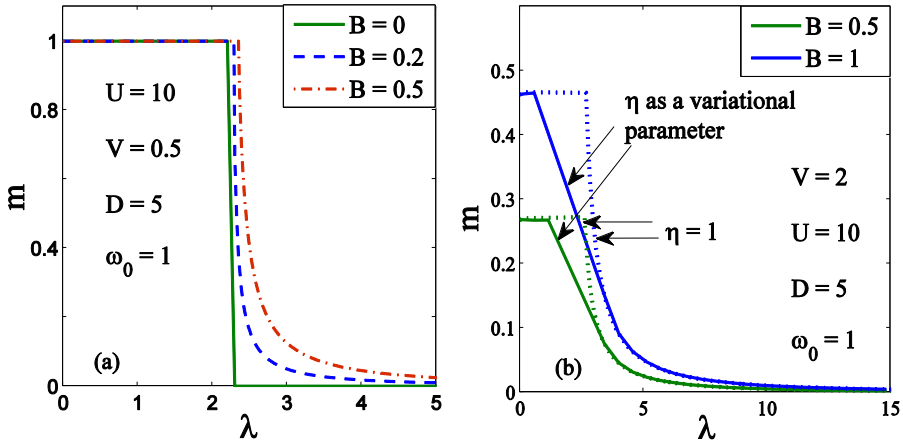


***Fig. 3*** *Local moment $m$ as a function of $\lambda$ with $U = 10$, for (a) an anti-adiabatic case ($V = 0.5$) with $B$ =0, 0.2, 0.5, (b) an adiabatic case ($V = 2$) with $B$ = 0.5, 1.*

On the other hand, as $B$ increases, the electron spins will be forced to align in the same direction and as a result the double occupancy will be prevented on the impurity site leading to a larger value of $m$. Thus the *el-ph* interaction and the magnetic field have opposite effects on $m$. Thus, for a given value

of $B$, if $V$ is small and $U$ is sufficiently large, as $\lambda$ increases, the effective Coulomb repulsion remains reasonably large below a critical value of $\lambda$ preventing a double occupancy at the impurity site. In this regime, we have $m = 1$ which can be described as a single-polaron state. At a critical value of $\lambda$ ($\lambda_c$), $m$ undergoes a sharp fall and then slowly goes to zero as $\lambda$ further increases. This is because the effective onsite Coulomb interaction changes sign at $\lambda_c$ leading to an effective attractive *el-el* interaction facilitating eventually the formation of a singlet bipolaronic state at the impurity site which corresponds to $m = 0$. Thus the transition from $m = 1$ state to $m = 0$ state can be interpreted as a polaron-bipolaron transition. It is interesting to mention that the polaron to bipolaron transition is not direct but goes through a mixed state which is a linear superposition of a polaron state and a bipolaron state. One can immediately see that the value of $\lambda_c$ obtained from Fig. 3(a) is the same as the one observed in the GS energy in Fig. 1. Thus the transition shown in $E_0$ is also a signature of the polaron-bipolaron transition. Fig. 3(b) shows the $m$ vs $\lambda$ graph for $V = 2$ and $U = 10$. Here one can see that again the value of $m$ remains constant, albeit small, up to a critical value of $\lambda$. That $m$ can have only small values in the adiabatic case (even for small values of $\lambda$) can be easily understood in the following way. In the adiabatic case, the probability of hopping of an electron from the conduction band to the impurity level is pretty high and as a result the double occupancy becomes partially possible, even if $\lambda$ is small and $U$ is reasonably large. It appears that for small values of $\lambda$, $m$ is hardly influenced by the *el-ph* interaction. However as $\lambda$ exceeds a certain critical value of $\lambda(\lambda_c)$, the effect of *el-ph* interaction becomes important so much so that the possibility of double occupancy then starts increasing with $\lambda$ and consequently $m$ starts decreasing almost linearly beyond $\lambda_c$ up to another critical value of $\lambda$ beyond which $m$ decreases very slowly to zero. Compared to the anti-adiabatic case, here $m$ becomes zero at a much larger value of $\lambda$. Another interesting observation one can make in the adiabatic

case is that here up to a large value of $\lambda$, $m$ is strongly dependent on $B$. To be more specific, $m$ increases with increasing $B$. Thus we can clearly have two limiting scenario in the adiabatic case. If the applied magnetic field is sufficiently large, then for large $V$, it is possible to have a polaronic state at the impurity site at small $\lambda$ and a bipolaronic state as $\lambda$ is increased. On the other hand, for small values of $B$, unless $U$ is extremely large, $m$ will have small non-zero values below a certain value of $\lambda$. At a large value $\lambda$, of course, $m$ becomes zero implying the formation a bipolaron on the impurity site. Thus in the adiabatic case, in the presence of a very large magnetic field, there can be a polaron-bipolaron transition as a function of $\lambda$. However, for a finite but not so large value of the magnetic field, if $V$ is not too large, then at small value of $\lambda$, the state on the impurity site can be a mixed one i.e., a linear superposition of the polaronic and bipolaronic states. As $\lambda$ increases, spectral weight of the bipolaron state will increase and that of polaron state will decrease so that at a certain value of $\lambda$, the state will collapse into a bipolaronic state corresponding to $m = 0$. However, if $V$ is very large, then the impurity state will be a bipolaronic state for all values of the *el-ph* coupling constant unless the magnetic field is too large. We have again compared our present results with the $\eta = 1$ results. It is interesting to note that the introduction of the variational parameter $\eta$ brings a qualitative change in the behavior of $m$. For example, according to the present improved calculation $m$ decreases continuously as $\lambda$ increases unlike in the $\eta = 1$ case and also the decrease is much less sharp. Furthermore the accuracy of the present calculation increases with increasing $B$. To study the issue of transition in some more detail, we plot in Fig. 4, the variation of $\eta$ as a function of $\lambda$ for different values of $B$ in anti-adiabatic and adiabatic cases. In the anti-adiabatic case (Fig. 4(a)), as $\lambda$ increases, $\eta$ initially remains constant and then undergoes a couple of jumps and eventually saturates to a constant with further increase in $\lambda$. The critical values of $\lambda$ where the jumps in $\eta$ take place become smaller with increasing $B$. The

behavior of $\eta$ vs $\lambda$ clearly shows three regions which agree with the $m$ *vs* $\lambda$ graphs. These critical values of $\lambda$ match exactly with the ones obtained from the energy and the magnetic moment graphs. Thus the sudden change in $\eta$ clearly reflects the formation of a bipolaron at the impurity atom.

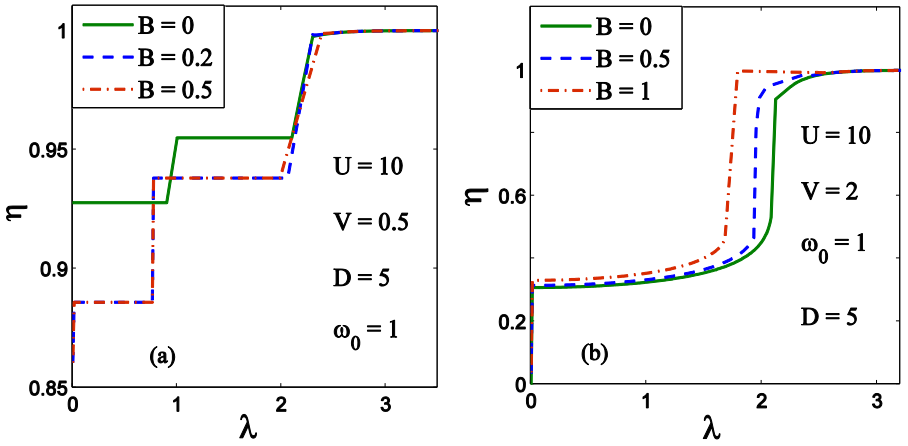


***Fig. 4*** *Variational parameter* $\eta$ *as a function of el-ph interaction strength* $\lambda$ *for* $(a)$ *an anti-adiabatic case* $(V = 0.5)$*with* $B = 0, 0.2, 0.5,$ $(b)$ *an adiabatic case* $(V = 2)$ *with* $B = 0, 0.5, 1.$

We have also studied the variation of $E_0$ as a function of $\eta$. We find that $E_0$ undergoes a sudden fall at the same value of $\eta$. In the adiabatic case (Fig. 4(b)), as $\lambda$ increases from zero, $\eta$ initially increases very slowly but as $\lambda$ attains a certain critical value, $\eta$ increases rapidly to the value 1 and remains constant with further increase in $\lambda$. This state corresponds to $m = 0$ which clearly indicates the formation of a bipolaron. Fig. 5 shows the dependence of $m$ on $U$. Fig. 5(a) shows the results for an anti-adiabatic case while Fig. 5(b) gives results for an adiabatic regime. We can observe several things from these figures. With increasing $U$, $m$ increases in both the regimes. However, for the same value of $U$, $m$ has in general much larger value in the anti- adiabatic case. In the adiabatic case, $m$ increases monotonically but

slowly with $U$ so that $m$ remains small as long as $V$ or $\lambda$ are not unreasonably large. On the other hand, in the anti-adiabatic case, $m$ saturates to 1 beyond a certain value of $U$ that depends on $B$. It is clear that in the adiabatic case, unless $U$ is unreasonably large,

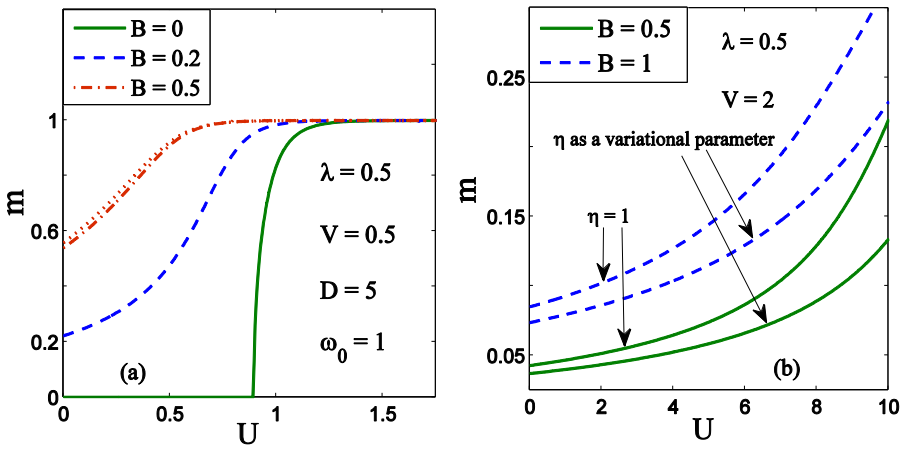


***Fig. 5*** *Local moment m as a function of el-el interaction strength U for (a) an anti-adiabatic case* ($V = 0.5$) *with* $B = 0, 0.2, 0.5$, *(b) an adiabatic case* ($V = 2$) *with* $B = 0.5, 1$.

the impurity site would be in a mixed state with spectral weight for the bipolaronic state being much larger. Of course, with increase in $U$, the spectral weight for the polaronic state increases. On the other hand, in the anti-adiabatic case, as $U$ increases, there is a transition from a mixed state to the polaronic state. It is clear that in the anti-adiabatic case (Fig. 5(a)), the improvement is only marginal, while in the adiabatic case (Fig. 5(b)), the variational LF transformation leads to a significant difference in the local moment results. In fact, the conventional LF transformation overestimates the local moment. One can also observe that the variational LF transformation becomes more and more important as the magnetic field increases. The main important objective of this work is to examine the

combined effect of *el-ph* and *el-el* interactions on BE between the localized and the conduction electrons in the presence of a magnetic field.

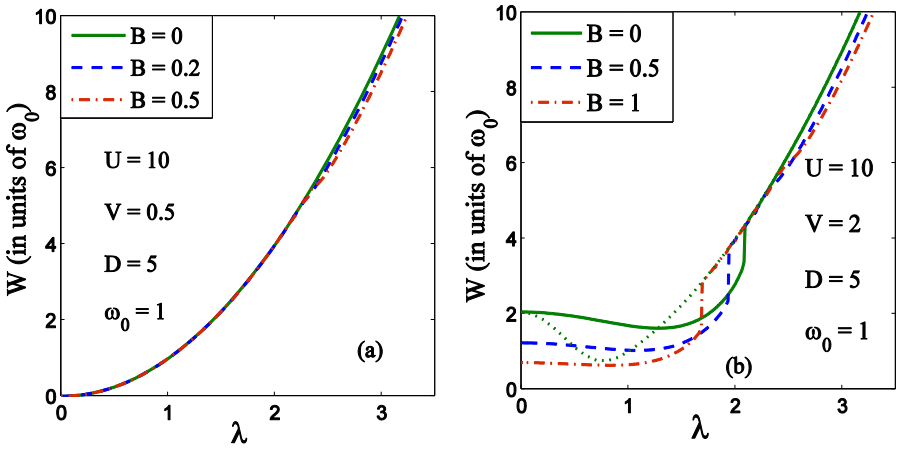


***Fig. 6*** *$W$ as a function of $\lambda$ for ($a$) an anti-adiabatic case ($V = 0.5$) with $B$ = 0, 0.2, 0.5, ($b$) an adiabatic case ($V = 2$) with $B$ = 0, 0.5, 1 (Dotted line is for $\eta = 1, B = 0$).*

In Fig. 6, we plot $W$ as a function of $\lambda$ for several values of $B$. Fig. 6(a) shows the variation in an anti-adiabatic case while Fig. 6(b) refers to an adiabatic case. In both cases, $W$ increases with $\lambda$. Quantitatively, however, at small $\lambda$, the binding is stronger in the adiabatic case. The reason is clear. The $s-d$ interaction favours hybridization between the conduction electrons and the localized electron. Therefore, an increase in $V$ would favour binding. However as $\lambda$ increases, the behavior becomes similar in the two cases. We present in Fig. 7, $W$ vs $U$ results for different values of $B$. As expected, the *el-el* interaction reduces $W$ in both adiabatic (Fig. 7(a)) and anti-adiabatic (Fig. 7(b)) regimes. However the fall in $W$ is sharper in the anti-adiabatic regime. This happens because a small $V$ is not favourable for the formation of a bound state between local and conduction electrons at the impurity site. Also as $B$ increases, $W$ usually decreases. This decrease reduces as $U$ increases. In the anti-adiabatic case, above a certain $U$, $W$

becomes almost independent of both $B$ and $U$. In the adiabatic case, as $U$ increases, $W$ eventually approaches zero. This represents a polaronic state.

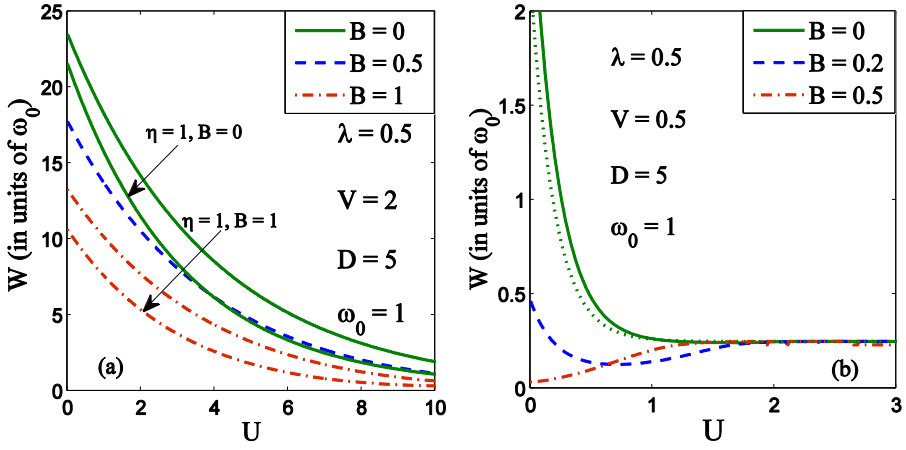


***Fig. 7*** *$W$ as a function of $U$ for (a) an adiabatic case ($V = 2$) with $B$ = 0, 0.5, 1, (b) an anti-adiabatic cases ($V = 0.5$) with $B$ = 0, 0.2,0.5 (Dotted line is for $\eta = 1, B = 0$).*

It is also clear from the figures that the conventional LF transformation ($\eta = 1$) underestimates BE at the impurity site. Variations of $W$ with $B$ are shown explicitly in Fig. 8 for different values of $\lambda$ in adiabatic and anti-adiabatic cases respectively. Fig. 8(a) shows that in an adiabatic case, as $B$ increases, $W$ decreases and becomes zero eventually. Fig. 8(b) shows that in the anti-adiabatic case, $W$ reduces to zero quite fast in the absence of *el-ph* interaction, while in the presence of the *el-ph* interaction, $W$ vs $B$ is very interesting. In fact $W$ does not become zero at all. It shows a complicated behavior and eventually saturates to a finite value. We also show our results for $\eta = 1$. In the adiabatic case, $\eta = 1$ provides weaker binding. From Figs. 5 and 7, it is clear that $m$ and $W$ are competing quantities. As $U$ increases, $m$ increases but $W$ decreases. In the anti-adiabatic case, in the presence of *el-ph* interaction, there exists a critical value of $U$ below which

the impurity will be in a bipolaron state and above this critical $U$, double occupancy will be prevented and one will have a polaronic state. This transition becomes more smoother as the magnetic field is increased.

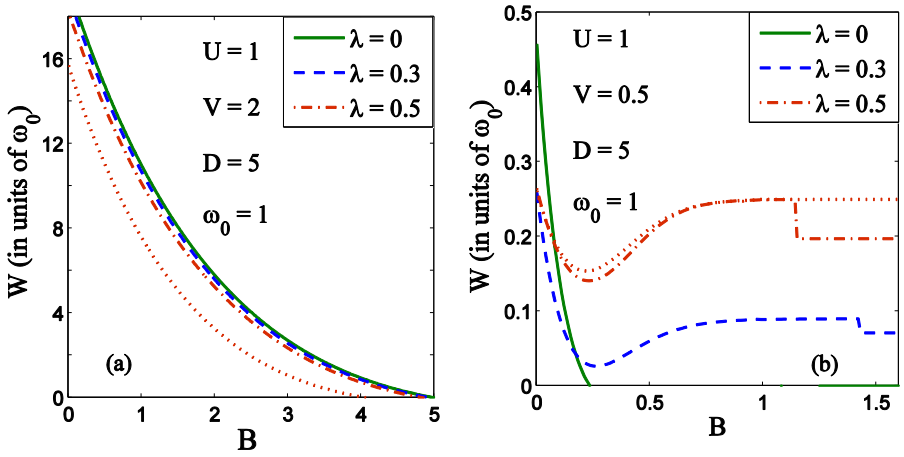


***Fig. 8*** *$W$ as a function magnetic field $B$ with $\lambda = 0, 0.3, 0.5$ for (a) an adiabatic case $(V = 2)$, (b) an anti-adiabatic case $(V = 0.5)$. (Dotted lines are for $\eta = 1$, $\lambda = 0.5$).*

In Fig. 9 we finally show the polaron-bipolaron phase diagram in an anti-adiabatic region.

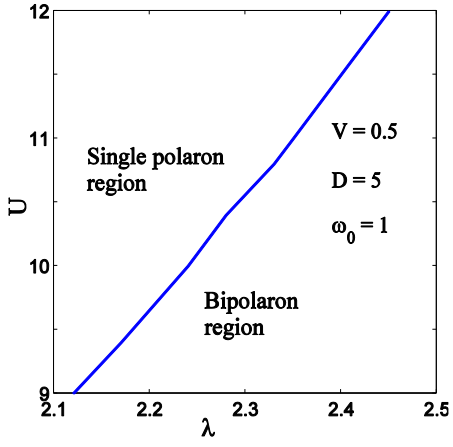


***Fig. 9*** *Polaron-bipolaron phase diagram in the $U - \lambda$ plane.*

## 5.4 Summary

In this chapter we have studied the AH model in the presence of an external magnetic field at zero temperature in three dimensions. The phonons have been eliminated by using a variational LF transformation followed by zero-phonon averaging and the resulting effective Anderson model has been solved by employing the CV method. We have investigated the effect of *el-ph* interaction on the total GS energy of the system, the BE between the impurity electron and the conduction electrons and the local magnetic moment of the impurity electron. The GS energy is found to increase with increasing $U$ and $B$, but with increasing $\lambda$ it is found to decrease due to the polaronic effect. We have shown that an increase in either $U$ or $B$ weakens the binding between the local and the conduction electrons, while that in $\lambda$ or $V$ strengthens it. The parameter $\eta$ is shown to undergo an increase at a critical $\lambda$ indicating a transition in the impurity state. In the anti-adiabatic case, $m$ is equal to 1 at $\lambda = 0$ which represents a polaronic state. As $\lambda$ increases, $m$ decreases and becomes zero at a critical value of $\lambda$ ($\lambda_c$) indicating the formation of a bipolaron on the impurity site. Thus at $\lambda = \lambda_c$, impurity state undergoes a polaron-bipolaron transition. Also for a given $\lambda$, there exists a critical value of $U$ at which the state at the impurity site undergoes a bipolaron-polaron transition that becomes smoother with increasing magnetic field. A slightly different kind of transition is observed in the adiabatic cases. For example, if $U$ and $B$ are not too large, the state on the impurity site at small $\lambda$ would be a linear superposition of a polaron and bipolaron states which would settle into a bipolaron state if $\lambda$ is increased beyond a critical value. We have shown the polaron-bipolaron phase diagram for a particular anti-adiabatic case in the $U - \lambda$ plane.

# References

[1] I. G. Lang & Yu. A. Firsov, Zh. Eksp. Teor. Fiz.**43**, 1843 (1962) [Sov. Phys. JETP**16**, 1301 (1963)];
A. N. Das & S. Sil, J. Phys.: Condens. Matter **5**, 8265 (1993);
Y. Takada & A. Chatterjee, Phys. Rev. B **67**, 081102 (R) (2003).

Chapter **6**

# Magnetic impurity in superconducting host: The Anderson-Holstein-BCS model

## 6.1 Introduction

In the previous chapters we have studied the properties of a magnetic impurity in a non-magnetic metal host using the Anderson-Holstein (AH) model. In the present chapter we consider the AH-BCS model to study a magnetic impurity in a BCS superconductor. The effects of a magnetic impurity on a superconductor [1] have been studied quite extensively in the past. These studies were mainly based on the Anderson model [2-4] and the $s-d$ exchange model [5, 6]. Abrikosov and Gor'kov (AG) have been the first to develop a theory for a superconductor in the presence of a few magnetic impurities [7]. It has been suggested that magnetic impurities would suppress superconductivity because of the de-pairing effect and furthermore, an intermediate impurity concentration may lead to a gapless superconductivity. Tunneling experiments on PbGd [8] and specific heat measurements on LaGd [9] have confirmed the prediction of gapless superconductivity. Also in the conventional superconductors the magnetic impurity forms a bound state within the superconducting gap with conduction electrons by de-pairing the Cooper pairs [6, 10, 11]. It leads to the competition between the Cooper pair formation and the Kondo effect [12-15].

The main goal of this chapter is to study the effect of the superconducting order parameter on the properties a magnetic impurity embedded in a superconducting host metal in the presence of an *el-ph* interaction in the localized impurity. Furthermore, we study the phase diagrams for the bound and unbound states, and the phase diagram for the polaron-bipolaron transition for both adiabatic and anti-adiabatic cases.

## 6.2 Effective Anderson-Holstein-BCS Hamiltonian

As introduced in Chapter 1, the AH-BCS Hamiltonian can be written as

$$H = \sum_{\boldsymbol{k},\sigma} \varepsilon_{\boldsymbol{k}\sigma} n_{\boldsymbol{k}\sigma} + \Delta \sum_{\boldsymbol{k},\sigma} \left(c^{\dagger}_{\boldsymbol{k},\sigma} c^{\dagger}_{-\boldsymbol{k},-\sigma} + h.c\right) + \sum_{\sigma} \varepsilon_d n_{d\sigma} + U n_{d\downarrow} n_{d\uparrow} + \sum_{\boldsymbol{k},\sigma} V_k \left(c^{\dagger}_{\boldsymbol{k}\sigma} c_{d\sigma} + h.c\right) + \hbar\omega_0 \left(b^{\dagger} b\right) + \lambda\hbar\omega_0 \left(b + b^{\dagger}\right) \sum_{\sigma} n_{d\sigma}. \tag{6.1}$$

Performing the variational Lang-Firsov (LF) transformation followed by the zero phonon averaging, we get the following effective Hamiltonian

$$H_{eff} = \sum_{\boldsymbol{k},\sigma} \varepsilon_{\boldsymbol{k}\sigma} n_{\boldsymbol{k}\sigma} + \Delta \sum_{\boldsymbol{k},\sigma} \left(c^{\dagger}_{\boldsymbol{k}\sigma} c^{\dagger}_{-\boldsymbol{k},-\sigma} + h.c\right) + \sum_{\sigma} \tilde{\varepsilon}_d n_{d\sigma} + \widetilde{U}\, n_{d\downarrow} n_{d\uparrow} + \sum_{\boldsymbol{k},\sigma} \widetilde{V} \left(c^{\dagger}_{\boldsymbol{k}\sigma} c_{d\sigma} + h.c\right), \tag{6.2}$$

where,

$$\tilde{\varepsilon}_d = \varepsilon_d - \eta\lambda^2\hbar\omega_0(2-\eta), \tag{6.3}$$

$$\widetilde{U} = U - 2\eta\lambda^2\hbar\omega_0(2-\eta), \tag{6.4}$$

$$\widetilde{V} = V\, e^{-(\lambda^2\eta^2/2)}. \tag{6.5}$$

## 6.3 Cluster variation method

As introduced in Chapter 4, the free energy of a system is defined as: $F = Tr\left[\rho_t \left(H_{eff} + K_B T\, ln\rho_t\right)\right]$, where $Tr$ is the trace operation, $K_B$ is the Boltzmann constant, $T$ is the absolute temperature and $\rho_t$ is the normalized density matrix given by

$$\rho_t = \frac{e^{-\beta H}}{Tr\,[e^{-\beta H}]}, \qquad \beta = \frac{1}{K_B T} \quad . \tag{6.6}$$

The free energy of a system is then given by

$$F = \sum_j tr_j h^{(1)}(j)\rho_t^{(1)}(j) + \sum_{j>\boldsymbol{k}} tr_{j,k} h^{(2)}(j,\boldsymbol{k})\,\rho_t^{(2)}(j,\boldsymbol{k}) + K_B T \sum_j \gamma^{(1)}(j) + K_B T \sum_{j>k} \gamma^{(2)}(j,\boldsymbol{k}) \tag{6.7}$$

$$\begin{aligned} F = {} & \sum_{\boldsymbol{k},\sigma} \varepsilon_{\boldsymbol{k}} tr_{\boldsymbol{k}\sigma}\rho_t^{(1)}(k\sigma) n_{\boldsymbol{k}\sigma} + \sum_{\sigma} \tilde{\varepsilon}_{d\sigma}\, tr_{d\sigma}\rho_t^{(1)}(d\sigma) n_{d\sigma} \\ & + \tilde{U}\left(tr_{d\sigma}\rho_t^{(1)}(d\sigma) n_{\boldsymbol{d}\sigma}\right)\left(tr_{d,-\sigma}\rho_t^{(1)}(d,-\sigma) n_{d,-\sigma}\right) \\ & + \Delta \sum_{\boldsymbol{k},\sigma} tr_{\boldsymbol{k}\sigma,-\boldsymbol{k}\sigma}\,\rho_t^{(2)}(\boldsymbol{k}\sigma,-\boldsymbol{k}\sigma)\left(c^{\dagger}{}_{\boldsymbol{k}\sigma} c_{-\boldsymbol{k}\sigma} + h.c\right) \\ & + \tilde{V} \sum_{\boldsymbol{k},\sigma} tr_{\boldsymbol{k}\sigma,d\sigma}\,\rho_t^{(2)}(\boldsymbol{k}\sigma,d\sigma)\left(c^{\dagger}{}_{d\sigma} c_{\boldsymbol{k}\sigma} + h.c\right) \\ & + K_B T \sum_{\boldsymbol{k},\sigma} tr_{\boldsymbol{k}\sigma}\rho_t^{(1)}(\boldsymbol{k}\sigma)\, ln\rho_t^{(1)}(\boldsymbol{k}\sigma) \end{aligned}$$

$$+ K_B T \sum_{\sigma} tr_{\sigma} \rho_t^{(1)}(d\sigma)\, ln\rho_t^{(1)}(d\sigma)$$

$$+ K_B T \sum_{\boldsymbol{k},\sigma} \Big[ tr_{\boldsymbol{k}\sigma,d\sigma} \rho_t^{(2)}(\boldsymbol{k}\sigma, d\sigma)\, ln\rho_t^{(2)}(\boldsymbol{k}\sigma, d\sigma)$$

$$- tr_{\boldsymbol{k}\sigma} \rho_t^{(1)}(\boldsymbol{k}\sigma)\, ln\rho_t^{(1)}(\boldsymbol{k}\sigma)$$

$$- tr_{\sigma} \rho_t^{(1)}(d\sigma)\, ln\rho_t^{(1)}(d\sigma)$$

$$+ tr_{\boldsymbol{k}\sigma,-\boldsymbol{k}\sigma} \rho_t^{(2)}(\boldsymbol{k}\sigma, -k\sigma)\, ln\rho_t^{(2)}(\boldsymbol{k}\sigma, -\boldsymbol{k}\sigma)$$

$$- tr_{\boldsymbol{k}\sigma} \rho_t^{(1)}(\boldsymbol{k}\sigma)\, ln\rho_t^{(1)}(\boldsymbol{k}\sigma)$$

$$- tr_{\boldsymbol{k}\sigma} \rho_t^{(1)}(-\boldsymbol{k}, -\sigma)\, ln\rho_t^{(1)}(-\boldsymbol{k}, -\sigma) \Big], \qquad (6.8)$$

In the previous chapter we have given the prescription for the reduced trial density matrices $\rho_t^{(1)}(\boldsymbol{k}\sigma)$, $\rho_t^{(1)}(d\sigma)$, and $\rho_t^{(2)}(\boldsymbol{k}\sigma, d\sigma)$. Here we choose the trial density matrix $\rho_t^{(2)}(\boldsymbol{k}\sigma, -\boldsymbol{k}\sigma)$ [16] as

$$\rho_t^{(2)}(\boldsymbol{k}\sigma, -\boldsymbol{k}\sigma) = \begin{bmatrix} a & 0 & 0 & e \\ 0 & b & 0 & 0 \\ 0 & 0 & c & 0 \\ f & 0 & 0 & d \end{bmatrix}, \qquad (6.9)$$

where

$$a = \langle n_{\boldsymbol{k}} n_{-\boldsymbol{k}} \rangle, \qquad b = \langle n_{\boldsymbol{k}} - n_{\boldsymbol{k}} n_{-\boldsymbol{k}} \rangle, \qquad c = \langle n_{-\boldsymbol{k}} - n_{\boldsymbol{k}} n_{-\boldsymbol{k}} \rangle,$$

$$d = \langle n_{\boldsymbol{k}} - n_{\boldsymbol{k}} n_{-\boldsymbol{k}} \rangle, \qquad e = \langle c_{\boldsymbol{k}} c_{-\boldsymbol{k}} \rangle, \qquad f = \langle c_{\boldsymbol{k}}^{\dagger} c_{-\boldsymbol{k}}^{\dagger} \rangle.$$

After diagonalization of $\rho_t^{(2)}(\boldsymbol{k}\sigma, d\sigma)$, the free energy reads

$$F = U^{(1)} + U^{(2)} - TS^{(1)} - TS^{(2)}, \tag{6.10}$$

with

$$U^{(1)} = \sum_{\boldsymbol{k},\sigma} \varepsilon_k \langle n_{\boldsymbol{k}\sigma} \rangle + \sum_{\sigma} \tilde{\varepsilon}_{d\sigma} \langle n_{d\sigma} \rangle \,, \tag{6.11}$$

$$U^{(2)} = \tilde{U} \langle d_{d\sigma} \rangle \langle n_{d-\sigma} \rangle + \tilde{V} \sum_{\boldsymbol{k},\sigma} \left( \xi_{\boldsymbol{k}d\sigma} + \xi_{\boldsymbol{k}d\sigma}^{\dagger} \right) + \Delta \sum_{\boldsymbol{k},\sigma} \left( \eta_{\boldsymbol{k},\sigma} + \eta_{\boldsymbol{k},\sigma}^{\dagger} \right), \tag{6.12}$$

where,

$$\xi_{\boldsymbol{k}d\sigma} = \langle c_{\boldsymbol{k}\sigma}^{\dagger} c_{d\sigma} \rangle, \tag{6.13}$$

$$\eta_{\boldsymbol{k},\sigma} = \langle c_{\boldsymbol{k}}^{\dagger} c_{-\boldsymbol{k}}^{\dagger} \rangle, \tag{6.14}$$

$$\begin{aligned} S^{(1)} \; = & -K_B \sum_{\boldsymbol{k},\sigma} [\, \langle n_{\boldsymbol{k}\sigma} \rangle \, ln \langle n_{\boldsymbol{k}\sigma} \rangle + (\, 1 - \langle n_{\boldsymbol{k}\sigma} \rangle \,) \, ln(\, 1 - \langle n_{\boldsymbol{k}\sigma} \rangle \,) \,] \\ & -K_B \sum_{\sigma} [\langle n_{d\sigma} \rangle \, ln \langle n_{d\sigma} \rangle + (1 - \langle n_{d\sigma} \rangle) \, ln(1 - \langle n_{d\sigma} \rangle)] \,, \end{aligned} \tag{6.15}$$

$$\begin{aligned} S^{(2)} \; = & - K_B \sum_{\boldsymbol{k},\sigma} \{A \, ln(A) + \; B \, ln(B) - \; K_B \sum_{\boldsymbol{k},\sigma} \{C \, ln(C) + \; D \, ln(D) \\ & - \langle n_{\boldsymbol{k}\sigma} \rangle \, ln \langle n_{\boldsymbol{k}\sigma} \rangle - (\, 1 - \langle n_{\boldsymbol{k}\sigma} \rangle \,) \, ln[1 - \langle n_{\boldsymbol{k}\sigma} \rangle] \\ & - \langle n_{d\sigma} \rangle \, ln \langle n_{d\sigma} \rangle - (1 - \langle n_{d\sigma} \rangle) \, ln[\, 1 - \langle n_{d\sigma} \rangle \,] \,\} \\ & - K_B \sum_{k,\sigma} \{E \, ln(E) + \; F \, ln(F) + G \, ln(G) + H \, ln(H) \end{aligned}$$

$$- \langle n_{k\sigma} \rangle \, ln\langle n_{k\sigma} \rangle \; - \; \langle n_{-k\sigma} \rangle \, ln\langle n_{-k\sigma} \rangle$$

$$- ( \, 1 - \langle n_{k\sigma} \rangle \, ) ln \, [1 - \langle n_{k\sigma} \rangle]$$

$$- (1 - \langle n_{-k\sigma} \rangle \, ) \, ln[1 - \langle n_{-k\sigma} \rangle] \, \} \, , \qquad (6.16)$$

where,

$$a = ( \, ( \, \langle n_{k\sigma} \rangle - \langle n_{d\sigma} \rangle \, )^2 + 4 \, |\xi_{kd\sigma}|^2 \, ),$$

$$b = (1 - \langle n_{k\sigma} \rangle - \langle n_{-k\sigma} \rangle \, )^2 + 4 \, \eta_{k,-k} \, \eta^{\dagger}_{k,-k} \, ,$$

$$A = \langle n_{k\sigma} \rangle \, \langle n_{d\sigma} \rangle \; ,$$

$$B = \frac{1}{2} \, \left[ \, \langle n_{k\sigma} \rangle + \langle n_{d\sigma} \rangle - 2 \langle n_{k\sigma} \rangle \langle n_{d\sigma} \rangle + \sqrt{a} \, \right],$$

$$C = \frac{1}{2} \left[ \, \langle n_{k\sigma} \rangle + \langle n_{d\sigma} \rangle - 2 \, \langle n_{k\sigma} \rangle \, \langle n_{d\sigma} \rangle - \sqrt{a} \right],$$

$$D = [1 - \langle n_{k\sigma} \rangle - \langle n_{d\sigma} \rangle + \langle n_{k\sigma} \rangle \, \langle n_{d\sigma} \rangle],$$

$$E = [ \, \langle n_{k\sigma} \rangle - \langle n_{k\sigma} \rangle \, \langle n_{-k\sigma} \rangle \, ],$$

$$F = [ \, \langle n_{-k\sigma} \rangle - \langle n_{k\sigma} \rangle \, \langle n_{-k\sigma} \rangle \, ],$$

$$G = \langle n_{k\sigma} \rangle \, \langle n_{-k\sigma} \rangle + \frac{1}{2} \left( 1 - ( \, \langle n_{k\sigma} \rangle + \langle n_{-k\sigma} \rangle \, ) - \sqrt{b} \right),$$

$$H = \langle n_{k\sigma} \rangle \, \langle n_{-k\sigma} \rangle + \frac{1}{2} \left( 1 - ( \, \langle n_{k\sigma} \rangle + \langle n_{-k\sigma} \rangle \, ) + \sqrt{b} \right).$$

We now introduce the following decouplings:

$$\langle n_{k\sigma} n_{-k\sigma} \rangle = \langle n_{\boldsymbol{k}\sigma} \rangle \langle n_{-\boldsymbol{k}\sigma} \rangle \tag{6.17}$$

$$\langle n_{k\sigma} n_{d\sigma} \rangle = \langle n_{\boldsymbol{k}\sigma} \rangle \langle n_{\boldsymbol{d}\sigma} \rangle \tag{6.18}$$

$$\langle n_{d\sigma} n_{d,-\sigma} \rangle = \langle n_{\boldsymbol{d}\sigma} \rangle \langle n_{\boldsymbol{d},-\sigma} \rangle. \tag{6.19}$$

The expectation values $\xi_{\boldsymbol{k}d\sigma}$, $\eta_{\boldsymbol{k},-\boldsymbol{k}}$, $\langle n_{\boldsymbol{k}\sigma} \rangle$ and $\langle n_{\boldsymbol{d}\sigma} \rangle$ are to be determined in such way that the free energy $F$ has a stationary value. After minimizing the free energy with respect to $\xi_{\boldsymbol{k}d\sigma}$ and $\eta_{\boldsymbol{k},-\boldsymbol{k}}$ in the limit $T \to 0$, we obtain the following equations:

$$\xi_{\boldsymbol{k}d\sigma} = -[\, \langle n_{\boldsymbol{k}\sigma} \rangle \langle n_{d\sigma} \rangle \, ( \, 1 - \langle n_{\boldsymbol{k}\sigma} \rangle \, ) \, ( \, 1 - \langle n_{d\sigma} \rangle \, ) \, ]^{1/2} \tag{6.20}$$

$$\eta_{\boldsymbol{k},-\boldsymbol{k}} = -[\, \langle n_{\boldsymbol{k}\sigma} \rangle \langle n_{-\boldsymbol{k}\sigma} \rangle \, ( \, 1 - \langle n_{\boldsymbol{k}\sigma} \rangle \, ) \, ( \, 1 - \langle n_{-\boldsymbol{k}\sigma} \rangle \, ) \, ]^{1/2}. \tag{6.21}$$

The free energy at $T = 0$, which is the ground state (GS) energy, then becomes

$$\begin{aligned} E_0 = & \sum_{\boldsymbol{k},\sigma} \varepsilon_{\boldsymbol{k}} \langle n_{\boldsymbol{k}\sigma} \rangle + \sum_{\sigma} \tilde{\varepsilon}_{d\sigma} \langle n_{d\sigma} \rangle + \tilde{U} \langle n_{d\sigma} \rangle \langle n_{d,-\sigma} \rangle \\ & -2 \left| \tilde{V} \right| \sum_{\boldsymbol{k},\sigma} [\, \langle n_{\boldsymbol{k}\sigma} \rangle \langle n_{d\sigma} \rangle \, ( \, 1 - \langle n_{\boldsymbol{k}\sigma} \rangle \, ) \, ( 1 - \langle n_{d\sigma} \rangle \, ) \, ]^{1/2} \\ & -2 \, \Delta \sum_{\boldsymbol{k},\sigma} [\, \langle n_{\boldsymbol{k}\sigma} \rangle \langle n_{-\boldsymbol{k}\sigma} \rangle \, ( \, 1 - \langle n_{\boldsymbol{k}\sigma} \rangle \, ) \, ( \, 1 - \langle n_{-\boldsymbol{k}\sigma} \rangle \, ) \, ]^{1/2} \, . \end{aligned} \tag{6.22}$$

Minimizing $E_0$ with respect to $\langle n_{\boldsymbol{k}\sigma} \rangle$ and $\langle n_{\boldsymbol{d}\sigma} \rangle$ we get the following equations

$$\varepsilon_{\boldsymbol{k}} - \left| \tilde{V} \right| \left( \frac{\eta_{d\sigma}}{\eta_{\boldsymbol{k}\sigma}} \right)^{\frac{1}{2}} ( \, 1 - 2 \langle n_{\boldsymbol{k}\sigma} \rangle \, ) - \Delta \left( \frac{\eta_{-\boldsymbol{k}\sigma}}{\eta_{\boldsymbol{k}\sigma}} \right)^{\frac{1}{2}} ( \, 1 - 2 \langle n_{\boldsymbol{k}\sigma} \rangle ) = 0, \tag{6.23}$$

$$\tilde{\varepsilon}_{d\sigma} - \frac{\epsilon_{0\sigma}}{2\sqrt{\eta_{d\sigma}}}\,(\,1 - 2\langle n_{d\sigma}\rangle\,) = 0, \tag{6.24}$$

where

$$\eta_{d\sigma} \;= \langle n_{d\sigma}\rangle\,(\,1 - \langle n_{d\sigma}\rangle\,), \tag{6.25}$$

$$\eta_{\boldsymbol{k}\sigma} \;= \langle n_{\boldsymbol{k}\sigma}\rangle\,(\,1 - \langle n_{\boldsymbol{k}\sigma}\rangle\,), \tag{6.26}$$

$$\eta_{-\boldsymbol{k}\sigma} = \langle n_{-\boldsymbol{k}\sigma}\rangle\,(\,1 - \langle n_{-\boldsymbol{k}\sigma}\rangle\,), \tag{6.27}$$

$$\varepsilon_{0\sigma} \;= 2\,\left|\tilde{V}\right| \sum_{\boldsymbol{k}} [\,\langle n_{\boldsymbol{k}\sigma}\rangle\,(\,1 - \langle n_{\boldsymbol{k}\sigma}\rangle\,)\,]^{1/2}\,. \tag{6.28}$$

Because of the symmetry of the problem, $\langle n_{-\boldsymbol{k}\sigma}\rangle \cong \langle n_{\boldsymbol{k}\sigma}\rangle$ as a result $\eta_{-\boldsymbol{k}\sigma} = \eta_{\boldsymbol{k}\sigma}$. From Eq. (6.23) we can get

$$\langle n_{\boldsymbol{k}\sigma}\rangle = \frac{1}{2}\left[\,1 - \frac{\tilde{\varepsilon}_{\boldsymbol{k}}}{\sqrt{\tilde{\varepsilon}_{\boldsymbol{k}}^2 + 4\,\eta_{d\sigma}\,\left|\tilde{V}\right|^2}}\,\right], \tag{6.29}$$

$$\varepsilon_{0\sigma} = 2\,\tilde{V}^2\,\sqrt{\eta_d} \sum_{\boldsymbol{k},\sigma} \left[\frac{1}{\sqrt{\tilde{\varepsilon}_{\boldsymbol{k}}^2 + 4\,\eta_{d\sigma}\,\tilde{V}^2}}\right], \tag{6.30}$$

where we use the notation $\tilde{\varepsilon}_{\boldsymbol{k}} = \sqrt{\varepsilon_{\boldsymbol{k}}^2 - \Delta^2}$ and consider only linear terms in $\eta_{\boldsymbol{k}\sigma}$. Thus we get

$$E_0 = \frac{\omega_D}{2}\left(\omega_D^2 - \Delta^2\right)^{1/2} + \frac{\Delta^2}{2} ln\left[\frac{1}{\Delta}\left(\omega_D + (\omega_D^2 - \Delta^2)^{1/2}\right)\right]$$

$$- \frac{1}{2}\left[\omega_D\left(\omega_D^2 + 4\,\tilde{V}^2\eta_d - \Delta^2\right)^{\frac{1}{2}} - 2\,\tilde{V}\,\Delta\,\eta_d^{1/2}\right] + \tilde{\varepsilon}_d N + \tilde{U}\,\eta_d$$

$$+ \frac{1}{2}\left(4\,\tilde{V}^2\,\eta_d - \Delta^2\right)\left[\sinh^{-1}\left(\frac{\omega_D}{\left(4\,\tilde{V}^2\,\eta_d - \Delta^2\right)^{1/2}}\right)\right.$$

$$\left. - \sinh^{-1}\left(\frac{\Delta}{\left(4\,\tilde{V}^2\,\eta_d - \Delta^2\right)^{1/2}}\right)\right], \qquad (6.31)$$

where $\langle n_{k\sigma}\rangle$ is the conduction electron distribution and the value of $\varepsilon_{0\sigma}$ has been obtained by replacing the summation over $\boldsymbol{k}$ by an integral over $\varepsilon_{\boldsymbol{k}}$ using the superconductor (SC) density of states

$$\frac{g(\varepsilon_{\boldsymbol{k}})}{g(0)} = \left(\frac{\varepsilon_{\boldsymbol{k}}}{\tilde{\varepsilon}_{\boldsymbol{k}}}\right)\theta(|\varepsilon_{\boldsymbol{k}}| - \Delta), \qquad (6.32)$$

with $\omega_D$ (Debye frequency) as the cutoff energy of the conduction band. Here we assume that the total number of electrons on the impurity atom is one i.e., $N = 1$. Using the definition of the local magnetic moment $(m)$ on the impurity atom, we can write $\eta_{d\sigma} = (1 - m^2)/4$. The binding energy (BE) $W$ between the impurity and the continuum electrons of SC is given by

$$W = (\varepsilon_d - E_0)$$

$$= \varepsilon - \eta\lambda^2\hbar\omega_0\,(2 - \eta) - (E_0 - \eta\lambda^2\hbar\omega_0(2 - \eta))$$

$$= \tilde{\varepsilon}_d - E_0 + \eta\lambda^2\hbar\omega_0(2 - \eta). \qquad (6.33)$$

## 6.4 Results and Discussion

In Figs. 1 and 2, we present results for the GS energy as a function of the *el-ph* coupling constant $\lambda$ for two values of the order parameter in anti-adiabatic and adiabatic regimes respectively. In both the cases the GS energy decreases with increase in $\lambda$. One can see from Fig. 1 that in the anti-adiabatic case, there is a sharp fall in the GS energy at a certain value of $\lambda$ ($\lambda_c$). This indicates the transition from a large polaron to a small localized

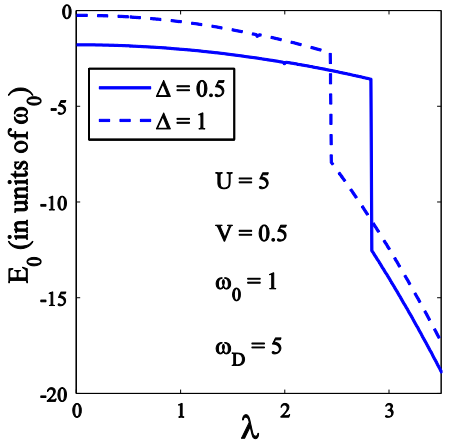


***Fig. 1*** *$E_0$ vs $\lambda$ with $V = 0.5, \Delta = 0.5$ and* 1.

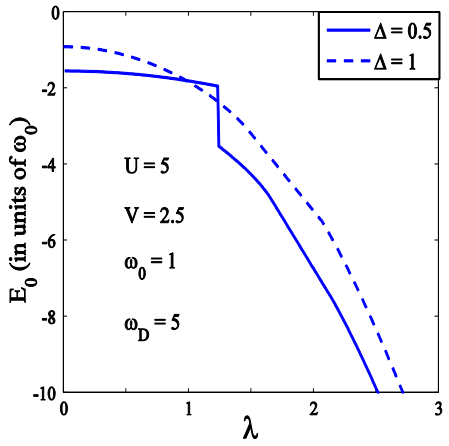


***Fig. 2*** *$E_0$ vs $\lambda$ with $V = 2.5$, $\Delta = 0.5$ and* 1.

polaron. The transition from an extended polaron state to the localized polaron state occurs for both $\Delta = 0.5$ and $\Delta = 1$, of course, at two different values of $\lambda_c$. It seems that $\lambda_c$ decreases as $\Delta$ increases. In the adiabatic case, for $\Delta = 0.5$, we again observe (Fig. 2) a similar situation i.e., a transition from an extended polaron to a localized polaron. However, it seems that for $\Delta = 1$, the GS is always a localized polaron state and so there is no transition. It may be pointed here that though there may exist a transition

from a large polaron to a small polaron at a critical value of $\lambda$, the discontinuity may be an artifact of the approximation employed in the cluster variation method. To probe the formation of a localized polaron in more detail we plot in Figs. 3 and 4, the variational parameter $\eta$ as a function of the *el-ph* coupling constant $\lambda$ for two different values of $\Delta$. Fig. 3 shows the results for the anti-adiabatic regime while in Fig. 4 we present the results for the adiabatic case.

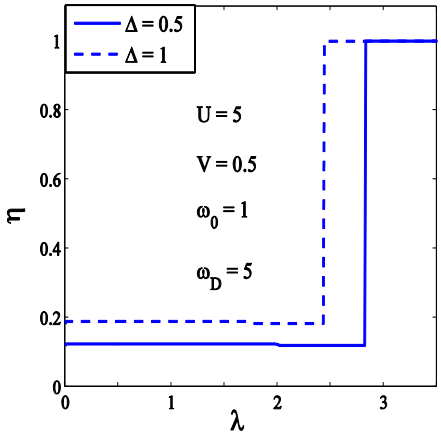


***Fig.3*** *$\eta$ vs $\lambda$ for $V = 0.5$ with $\Delta = 0.5$ and 1.*

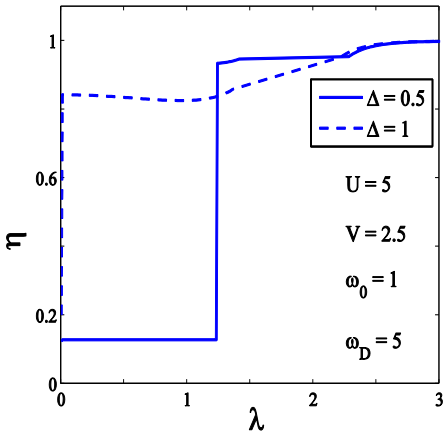


***Fig. 4*** *$\eta$ vs $\lambda$ for $V = 2.5$ with $\Delta = 0.5$ and 1.*

We observe that in both regimes, as $\lambda$ increases, $\eta$ also increases and finally saturates to the value 1 indicating localization. The discontinuities occurring in the variational parameters at the transition may again be artifact of the approximation involved. The values of $\lambda_c$'s obtained from Figs. 1 and 2 match exactly with those obtained from Figs. 3 and 4.

Our main objective in this work is to understand the bound state formation on the magnetic impurity in a superconductor. In Figs. 5 and 6 we plot BE ($W$) between the impurity electron and the conduction electrons for

two values of the order parameter Δ. Fig. 5 shows the results for the adiabatic case while in Fig. 6 we present the results for the anti-adiabatic case. $W$ increases with $\lambda$ in both adiabatic and anti-adiabatic regimes.

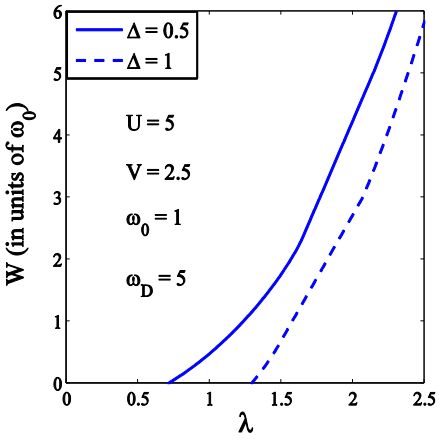


***Fig. 5*** *W vs* $\lambda$ *for* $V = 2.5, \Delta = 0.5$ *and* 1.

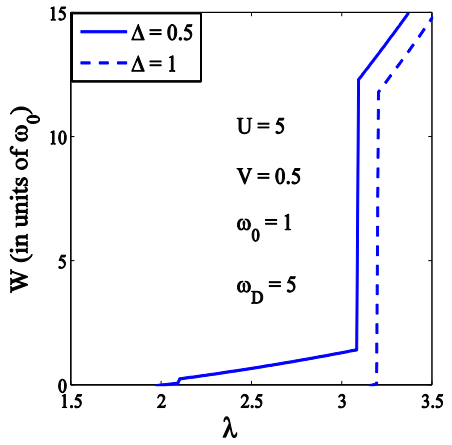


***Fig. 6*** *W vs* $\lambda$ *for* $V = 0.5, \Delta = 0.5$ *and* 1.

It also appears that there is a threshold value of $\lambda$ ($\lambda_t$) below which $W$ is zero. The value of $\lambda_t$ is smaller in the adiabatic case. This is because the $s-d$ interaction favours hybridization between the conduction and localized electrons. Therefore adiabatic case is more favorable to induce a bound state on the impurity site.

In Figs. 7 and 8, we study the variation of the BE $W$ with respect to the order parameter Δ explicitly. Fig. 7 gives results for an adiabatic case while Fig. 8 shows the data for an anti-adiabatic regime. The behavior is qualitatively similar in the two regimes. As Δ increases, $W$ decreases in a continuous way and becomes zero beyond a critical Δ. Thus it is clear that binding will be inhibited in a good superconducting host. As $\lambda$ increases, a higher value of Δ is required to make the binding disappear. Since the local

magnetic moment $m$ on the impurity is intimately related with the BE $W$, we would also like to study the effect of $\lambda$ on $m$.

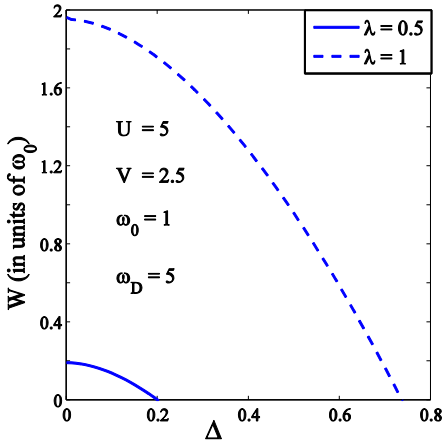


***Fig. 7*** *W vs Δ for* $V = 2.5, \lambda = 0.5$ *and* 1.

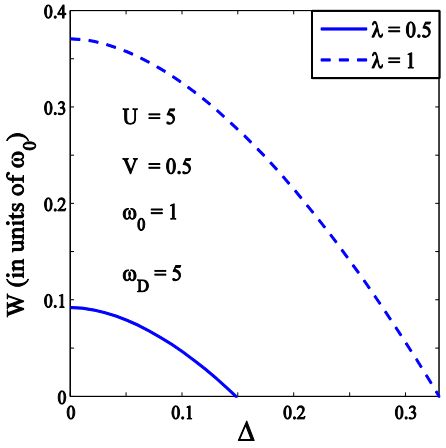


***Fig. 8*** *W vs Δ for* $V = 0.5, \lambda = 0.5$ *and* 1.

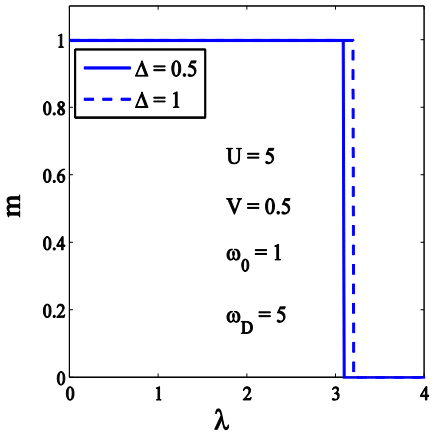


***Fig. 9*** *m vs* $\lambda$ *for* $V = 0.5, \Delta = 0.5$ *and* 1.

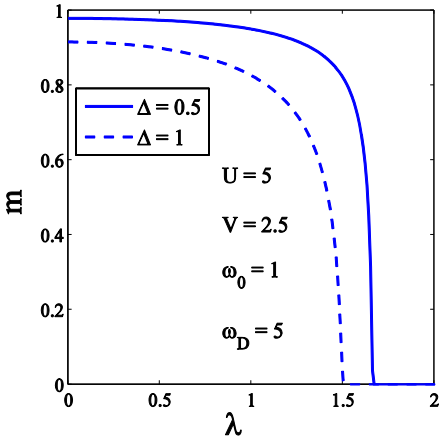


***Fig. 10*** *m vs* $\lambda$ *for* $V = 2.5, \Delta = 0.5$ *and* 1.

Figs. 9 and 10 show the variation of $m$ as a function of $\lambda$ for anti-adiabatic and adiabatic regimes respectively. As $\lambda$ increases, the local effective *el-el*

interaction decreases leading to a reduction in the value of $m$. In the anti-adiabatic case, for both $\Delta = 0.5$ and $1$, $m$ remains equal to 1 till $\lambda$ remains below a critical value of $\lambda$ ($\lambda_c$) (which depends on $\Delta$). At $\lambda = \lambda_c$, the state characterized by $m = 0$ is purely a bipolaron state. This is because the effective *el-el* interaction becomes attractive at $\lambda = \lambda_c$ leading to the formation of a bipolaron state at the impurity site. Thus, the polaron to bi-polaron transition at the impurity can be described as a transition from $m = 1$ state to $m = 0$ state. As $\Delta$ increases, the value of $\lambda_c$ increases. It can be easily observed that the value of $\lambda_c$ obtained from Fig. 9 is the same as that obtained from the BE curve shown in Fig. 6. One can also see that as $\Delta$ increases, the value of $\lambda_c$ also increases. The reason can be easily understood. A larger $\Delta$ corresponds to a better superconductor. In such a case, one would expect the host material to have more cooper pairs and consequently, lesser number of un-paired electrons will be available in the system. Furthermore, as $\Delta$ becomes larger, it requires a larger energy to excite the unpaired electrons to overcome the gap of the superconducting host to occupy the impurity site. Obviously, such a situation will lead to an enhancement in $m$. In the adiabatic case, $m$ shows a rapid but continuous fall to zero. The discontinuity observed in the anti-adiabatic case may again be due to the approximation employed. The $s - d$ interaction strength ($V$) increases the hybridization between conduction electrons and impurity electron. As a result the value of $\lambda_c$ is large in an anti-adiabatic case. Furthermore, since $\Delta$ separates the conduction electrons from the cooper pairs in SC, as $\Delta$ increases, one would expect to have lesser number of unpaired conduction electrons available to compensate for the impurity spin.

In Fig. 11 we present the phase diagrams for the bound and unbound states in adiabatic and anti-adiabatic cases. The value of $\lambda_t$ increases almost

linearly with $\Delta$ in both the cases. But the effect of $\Delta$ on the $\lambda -$ dependence of bound-unbound transition is strong in the anti-adiabatic case.

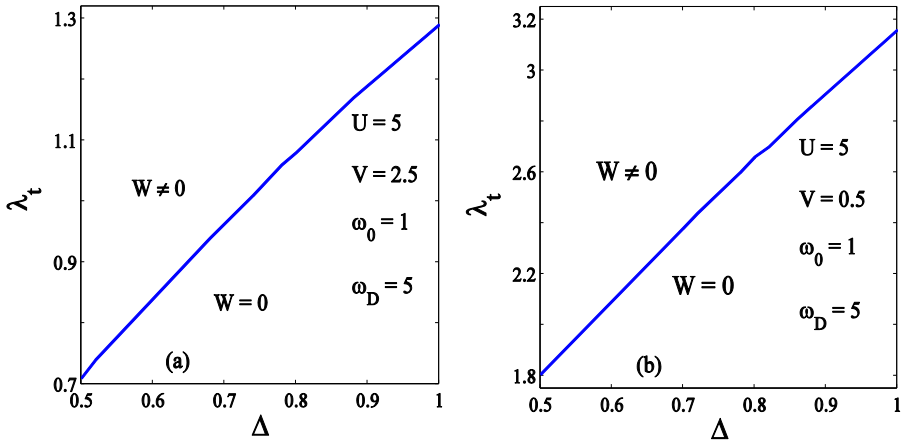


***Fig. 11*** *Bound-Unbound state phase diagram in the $\lambda_t - \Delta$ plane for (a) $V = 2.5$ (b) $V = 0.5$.*

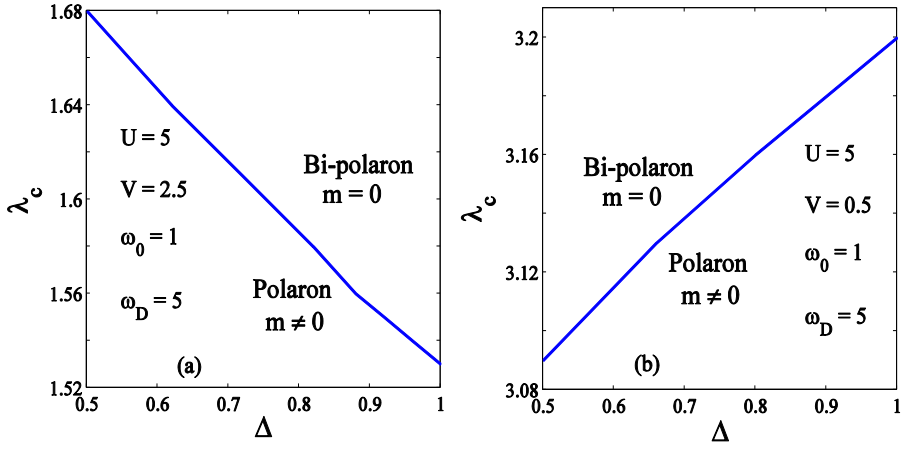


***Fig. 12*** *Polaron-Bipolaron phase diagram in the $\lambda_c - \Delta$ plane for (a) $V = 2.5$ (b) $V = 0.5$.*

Finally, we show in Fig. 12 the dependence of $\lambda_c$ on $\Delta$ in both adiabatic and anti-adiabatic cases. In the anti-adiabatic case the value of $\lambda_c$ increases with the order parameter $\Delta$, as normally expected, while in the adiabatic case $\lambda_c$ decreases with $\Delta$. In the adiabatic case, the $s-d$ interaction strength $V$ enhances the probability of hopping of an electron from the conduction band to the impurity site. This happens because of the strong hybridization of the conduction band with the impurity level. In the present case, the impurity level may lie within the superconducting band so that a Cooper pair itself can occupy the impurity level. Thus if $V$ is large enough, a lesser value of $\lambda$ is required to achieve a double occupancy on the impurity atom as $\Delta$ increases. Thus $\lambda_c$ decreases with $\Delta$.

## 6.5 Summary

In this chapter we have studied the many-body bound state formation on the magnetic impurity atom embedded in a BCS superconductor. We have described the system by adding the BCS interaction term to the single-level AH model. Using the cluster variation method we have calculated the GS energy and BE between the impurity electron and s electrons of SC. We have shown that the local magnetic moment decreases with increasing *el-ph* interaction. We have also shown that BE increases with *el-ph* interaction, but decreases with the superconducting gap parameter. We have finally shown the bound-unbound and the polaron-bipolaron phase diagrams for adiabatic and anti-adiabatic cases.

# References


[1] T. Sugawara, Physics **55**, 143 (1971);
S. V. Vonsovsky, Yu A. Izyumov & E. Z. Kurmaev, *Superconductivity of Transition Metals* (Springer-Verlag, 1982).

[2] C. Inoue & F. Takano, Prog. Theor. Phys. **48**(4), 1080 (1972).

[3] C. F. Ratto & A. Blandin, Phys. Rev. **156**, 513 (1967).

[4] I. Tifrea & M. Crisan, J. Superconductivity. **10**(2), 127 (1997).

[5] M. J. Zuckermann, Phys. Rev. **168**, 390(1968).

[6] H. Shiba, Prog. Theor. Phys. **40**, 435 (1968).

[7] A. A. Abrikosov & L. P. Gorkov, Soy. Phys. JETP. **12**, 1243 (1961).

[8] M. A. Woolf, F. Reif, Phys. Rev. A. **137**, 557 (1965);
*ibid*. **12**, 1243(1961).

[9] D. K. Finnemore, *et al*., Phys. Rev. **137**, A550 (1965).

[10] L. Yu, Acta Phys. Sin. **21**, 75 (1965).

[11] A. I. Rusinov, Sov. Phys. JETP **29**, 1101 (1969).

[12] K. Satori *et al*., J. Phys. Soc. Jpn. **61**, 3239 (1992).

[13] O. Sakai *et al*., J. Phys. Soc. Jpn. **62**, 3181 (1993).

[14] T. Yoshioka & Y. Ohashi, J. Phys. Soc. Jpn. **69**, 1812 (2000);
A. Oguri *et al*., J. Phys. Soc. Jpn. **73**, 2494 (2004).

[15] J. Bauer *et al*., J. Phys.: Condens. Matter. **19**, 486211 (2007).

[16] T. Tanaka, *Methods of statistical physics*, (Cambridge University Press, New York, 2002).

Chapter **7**

# Quantum dissipative effects on non-equilibrium transport through a single-molecular transistor: Anderson-Holstein-Caldeira-Leggett model

## 7.1 Introduction

Moletronics (molecular electronics) is the study and application of molecules as building blocks of electronic components. Aviram and Ratner [1] made a theoretical proposal for the first time in 1974, a single organic molecule as a rectifier and Park et al. were the first to fabricate the single C60 molecule transistor [2] in 2000. The transport properties of a single molecular transistor (SMT) device have been studied both experimentally [3-9] and theoretically [10-16] by several groups. In this transistor device the charge transport takes place through a single molecule (or a quantum dot) which are connected with two metal electrodes that act as source and drain. The entire structure is constructed on a metal oxide layer that acts as a substrate below which a gate electrode is placed. Each electron-transfer from the lead to the molecule creates a distortion in the molecule. Quanta of this distortion, called phonons, interact with a local electron of the molecule giving rise to what is known as the electron-phonon (*el-ph*) interaction. Of

late, the phononic effects on molecular devices have been studied by many research groups [2, 5, 8]. It would be interesting to study how these local phonon modes interact with the phonons or plasmons of the substrate in which the molecule is placed. An investigation in this direction can answer the question: "what is the effect of dissipation on non-equilibrium transport through an SMT device". In the present chapter our main aim is to study the damping effect on the non-equilibrium transport properties of the SMT due to the presence of the substrate in ohmic case at zero temperature using the Anderson-Holstein (AH) Hamiltonian in combination with the Caldeira-Leggett model which was proposed by Caldeira and Leggett [17] in 1981 to describe the dissipation of a quantum system due to its interaction with a set of independent harmonic oscillators.

## 7.2 Decoupling of oscillator-bath interaction

In the Introduction chapter we have described the SMT device using AH-Caldeira-Leggett model. We have described the substrate as set of independent harmonic oscillators in Eq. (1.14) and it is fully characterized by a spectral function $J(\omega)$ given by

$$J(\omega) = \sum_{j=1}^{N} \frac{\beta_j^2}{2m_j\omega_j}\delta(\omega - \omega_j). \tag{7.1}$$

The linear oscillator-bath interaction term in Eq. (1.15) can be exactly eliminated from the theory by performing simple transformations and we obtain

$$H_{vib} + H_B = \left(\frac{p_0^2}{2m_0} + \frac{1}{2}\, m_0 \tilde{\omega}_0{}^2 x_0^2\right) + \sum_{j=1}^{N}\left(\frac{\tilde{p}_j^2}{2m_j} + \frac{1}{2}\, m_j \omega_j{}^2 \tilde{x}_j{}^2\right), \tag{7.2}$$

where,

$$\tilde{x}_j = x_j + \frac{\beta_j x_0}{m_j \omega_j^2}\,, \qquad \tilde{p}_j = -i\hbar \frac{\partial}{\partial \tilde{x}_j}\,, \tag{7.3}$$

$$\widetilde{\omega}_0 = (\omega_0^2 - \Delta\omega^2)^{1/2} = \left( \omega_0^2 - \sum_{j=1}^{N} \frac{\beta_j^2}{m_0 m_j {\omega_j}^2} \right)^{1/2}, \tag{7.4}$$

where $\Delta\omega^2$ is the shift in the square of the quantum dot (QD) oscillator frequency caused by the linear oscillator-bath coupling. For very large $N$, we can replace the summation over $j$ by an integration over $\omega_j$. $\Delta\omega^2$ can be written as

$$\Delta\omega^2 = \frac{2}{m_0} \int_0^\infty \frac{J(\omega)}{\omega}\, d\omega, \tag{7.5}$$

where $J(\omega)$ is the spectral function for which we choose the Lorentz-Drude form:

$$J(\omega) = \frac{2 m_0 \gamma \omega}{[1 + (\omega/\omega_c)^2]}\,, \tag{7.6}$$

where $\omega_c$ is the cutoff frequency which is much larger than the other frequencies in the system and $\gamma$ is the damping rate. The Lorentz-Drude form for $J(\omega)$ satisfies the Ohmic dissipation condition. The shift in the QD frequency turns out be: $\Delta\omega^2 = 2\pi\gamma\omega_c$. The total Hamiltonian finally reduces to

$$H = \sum_{\boldsymbol{k},\sigma\in S,D} \varepsilon_{\boldsymbol{k}}\, n_{\boldsymbol{k}\sigma} + \sum_{\sigma} (\varepsilon_d - eV_G)\, n_{d\sigma} + U\, n_{d\uparrow}\, n_{d\downarrow} + \hbar\tilde{\omega}_0 b^{\dagger} b$$

$$+ \sum_{\boldsymbol{k},\sigma\in S,D} \left(V_{\boldsymbol{k}} c_{k\sigma}^{\dagger} c_{d\sigma} + h.c\right) + \lambda\, \hbar\tilde{\omega}_0 \left(b^{\dagger} + b\right) \sum_{\sigma} n_{d\sigma}, \qquad (7.7)$$

where, $b^{\dagger}(b)$ is the creation (annihilation) operator for a QD phonon of frequency $\tilde{\omega}_0$. It may be noted that we have neglected the decoupled bath-oscillator Hamiltonian because that merely contributes a constant to the energy.

## 7.3 Effective Anderson-Holstein-Caldeira-Leggett model Hamiltonian

To investigate the effects of the polaronic interactions in the system, a Lang-Firsov transformation with the generator $S = \lambda \left(b^{\dagger} - b\right) \sum_{\sigma} n_{d\sigma}$, is applied to the Hamiltonian. The transformed Hamiltonian $\tilde{H} = e^{S} H e^{-S}$ reads

$$\tilde{H} = \sum_{\boldsymbol{k},\sigma\in S,D} \varepsilon_{\boldsymbol{k}}\, n_{\boldsymbol{k}\sigma} + \sum_{\sigma} \tilde{\varepsilon}_d\, n_{d\sigma} + \tilde{U}\, n_{d\uparrow} n_{d\downarrow} + \hbar\tilde{\omega}_0 b^{\dagger} b$$

$$+ \sum_{\boldsymbol{k},\sigma\in S,D} \left(V'_{\boldsymbol{k}} c_{\boldsymbol{k}\sigma}^{\dagger} c_{d\sigma} + h.c\right), \qquad (7.8)$$

with

$$\tilde{\varepsilon}_d = \left(\varepsilon_d - eV_G - \varepsilon_p\right) = \varepsilon_d - eV_G - \hbar\tilde{\omega}_0\lambda^2, \qquad (7.9)$$

$$\tilde{U} = U - 2\hbar\tilde{\omega}_0\lambda^2, \qquad (7.10)$$

$$V'_{\boldsymbol{k}} = V_{\boldsymbol{k}} X = V_{\boldsymbol{k}}\, e^{\lambda(b - b^{\dagger})}, \qquad (7.11)$$

where $V_{\boldsymbol{k}}'$ is the phonon-mediated hybridization strength, $\tilde{\varepsilon}_d$ is the renormalized QD energy level due to the polaronic effect and $\varepsilon_p$ is the polaron binding energy.

## 7.4 Tunneling Current

The current expression through the interacting region coupled to two metallic leads can be expressed as [18, 19]

$$J = \frac{e}{2h}\int [\{ f_S(\varepsilon)\Gamma_S(\varepsilon) - f_D(\varepsilon)\Gamma_D(\varepsilon)\}\, A(\varepsilon) + \{\big(\Gamma_S(\varepsilon) - \Gamma_D(\varepsilon)\big)G^{<}(\varepsilon)\}\big]\, d\varepsilon. \quad (7.12)$$

Similarly, the occupation number of the QD is given by

$$\langle n_{d\uparrow}\rangle = \int \frac{d\varepsilon}{2\pi\Gamma}\{f_S(\varepsilon)\Gamma_S(\varepsilon) + f_D(\varepsilon)\Gamma_D(\varepsilon)\}\, A(\varepsilon), \quad (7.13)$$

where $\Gamma_S(\varepsilon)$ and $\Gamma_D(\varepsilon)$ are the coupling strengths of the QD with source and drain. $G^{<}(\varepsilon)$ is the Fourier transformed Keldysh lesser Green function for the QD electron. $f_{S,D}(\varepsilon)$ are the Fermi distribution functions of the source and drain whose chemical potentials are related to the bias voltage ($V_B$) and mid-voltage ($V_m$) as

$$(\mu_S - \mu_D) = eV_B, \quad (7.14)$$

and

$$\frac{(\mu_S + \mu_D)}{2} = eV_m. \quad (7.15)$$

For symmetric coupling of the QD with the source and the drain,

$$\tilde{\Gamma}(\varepsilon) = \frac{\tilde{\Gamma}_S(\varepsilon) + \tilde{\Gamma}_D(\varepsilon)}{2} = \tilde{\Gamma}, \tag{7.16}$$

where,

$$\tilde{\Gamma}_{S(D)}(\varepsilon) = \pi\rho_{S(D)}(0)\left|\tilde{V}_k\right|^2 = \Gamma_{S(D)}e^{-(\lambda^2)}, \tag{7.17}$$

where $\Gamma_{S(D)}(=\pi\rho_{S(D)}(0)|V_k|^2)$, $\rho_{S(D)}$ being the density of states in the source (drain) channel. Here we consider constant density of states in the source and drain. The possible excitation energy spectrum is described by the quantity called spectral (SP) function, which is defined as

$$A(\varepsilon) \;= i\,[G^r(\varepsilon) - G^a(\varepsilon)] = i[G^>(\varepsilon) - G^<(\varepsilon)], \tag{7.18}$$

where,

$$G^>(t) = -i\,\langle 0\left|c(t)c^\dagger(0)\right|0\rangle\,, \tag{7.19}$$

$$G^<(t) \;=\; i\,\langle 0\left|c^\dagger(0)c(t)\right|0\rangle\,, \tag{7.20}$$

$$G^{r(a)}(t,t') = \mp i\,\theta(t-t')\,\langle\{c_d(t), c_d^\dagger(t')\}\rangle, \tag{7.21}$$

where the superscript '>' ('<') refers to greater (lesser), '$r$' ('$a$') refers to retarded (advanced) and $|0\rangle$ represents the true electronic ground state of the system. Thus $G^{r(a)}(\varepsilon)$ and $G^{>(<)}(\varepsilon)$ are the energy-dependent retarded (advanced) and lesser (greater) electron Green's functions of the QD respectively. The phonon operator $X$ in the Hamiltonian Eq. (7.8) can be absorbed into renormalized electron annihilation ($\tilde{c}_d = Xc_d$) and creation ($\tilde{c}_d^\dagger = X^\dagger c_d^\dagger$) operators in the QD region. So the Hamiltonian Eq. (7.8) is the

usual resonant tunneling Hamiltonian with the dressed QD electron operators. So the Hamiltonian Eq. (7.8) can be written as

$$\widetilde{H} = \widetilde{H}_{el} + \widetilde{H}_{ph}\,, \tag{7.22}$$

where,

$$\widetilde{H}_{el} = \sum_{\boldsymbol{k}\sigma\in S,D} \varepsilon_{\boldsymbol{k}}\, n_{\boldsymbol{k}\sigma} + \sum_{\sigma} \tilde{\varepsilon}_d\, n_{d\sigma} + \widetilde{U}\, n_{d\uparrow} n_{d\downarrow} + \sum_{\boldsymbol{k}\sigma\in S,D} \left(V'_{\boldsymbol{k}} c^{\dagger}_{\boldsymbol{k}\sigma} \tilde{c}_{d\sigma} + h.c\right), \tag{7.23}$$

$$\widetilde{H}_{ph} = \hbar\widetilde{\omega}_0 b^{\dagger} b\,. \tag{7.24}$$

The retarded Green function for the dressed dot electron can be written as,

$$\tilde{G}^{r(a)}(t,t') = \mp i\,\theta(t-t')\,\langle\{c_d(t), c_d^{\dagger}(t')\}\rangle_{el}\,\langle X^{\dagger}(0)X(\tau)\rangle_{ph}\,, \tag{7.25}$$

$$= G_{dd}^{r(a)}(\varepsilon)\;\langle X^{\dagger}(0)X(\tau)\rangle_{ph}\,. \tag{7.26}$$

Using the EOM approach $G_{dd}^{r(a)}(\varepsilon)$ can be calculate as,

$$G_{dd}^{r(a)}(\varepsilon) = \frac{1}{\varepsilon - \tilde{\varepsilon}_d - \widetilde{U}\langle n_{d\downarrow}\rangle - S^{r(a)}(\varepsilon)}\,, \tag{7.27}$$

where the retarded (advanced) self-energy $S^{r(a)}(\varepsilon)$ due to hybridization interaction is given by

$$S^{r(a)}(\varepsilon) = \sum_{k\in S,D} \frac{\left|\tilde{V}_k\right|^2}{(\varepsilon - \varepsilon_k \pm i0^{+})} = \widetilde{\Lambda}(\varepsilon) \mp i\widetilde{\Gamma}(\varepsilon)\,, \tag{7.28}$$

where the real part of the self-energy can be absorbed into the QD energy level. We assume that $\widetilde{\Lambda}(\varepsilon)$ and $\tilde{\Gamma}(\varepsilon)$ are constants in the flat band approximation. Similarly the interacting lesser and greater Green's function for the electrons on the QD can be written as

$$\tilde{G}^{<}(\tau) = i\langle \tilde{c}_d^{\dagger}(0)\tilde{c}_d(\tau)\rangle = i\,\langle c_d^{\dagger}(0)c_d(\tau)\rangle_{el}\;\langle X^{\dagger}(0)X(\tau)\rangle_{ph}\,,$$

$$\cong G^{<}(\tau)\, e^{-\phi(-\tau)} \tag{7.29}$$

$$\tilde{G}^{>}(\tau) \cong G^{>}(\tau)\, e^{-\phi(\tau)}, \tag{7.30}$$

where the factors $e^{-\phi(\mp\tau)}$ which arise from the phonon averages are given by [20]

$$\phi(\mp\tau) = -\lambda^2\left[N_{ph}\left(1 - e^{\pm i\hbar\tilde{\omega}_0\tau}\right) + \left(1 + N_{ph}\right)\left(1 + e^{\mp i\hbar\tilde{\omega}_0\tau}\right)\right], \tag{7.31}$$

$$\phi(\mp\tau) = -\lambda^2\left[\left(2N_{ph}+1\right) \mp 2i\sqrt{N_{ph}\left(1+N_{ph}\right)}\;\; sin\left\{\hbar\tilde{\omega}_0\left(\tau + i\frac{\beta}{2}\right)\right\}\right], \tag{7.32}$$

with $N_{ph} = \left(e^{\beta\hbar\tilde{\omega}_0} - 1\right)^{-1}$. Using the relation,

$$e^{iz\sin(\theta)} = \sum_{n=-\infty}^{\infty} I_n(z)\, e^{i\,n\theta}, \tag{7.33}$$

$$z = 2\lambda^2\sqrt{N_{ph}\left(N_{ph}+1\right)}\;, \qquad \theta = \hbar\tilde{\omega}_0(\tau + i\beta/2). \tag{7.34}$$

$$\langle X^{\dagger}(0)X(\tau)\rangle_{ph} = e^{-\phi(\tau)} = \sum_{n=-\infty}^{\infty} L_n\, e^{-in\hbar\tilde{\omega}_0\tau}, \tag{7.35}$$

where,

$$L_n = e^{-\lambda^2(2N_{ph}+1)} e^{(n\hbar\tilde{\omega}_0\beta/2)}\, I_n(z), \tag{7.36}$$

where $I_n(z)$ is the $n$ th order Bessel function of complex argument. The lesser and greater Green functions can be expanded as

$$\tilde{G}^{<}(\varepsilon) = \sum_{n=-\infty}^{\infty} L_n\, G^{<}(\varepsilon + n\hbar\tilde{\omega}_0), \tag{7.37}$$

$$\tilde{G}^{>}(\varepsilon) = \sum_{n=-\infty}^{\infty} L_n\, G^{>}(\varepsilon - n\hbar\tilde{\omega}_0), \tag{7.38}$$

From Eq. (7.18) the SP function can be written as,

$$\tilde{A}(\varepsilon) = \sum_{n=-\infty}^{\infty} i\, L_n\, [G^{>}(\varepsilon - n\hbar\tilde{\omega}_0)\ - G^{<}(\varepsilon + n\hbar\tilde{\omega}_0)]. \tag{7.39}$$

Here we will use Keldysh formalism [21, 22] to calculate the lesser and greater Green's functions. By applying Langreth analytical continuation rules to the Dyson equations for the lesser and greater Green's functions can written as

$$G^{<}(\varepsilon) = G^{r}_{dd}(\varepsilon)\, S^{<}(\varepsilon)\, G^{a}_{dd}(\varepsilon) \tag{7.40}$$

$$G^{>}(\varepsilon) = G^{r}_{dd}(\varepsilon)\, S^{>}(\varepsilon)\, G^{a}_{dd}(\varepsilon) \tag{7.41}$$

with

$$S^{<}(\varepsilon) = i\, \tilde{\Gamma}\, [f_S(\varepsilon) + f_D(\varepsilon)], \tag{7.42}$$

$$S^{>}(\varepsilon) = -i\, \tilde{\Gamma}\, [2 - f_S(\varepsilon) - f_D(\varepsilon)], \tag{7.43}$$

$$G^{<}(\varepsilon) = \sum_{n=-\infty}^{\infty} L_n \, \tilde{G}^{<}(\varepsilon + n\hbar\tilde{\omega}_0)$$

$$= \sum_{n=-\infty}^{\infty} L_n \; (i) \frac{[f_S(\varepsilon) + f_D(\varepsilon)]}{2} \; \tilde{A}(\varepsilon), \tag{7.44}$$

$$G^{>}(\varepsilon) = \sum_{n=-\infty}^{\infty} L_n \, \tilde{G}^{>}(\varepsilon - n\hbar\tilde{\omega}_0)$$

$$= \sum_{n=-\infty}^{\infty} L_n \; (-i) \frac{[2 - f_S(\varepsilon) - f_D(\varepsilon)]}{2} \; \tilde{A}(\varepsilon). \tag{7.45}$$

The SP function of the QD electron can be obtained by substituting Eqs. (7.44) and (7.45) into Eq. (7.39).

## 7.5 Results and Discussion

In our calculation we take $\varepsilon_d = V_G = 0$, $\Gamma = 0.2$ and $eV_m = 0.1$. In Fig. 1, we show the variation of the SP function $A(\varepsilon)$ of an SMT with $\varepsilon$ for different values of the damping rate $\gamma$ and a given value of the *el-ph* coupling constant $\lambda$ ($\lambda = 0.6$). The inset shows the behavior of $A(\varepsilon)$ as a function of $\varepsilon$ for the case: $\lambda = \gamma = 0$, which is a simple lorentzian with a single resonant peak at $\varepsilon_d = 0$. The *el-ph* interaction induces polaronic effects that renormalize the SMT parameters and shift the SP function peak from $\varepsilon_d = 0$ towards red and also make them sharper. Most importantly, the SP function also develops side peaks at $\tilde{\varepsilon}_d \mp n\tilde{\omega}_0$ in the presence of the *el-ph* interaction. These, so called, phonon side bands in the SP function at zero temperature represent the phononic excitation energy levels created by the electrons tunneling on to QD by absorbing or emitting phonons. Due to

the damping effect of the substrate the phonon frequency gets renormalized to $\tilde{\omega}_0$. As the damping rate increases, the heights of the phonon side bands decrease and broaden. This suggests that as the damping rate increases, the occupation probability of the phonon side bands decreases.

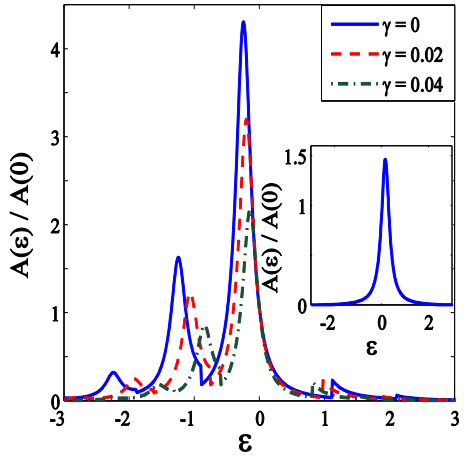


***Fig. 1*** *Dimensionless spectral function as a function of energy with* $\mu_S = \mu_D = 0,\ \lambda = 0.6$. *(**Inset**: SP function for* $\lambda = \gamma = 0$).

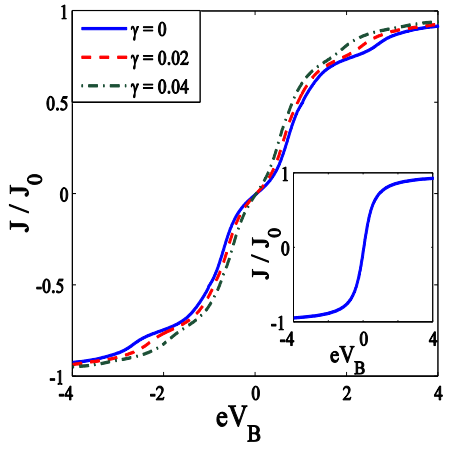


***Fig. 2*** $J/J_0$ *as a function of* $eV_B$ *with* $\lambda = 0.6$. *(**Inset**:* $J/J_0$ *for* $\lambda = \gamma = 0$)

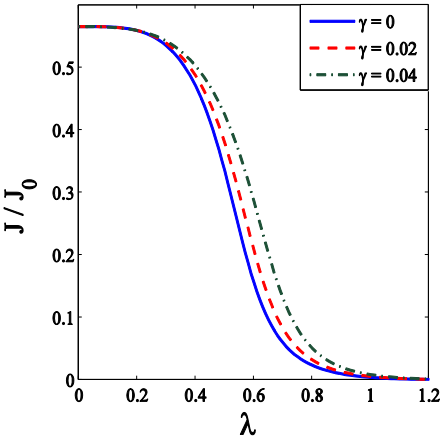


***Fig. 3*** $J/J_0$ *vs* $\lambda$ *with* $eV_B = 0.5$.

In Fig. 2 we present the results for the normalized tunneling current $J(eV_B, eV_m)$ of the SMT system as a function of bias voltage for different values of $\gamma$ in the presence of the *el-ph* interaction. The normalized tunneling current for the case: $\lambda = \gamma = 0$ is shown in the inset for comparison. As the damping rate increases the current also increases. To see the effect of *el-ph* interaction on current, we plot, in Fig. 3, the current as a function of $\lambda$ for different values of $\gamma$ at constant bias voltage $V_B$. As $\lambda$ increases, the current decreases smoothly but rapidly and becomes zero at a critical value of $\lambda$, say $\lambda_c$. This is easy to understand physically, though mathematically, Eq. (7.17) explicitly shows that the current decreases exponentially with $\lambda$. At the same time as $\lambda$ increases, the separation between the QD energy level and the chemical potential of source increases. As $\gamma$ increases, $\lambda_c$ is also found to increase.

In Fig. 4, we present the results for the differential conductance $G(eV_B, eV_m)$ $(= dJ/dV_B)$ as a function of the bias voltage in the absence of the *el-ph* interaction and the damping effect. It reveals the excitation spectrum of the central QD.

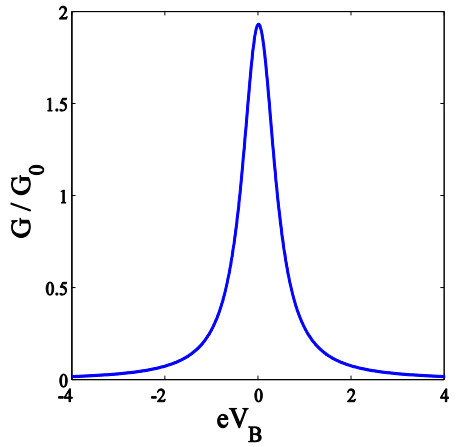


***Fig. 4*** *The dimensionless differential conductance $G/G_0$ as a function of $eV_B$ with $\lambda = \gamma = 0$.*

The excitation in the QD is commonly detected by peak in differential conductance. The symmetry in the conductivity peak is clearly visible. In Fig. 5 we show the behavior of $G$ in the presence of *el-ph* interaction ($\lambda = 0.6$) for different values of $\gamma$. The *el-ph* interaction and damping have visible independent effects on $G$.

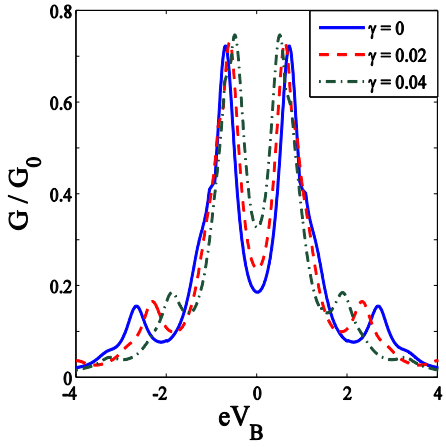


***Fig. 5*** *$G/G_0$ vs $eV_B$ for a few values of $\gamma$ with $\lambda = 0.6$.*

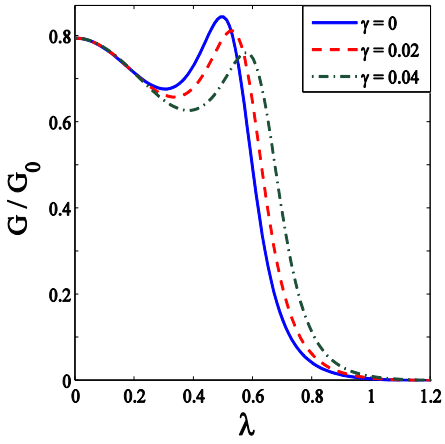


***Fig. 6*** *$G/G_0$ vs $\lambda$ for a few values of $\gamma$ with $eV_B = 0.6$.*

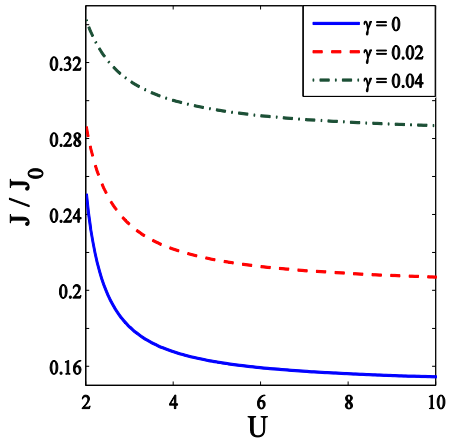


***Fig. 7*** *$J/J_0$ vs $U$ for a few values of $\gamma$ with $\lambda = 0.6$.*

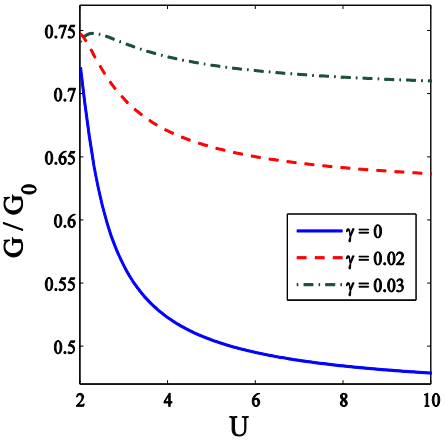


***Fig. 8*** *$G/G_0$ vs $U$ for a few values of $\gamma$ with $\lambda = 0.6$.*

The effect of the *el-ph* interaction is two-fold. First, it sharpens the conductivity peaks and secondly and more importantly it gives rise to new satellite peaks that originate because of phonon-assisted tunneling transport. To show the effect of *el-ph* interaction on the differential conductance explicitly, we plot in Fig. 6, $G/G_0$ as a function of $\lambda$ for different values of $\gamma$. For a given $\gamma$, the differential conductance has a peak at a certain value of $\lambda$ and as $\gamma$ increases, the peak reduces in height and also shifts towards right. Both shifting and reduction in height of the conductance peaks are the expected behavior. In Figs. 7 and 8 we plot $J$ and $G$ respectively as a function of the *el-el* interaction strength $U$ for different values of the damping rate. As $U$ increases, both $J$ and $G$ decrease, while they increase with increasing $\gamma$. These variations can be explained in the following way. Due to the Coulomb blockade effect the onsite Coulomb correlation opposes the double occupancy on the QD as a result of which the current decreases with increasing $U$, while as $\gamma$ increases, the effective phonon frequency decreases leading to an increase in the current and the conductance. Finally, we make a three-dimensional plot for $J$ as a function of both $\gamma$ and $\lambda$ in Fig. 9 and for $G$ as a function of $\gamma$ and $\lambda$ in Fig. 10.

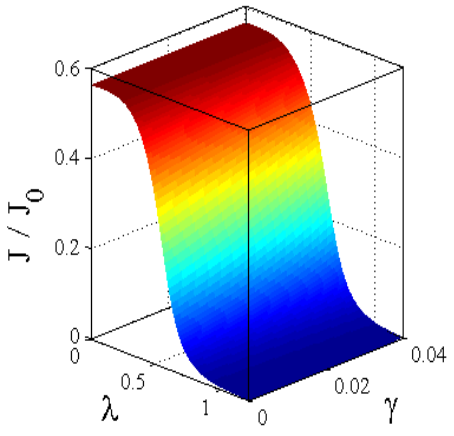


***Fig. 9*** *$J/J_0$ as a function of both $\lambda$ and $\gamma$ for $eV_B = 0.5, U = 5$.*

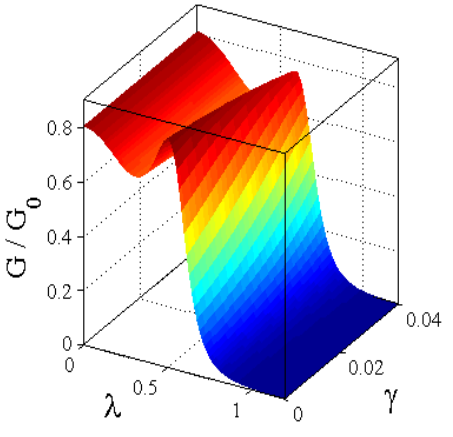


***Fig. 10*** *$G/G_0$ as a function of both $\lambda$ and $\gamma$ for $eV_B = 0.5, U = 5$.*

## 7.6 Summary

In this chapter we have considered an SMT system, which is modeled by the AH model with a linear Caldeira-Leggett term to include the linear coupling between the substrate and the molecule which describes the damping effect. We have calculated the spectral function, tunneling current and differential conductance of the SMT system using the Keldysh non-equilibrium Green function technique. We have also analyzed the effect of *el-ph* interaction and the damping effect in ohmic case due to the substrate. We have shown that the *el-ph* interaction induces polaronic effects that renormalize the SMT parameters and shift the peak of the spectral function towards red and also make them sharper. The spectral function also develops side bands whose heights decrease and the widths broaden with increasing damping rate. As $\lambda$ increases, the tunneling current is found to decrease smoothly but rapidly to zero at a critical value of $\lambda$. The *el-ph* interaction also sharpens the conductivity peaks and gives rise to new satellite peaks that originate because of phonon-assisted tunneling transport. It is also shown that the local *el-el* interaction causes a reduction in both the tunneling current and the differential conductance. Due to the damping effect of the substrate, the effective phonon frequency of the QD oscillator decreases as a result of which the tunneling current increases.

## References

[1] A. Aviram & M. A. Ratner, Chem. Phys. Lett. **29**(2), 277 (1974).

[2] H. Park *et al.*, Nature **407**, 57 (2000).

[3] M. A. Reed, *et al*., Science **278**, 252 (1997).

[4] J. Park, *et al*., Nature **417**, 722 (2002).

[5] W. Liang, *et al*., Nature **417**, 725 (2002).

[6] R. H. M. Smit, *et al*., Nature **419**, 906 (2002).

[7] N. B. Zhitenev, *et al*., Phys. Rev. Lett. **88**, 226801 (2002).

[8] A. N. Pasupathy, *et al*., Cond-mat/0311150.

[9] L. H. Yu and D. Natelson, Nano Lett. **4**, 79 (2004).

[10] T. Koch *et al*., J. Phys.: Conf. Ser. **220**, 012014-9 (2010).

[11] J. Loos *et al.*, J. Phys.: Condens. Matter. **21**, 395601 (2009).

[12] D. M. T. Kuo & Y. C. Chang, Phys. Rev. B **66**, 085311 (2002).

[13] R. Świrkowicz *et al*., Phys. Rev. B **68**, 195318 (2003).

[14] Z. Z. Chen, R. Lü & B. F. Zhu, Phys. Rev. B **71**, 165324 (2005).

[15] J. X. Zhu & A. V. Balatsky, Phys. Rev. B **67**, 165326 (2003).

[16] U. Lundin & R. H. McKenzie, Phys. Rev. B **66**, 075303 (2002).

[17] A. O. Caldiera & A. J. Legget, Phys. Rev. Lett. **46**, 211 (1981).

[18] A.-P. Jauho *et al.*, Phys. Rev. B **50**, 5528 (1994).

[19] Y. Meir & N. S. Wingreen, Phys. Rev. Lett. **68**, 2512 (1992).

[20] G. D. Mahan, *Many-Particle Physics* (Plenum Press, New York, 1990).

[21] H. Haug and A. –P. Jauho, in *Quantum Kinetics in Transport and Optics of Semiconductors*, edited by Dr. –Ing. Helmut K. V. Lotsch (Springer-Verlag, Berlin Heidelberg, 1996).

[22] D. C. Langreth, in *Linear and Nonlinear Electron Transport in Solids*, edited by J. T. Devreese and V. E. Van Doren (Plenum, New York, 1976).

# Chapter 8

# Conclusions

In this thesis we have considered the Anderson-Holstein (AH) model to study the quantum impurity problem and quantum transport in a three terminal mesoscopic electronic device like single molecular transistor (SMT). The standard AH model describes a localized impurity energy level incorporating both local electron-electron (*el-el*) and electron-phonon (*el-ph*) interactions and also its interaction with the continuum states of the host matrix. We have treated the phonon part of the Hamiltonian variationally using a canonical transformation. To be specific, we have eliminated the phonon degrees of freedom using the Lang-Firsov (LF) transformation followed by a zero-phonon averaging to obtain an effective AH Hamiltonian with renormalized parameters. Subsequently the effective AH model has been solved using several theoretical methods such as the equation of motion (EOM) Green function technique, spectral density approximation (SDA) method and cluster variation (CV) method. One of the main aims of this thesis has been to study the effect of local *el-ph* interaction on the properties of the impurity. Our EOM method results show that the ground state (GS) energy of the AH model increases with the Coulomb interaction strength $U$ and decreases with the *el-ph* interaction strength $\lambda$ due to the polaronic effect. Furthermore, the GS energy is found to be lower in the adiabatic case than in the anti-adiabatic case. We have next observed that the binding energy $W$ between the localized and the conduction electrons increases with $\lambda$ and decreases with $U$ in both adiabatic and anti-adiabatic cases. But the binding turns out to be stronger in

the adiabatic regime than in the anti-adiabatic regime. We have also obtained the spectral function for the impurity and calculated the impurity specific heat and our results show that the specific heat initially increases with increasing $\lambda$ and beyond $\lambda_c$ it starts decreasing to zero.

Application of the SDA method has given us results for the spectral function, and the impurity specific heat beyond the mean-filed approximation. We find that as $\lambda$ increases, the width of the of spectral function decreases as a result of which the life time of an electron on the impurity increases leading to the electron localization on the impurity. For further conformation of localzation we have studied the $\lambda$ dependence of the specific heat. We have observed that the specific heat increases in the weak *el-ph* interaction regime and falls sharply to zero at a critical *el-ph* coupling constant ($\lambda_c$) which is independent of temperature.

To improve the phonon part of the solution, we next applied the variational LF transformation to the AH Hamiltonian and solved the effective AH Hamiltonian using CV method in the presence of an external magnetic field. Here we have treated the local magnetic moment ($m$) as a variational parameter. The GS energy is again shown to increase with increasing $U$ and external magnetic field $B$, but to decrease with increasing $\lambda$. We have also confirmed that an increase in either $U$ or $B$ weakens the binding energy of the bound state between the local and the conduction electrons, while that in $\lambda$ or $V$ strengthens it. By comparison we find the variational LF transformation provides more accurate results particularly in the adiabatic regime than the conventional LF transformation. We have also studied the polaron ($m = 1$) to bipolaron ($m = 0$) transition of the impurity. In the anti-adiabatic case, as $\lambda$ increases the local magnetic moment $m$ decreases and becomes zero at a critical value of $\lambda$ ($\lambda_c$), indicating that the impurity state undergoes a polaron-bipolaron

transition. Also for a given $\lambda$, there exists a critical value of $U$ at which, the impurity state undergoes a bipolaron-polaron transition that becomes smoother with increasing magnetic field. But in the adiabatic case for intermediate values of $U$ and $B$ the impurity state is a linear superposition of a polaron and bipolaron states, and as $\lambda$ increases beyond $\lambda_c$ it turns into a complete bipolaron state.

Then we have studied the many-body bound state formation on a magnetic impurity atom embedded in a BCS superconductor using the CV method for the effective electronic problem. We have specifically studied the effect of superconducting gap on the properties of the impurity. We have observed that the binding energy ($W$) increases with *el-ph* interaction strength $\lambda$, but decreases with the superconducting gap parameter $\Delta$. The local magnetic moment ($m$) decreases with increasing $\lambda$ in both adiabatic and anti-adiabatic regimes. As $\Delta$ increases, the critical value of $\lambda$ ($\lambda_c$) at which $m$ becomes zero, increases. Because at large value of $\Delta$, a very few unpaired electrons will be available in the host to compensate the impurity spin. So it requires a large energy to excite the unpaired electron, so that it can occupy the impurity site. Finally we have studied the effect of $\Delta$ on the polaron-bipolaron phase transition and bound-unbound state phase transition in both adiabatic and anti-adiabatic cases.

Finally we have considered AH-Caldeira-Leggett Hamiltonian to study the transport properties of an SMT device. Caldeira-Leggett term in the Hamiltonian describes the linear coupling between the substrate and the molecule, which takes care of the damping effect. Here we have employed the Keldysh non-equilibrium Green function method to calculate the tunneling current and differential conductance. We have analyzed the effect of local *el-ph* interaction and the damping effect in Ohmic case on the transport properties of SMT. We have observed the polaronic effects on the

spectral function in the form of redshift of the spectral function peak and the emergence of vibrational sidebands due to phonon-assisted tunneling process. Increase in the damping rate decreases the heights of the vibrational sidebands and broadens their widths. We have shown that the local *el-el* interaction causes a reduction in both the tunneling current and the differential conductance. Due to the damping effect of the substrate, the effective phonon frequency of the QD decreases as a result of which the tunneling current increases.